UNIVERSIDADE FEDERAL DO CEARÁ
CENTRO DE CIÊNCIAS
PROGRAMA DE PÓS-GRADUAÇÃO EM QUÍMICA

DEOMAR NOGUEIRA RODRIGUES JÚNIOR

PROPRIEDADES ELETROCATALÍTICAS E ANTICORROSIVAS DE REVESTIMENTOS DE ZnCo OBTIDOS EM MEIO DE SOLVENTE EUTÉTICO

FORTALEZA
2024

DEOMAR NOGUEIRA RODRIGUES JÚNIOR

PROPRIEDADES ELETROCATALÍTICAS E ANTICORROSIVAS DE REVESTIMENTOS DE ZnCo OBTIDOS EM MEIO DE SOLVENTE EUTÉTICO

Tese apresentada ao Programa de Pós-Graduação em Química da Universidade Federal do Ceará, como requisito parcial à obtenção do título de Doutor em Química. Área de concentração: Físico-Química.

Orientadora: Prof.ª Dra. Adriana Nunes Correia

FORTALEZA

2024

Dados Internacionais de Catalogação na Publicação
Universidade Federal do Ceará
Sistema de Bibliotecas
Gerada automaticamente pelo módulo Catalog, mediante os dados fornecidos pelo(a) autor(a)

R612 Rodrigues Júnior, Deomar Nogueira.
Propriedades eletrocatalíticas e anticorrosivas de revestimentos de ZnCo obtidos em meio de solvente eutético / Deomar Nogueira Rodrigues Júnior. – 2024.
107 f. : il. color.

Tese (doutorado) – Universidade Federal do Ceará, Centro de Ciências, Programa de Pós-Graduação em Química, Fortaleza, 2024.
Orientação: Profa. Dra. Adriana Nunes Correia.

1. Eletrodeposição. 2. Solvente eutético. 3. Zinco. 4. Cobalto. 5. Zn-Co. I. Título.

CDD 540

DEOMAR NOGUEIRA RODRIGUES JÚNIOR

PROPRIEDADES ELETROCATALÍTICAS E ANTICORROSIVAS DE REVESTIMENTOS DE ZnCo OBTIDOS EM MEIO DE SOLVENTE EUTÉTICO

Tese apresentada ao Programa de Pós-Graduação em Química da Universidade Federal do Ceará, como requisito parcial à obtenção do título de Doutor em Química. Área de concentração: Físico-Química.

Aprovada em: 08/12/2023.

BANCA EXAMINADORA

Profa. Dra. Adriana Nunes Correia (Orientadora)

Universidade Federal do Ceará (UFC)

Prof. Dr. Pedro de Lima Neto

Universidade Federal do Ceará (UFC)

Prof. Dr. Dieric dos Santos de Abreu

Universidade Federal do Ceará (UFC)

Prof. Dr. Paulo Naftali da Silva Casciano

Universidade Federal do Ceará (UFC)

Prof. Dr. Thiago Mielle Brito Ferreira Oliveira

Universidade Federal do Cariri (UFCA)

AGRADECIMENTOS

Este trabalho foi realizado com apoio da Coordenação de Aperfeiçoamento de Pessoal de Nível Superior – Brasil (CAPES) – Código de Financiamento 001.

Sempre a Deus em primeiro lugar, por tudo que me deu, uma vida, uma família linda e graciosa.

À minha amada mãe, Nilce Silveira, que sempre estará em minha memória, como uma mulher lutadora, guerreira, amável, uma verdadeira matriarca.

À minha amada esposa Luciana Pinto, que pacientemente, sempre esteve comigo nessa empreitada tão difícil e longa. Muito obrigado por tudo que sempre fez de melhor em minha vida.

Aos meus amados filhos, Dante e Dafne, por tudo que fizeram em minha vida, uma verdadeira renovação de amor e fraternidade. Que Deus esteja sempre em suas vidas, olhando para vocês e levando-os sempre para o caminho da sabedoria. Tudo que faço é por vocês.

À minha grande professora e orientadora, Dra. Adriana Correia, por ter me aceitado como seu orientando no doutorado, mesmo sabendo de minhas limitações, que são inúmeras. Muito obrigado professora, aprendi muito com a senhora, com suas virtudes, com seus ensinamentos acadêmicos e de vida. Levarei sempre em meus caminhos pessoais e profissionais a pessoa como a senhora é, dedicada, atenciosa e de extrema responsabilidade. Meus sinceros agradecimentos.

À minha amiga Natalia Gomes, que, sem sua ajuda incansável, jamais teria conseguido realizar esse sonho.

À banca examinadora, Profa. Dra. Adriana Nunes Correia, Prof. Dr. Paulo Naftali da Silva Casciano, Prof. Dr. Pedro de Lima-Neto, Prof. Dr. Dieric dos Santos de Abreu e ao Prof. Dr. Thiago Mielle Brito Ferreira Oliveira, por todo conhecimento e contribuições que deram em minha vida acadêmica.

Aos meus colegas do GELCORR, Ana Aline, Andreza, Janevane, Gisele, Juliermes, Marcus, Mesaque, Natalia, Raíssa, Ronnie, Valdessandro, Gilvane, Alexandre e Wanderson, pela amizade e conhecimentos compartilhados.

Ao Professor Nazareno Oliveira, representando o Colégio Master, que sempre me apoiou quando necessitei.

À SEDUC-CE, que, por três anos, me liberou para realizar esse estudo.

A todos os órgãos de fomento que possibilitaram essa empreitada.

Ao programa de Pós-Graduação em Química, que possibilitou com toda a sua estrutura a realização desse sonho.

À UFC por toda estrutura física e recursos humanos disponibilizados desde o início da minha formação acadêmica.

À Central Analítica-UFC/CT-INFRA/MCTI-SISNANO/Pró-Equipamentos CAPES pelas análises de microscopia eletrônica de varredura.

“O que realmente conta na vida não é apenas o fato de termos vivido; é a diferença que fizemos nas vidas dos outros [...].” (MANDELA, N.)

RESUMO

O desempenho de revestimentos de Zn, Co e Zn-Co na eletrocatálise da RDH foi avaliado por meio de parâmetros de Tafel calculados a partir de experimentos de LSV em meio de KOH 1 mol L^{-1} a 298 K, sob velocidade de varredura de 0,5 mV s^{-1}. Os filmes de Zn e Zn-Co foram eletrodepositados a partir de soluções eletrolíticas preparadas utilizando solvente eutético baseado em cloreto de colina (ChCl) e etilenoglicol (EG) em proporção molar 1:2 (ChCl:2EG), variando as concentrações dos íons Zn^{2+} e Co^{2+} de 0 a 0,4 mol L^{-1}. O substrato utilizado foi Cu e o modo de deposição foi potenciostático a −1,3 V e a 343 K. Os voltamogramas cíclicos explicitaram processos característicos de redução de oxidação dos metais em meio de ChCl:2EG. Os coeficientes de difusão do Zn^{2+} variaram entre 8,93 (± 0,77) $\times 10^{-11}$ cm^2 s^{-1} (303 K) e 4,55 (± 0,34) $\times 10^{-10}$ cm^2 s^{-1} (343 K); já os coeficientes de difusão determinados para o Co^{2+} variaram entre 2,64 (± 0,07) $\times 10^{-7}$ cm^2 s^{-1} (303 K) e 4,43 (± 0,48) $\times 10^{-7}$ cm^2 s^{-1} (343 K). A energia de ativação (E_a) aparente, calculada a partir de gráficos ln D em função do inverso da temperatura absoluta, para a difusão dos íons Zn^{2+} e Co^{2+} foi de 35,93 kJ mol^{-1} e 11,07 kJ mol^{-1}, respectivamente. As imagens de MEV mostraram que o aumento da quantidade de Co nos revestimentos levou à formação de trincas, favorecendo a utilização das ligas como eletrocatalisadores. Além disso, observou-se estreita correlação entre a composição da solução eletrolítica e a dos eletrodepósitos. Os filmes de Zn e Zn-Co apresentaram atividade eletocatalítica frente à RDH em meio alcalino, com coeficientes de Tafel de 170,28 mV dec^{-1} e sobrepotencial, a 10 mA cm^{-2}, de −641 mV para o Zn; 123,50 mV dec^{-1} e −494 mV para a liga $Zn_{96}Co_4$ e 113,46 mV dec^{-1} e −377 mV para a liga Zn_3Co_{97}. No que envolve aos revestimentos de Zn, Co e ZnCo no estudo de corrosão, em meio de NaCl 3,5% m/m, foi obtido voltamogramas, em substrato de aço carbono 1020, em meio de DES ChCl:2EG como solvente, variando as concentrações dos íons Zn^{2+} e Co^{2+} de 0 a 0,4 mol L^{-1}. Foi usado o modo potenciostático, aplicando um potencial de −1,4 V a 343 K. A caracterização morfológica da superfície dos eletrodepósitos foi feita por meio de MEV e a distribuição dos metais Zn e Co foi determinada por EDS. Os ensaios de curvas de polarização das espécies obtidos a 293 K, em substrato de aço carbono 1020, com concentrações variando de Zn^{2+} e Co^{2+} de 0 a 0,4 mol L^{-1}. Observou-se que, no comparativo frente ao aço carbono 1020, o revestimento de Zn apresentou maior corrente de corrosão, devido ao caráter sacrificial do Zn em relação ao aço.

Palavras-chave: eletrodeposição; solvente eutético; zinco; cobalto; Zn-Co.

ABSTRACT

The performance of Zn, Co and Zn-Co coatings in RDH electrocatalysis was evaluated using Tafel parameters calculated from LSV experiments in 1 mol L^{-1} KOH at 0.5 mV s^{-1} and 298 K. The Zn and Zn-Co films were electrodeposited from electrolytic solutions prepared using a deep eutectic solvent based on choline chloride (ChCl) and ethylene glycol (EG) in molar ratio of 1:2 (ChCl:2EG), varying the concentrations of Zn^{2+} and Co^{2+} ions from 0 to 0.4 mol L^{-1}. The substrate used was Cu and the deposition mode was potentiostatic at −1.3 V and 343 K. The cyclic voltammograms showed characteristic processes of reduction and oxidation of metals in ChCl:2EG. The Zn^{2+} diffusion coefficients varied between 8.93 (± 0.77) × 10^{-11} cm^2 s^{-1} (303 K) and 4.55 (± 0.34) × 10^{-10} cm^2 s^{-1} (343 K). The diffusion coefficients determined for Co^{2+} varied between 2.64 (± 0.07) ×10^{-7} cm^2 s^{-1} (303 K) and 4.43 (± 0.48) ×10^{-7} cm^2 s^{-1} (343 K). The apparent activation energy (E_a), calculated from ln D graphs as a function of the inverse of the absolute temperature, for the diffusion of Zn^{2+} and Co^{2+} ions was 35.93 kJ mol^{-1} and 11.07 kJ mol^{-1}, respectively. The SEM images showed that the increase in the amount of Co in the coatings led to the formation of cracks, favoring the use of the alloys as electrocatalysts. Furthermore, a close correlation was observed between the composition of the electrolyte solution and that of the electrodeposits. The Zn and Zn-Co films showed electrocatalytic activity against RDH in an alkaline medium, with Tafel coefficients of 170.28 mV dec^{-1} and overpotential, at 10 mA cm^{-2}, of −641 mV for Zn; 123.50 mV dec^{-1} and −494 mV for the $Zn_{96}Co_4$ alloy and 113.46 mV dec^{-1} and −377 mV for the Zn_3Co_{97} alloy. Regarding the Zn, Co and ZnCo coatings in the corrosion study, in a medium of NaCl 3.5% m/m, voltammograms were obtained, on a 1020 carbon steel substrate, in DES ChCl:2EG as solvent, varying the concentrations of Zn^{2+} and Co^{2+} ions from 0 to 0.4 mol L^{-1}. The potentiostatic mode was used, applying a potential of −1.4 V at 343 K. The morphological characterization of the electrodeposit surface was carried out using SEM and the distribution of the metals Zn and Co was determined by EDS. The polarization curve tests of the species obtained at 293K, on a 1020 carbon steel substrate, with concentrations ranging from Zn^{2+} and Co^{2+} from 0 to 0.4 mol L^{-1}. It was observed that, in comparison with 1020 carbon steel, the Zn coating presented a higher corrosion current, due to the sacrificial nature of Zn in relation to steel.

Keywords: electrodeposition; deep eutectic solvent; zinc; cobalt; Zn-Co.

SUMÁRIO

1 INTRODUÇÃO 9

1.1 Eletrodeposição em meio aquoso e em meio de líquido iônico 9

1.2 Eletrodeposição em DES 12

1.3 Eletrodeposição de revestimentos contendo Zn e Co 15

1.4 Aplicações 19

1.4.1 Eletrocatálise 19

1.4.1.1 Reação de desprendimento de hidrogênio 21

1.4.1.2 Eletrocatalisadores 22

1.4.1.3 Eletrocatalisadores produzidos via eletrodeposição 23

1.4.2 Corrosão 23

2 MANUSCRITO 1 27

3 MANUSCRITO 2 69

REFERÊNCIAS 87

APÊNDICE A – MANUSCRITO 1 - ZnxCo(1-x) *COATINGS FROM CHOLINE CHLORIDE-ETHYLENE GLYCOL DEEP EUTECTIC SOLVENT AS ELECTROCATALYSTS FOR HYDROGEN EVOLUTION REACTION* - PUBLICADO NO PERIÓDICO *JOURNAL OF ELECTROANALYTICAL CHEMISTRY* 93

APÊNDICE B – MATERIAL SUPLEMENTAR DO MANUSCRITO 1 - ZnxCo(1-x) *COATINGS FROM CHOLINE CHLORIDE-ETHYLENE GLYCOL DEEP EUTECTIC SOLVENT AS ELECTROCATALYSTS FOR HYDROGEN EVOLUTION REACTION* - PUBLICADO NO PERIÓDICO *JOURNAL OF ELECTROANALYTICAL CHEMISTRY* 100

1 INTRODUÇÃO

De acordo com a IUPAC (*International Union of Pure and Applied Chemistry*), eletrodeposição é a deposição, sobre um eletrodo, de um material dissolvido ou suspenso, por ação de um campo elétrico. (1) No caso da eletrodeposição de metais, em geral, esta ocorre por meio da redução de íons sobre a superfície eletródica, com a formação de uma fase sólida. (2)

Pode-se dizer, ainda, que a eletrodeposição utiliza os princípios da eletrólise para promover a deposição de algum material (geralmente, metálico) de revestimento na superfície de um eletrodo. Esse processo ocorre por meio da imposição de uma densidade de corrente (método galvanostático) ou de um potencial (método potenciostático) a um eletrodo imerso em uma solução que contém as espécies a serem depositadas na superfície de trabalho. Desse modo, a eletrodeposição e, consequentemente, o revestimento metálico, tem como objetivo alterar as propriedades de determinada superfície para um fim específico. (3)

A eletrodeposição tem sido amplamente utilizada, uma vez que as aplicações que abrangem a proteção de materiais contra a corrosão, a produção de eletrocatalisadores para reações como a reação de desprendimento de hidrogênio (RDH) e, até o embelezamento de superfícies. Além disso, pode-se controlar características como morfologia, espessura, textura e composição dos revestimentos pela modificação de parâmetros experimentais, como potencial aplicado, densidade de corrente imposta, tempo de deposição e composição do banho eletrolítico. (3)

1.1 Eletrodeposição em meio aquoso e em meio de líquido iônico

A eletrodeposição tem sido aplicada industrialmente por mais de 150 anos. Durante esse período, soluções aquosas denominadas banhos com diferentes características foram desenvolvidas para aplicações industriais. A composição desses banhos inclui, em geral, aditivos para diferentes finalidades. Entre elas, estão abrilhantamento, alívio de estresse, aumento da eficiência de corrente ou eficiência faradaica, inibição da fragilização por hidrogênio, entre outras. Essa necessidade de aditivos tem sido apontada como uma desvantagem para a utilização da água como solvente para eletrodeposição. (4)

No entanto, diversos revestimentos eletrodepositados à base de metais têm sido obtidos em meio aquoso para diferentes fins, especialmente na produção de eletrocatalisadores da RDH e de revestimentos para proteção à corrosão. (4-6) A eletrocatálise da RDH tem tido destaque nos últimos anos na obtenção de energias limpas, especialmente na produção de hidrogênio

verde, que é aquele obtido por eletrólise da água utilizando fontes renováveis de energia elétrica, tais como energia solar, energia eólica e biomassa. (7)

Nesse âmbito, a região nordeste do Brasil tem sido pioneira na utilização de fontes renováveis de energia elétrica, visto que ela é responsável por cerca de 82,3 % de toda energia eólica e solar produzida no país. (8) Esse contexto levou à instalação de um *hub* de hidrogênio verde no Complexo Industrial e Portuário do Pecém (CIPP S/A), no estado do Ceará, tornando o estudo da eletrocatálise da RDH para a produção desse combustível ainda mais relevante para pesquisas realizadas em território brasileiro. (9)

Já a proteção à corrosão tem sua importância devido aos custos e aos riscos associados à corrosão de estruturas e componentes. (4) Pode-se evidenciar, por exemplo, dentre os materiais metálicos, os aços carbono de baixa liga, devido à sua larga utilização na construção civil. Especialmente em meios contendo o íon cloreto, que acelera a corrosão desse tipo de material, como a umidade presente na atmosfera de regiões litorâneas, o controle da corrosão dos aços é fundamental. (10)

Vale ressaltar que, no Ceará, a Praia do Futuro tem sido apontada como a região cuja atmosfera tem a maior agressividade do mundo, devido à maior concentração de cloreto medida, de 1498,77 mg m^{-2} dia^{-1}, quase o dobro da costa da Nigéria, que é a segunda colocada, com cerca de 800 mg m^{-2} dia^{-1}. (11)

No que concerne à produção de eletrocatalisadores da RDH, cita-se, por exemplo, o trabalho de Carim e colaboradores, em que estudaram a utilização de revestimentos Co-Se eletrodepositados sobre Ti como catalisadores da RDH em meio de H_2SO_4 0,500 mol L^{-1}. Para uma densidade de corrente de 10 mA cm^{-2}, o sobrepotencial observado foi, aproximadamente, 135 mV e o eletrodepósito manteve-se estável por 16 h de operação contínua a 10 mA cm^{-2}. (12)

Já o trabalho de Kublanovsky e Yapontseva foi sobre a atividade eletocatalítica de depósitos de Co-Mo frente à RDH em três diferentes soluções aquosas, H_2SO_4 0,01 mol L^{-1}, Na_2SO_4 0,5 mol L^{-1} e KOH 1,0 mol L^{-1}, desaeradas com Ar por 30 min antes dos experimentos, a 25 ºC (298,15 K), utilizando sistema convencional de três eletrodos, sendo o contra-eletrodo de fio Pt e o de referência, um eletrodo Ag/AgCl (solução não especificada). A eletrodeposição foi realizada utilizando sistema de dois eletrodos, em que um eletrodo de Pt foi o eletrodo auxiliar. Esses autores pontuaram que, devido à dependência do mecanismo da RDH em relação ao pH do meio, o sobrepotencial mais baixo para a RDH sobre Co foi obtido em meio ácido e o mais alto, em meio neutro. Ainda para o cátodo de Co, os coeficientes de Tafel foram 0,122 V, 0,142 V e 0,125 V em meio ácido, alcalino e neutro, respectivamente; enquanto os

valores de densidade de corrente de troca foram 1,93 × 10^{-2} mA cm^{-2} em meio ácido, 4,59 × 10^{-2} mA cm^{-2} em meio alcalino e 6,31 × 10^{-3} mA cm^{-2} em meio neutro. Além disso, citaram que os revestimentos Co-Mo obtiveram melhor atividade eletrocatalítica em meio alcalino e discutiram apenas os resultados relativos a este meio. As curvas de densidade de corrente *vs* potencial para a RDH em meio de KOH 1 mol L^{-1} para os revestimentos eletrodepositados com densidade de corrente de 30 mA cm^{-2} mostraram que o revestimento que continha apenas Co apresentou maiores sobrepotenciais que os filmes Co-Mo, sendo que o depósito obtido a partir de solução contendo $CoSO_4$ 0,1 mol L^{-1} + Na_2MoO_4 0,01 mol L^{-1} exibiu os menores sobrepotenciais, indicando maior atividade eletrocatalítica. (13)

Já em relação à eletrodeposição de revestimentos para proteção à corrosão, pode-se citar o trabalho de Baht e colaboradores, que produziram eletrodepósitos de Zn-Ni-Fe sobre aço carbono baixa liga, utilizando uma célula de Hull com banho contendo $ZnCl_2 \cdot 6H_2O$, $NiCl_2 \cdot 6H_2O$, $FeCl_2 \cdot 4H_2O$, NH_4Cl, KCl, ácido ascórbico, além de ácido sulfanílico e gelatina como aditivos, variando o pH do meio e a densidade de corrente aplicada. De acordo com esses autores, a maior resistência à corrosão foi observada para o revestimento de Zn-Ni-Fe obtido a 40 mA cm^{-2}, que contém aproximadamente 19,61% em peso de Ni e 5,70% em peso de Fe, cuja taxa de corrosão foi de 26,4 μm por ano em meio de NaCl 3,5 %. (14)

O trabalho de Lin e colaboradores, por sua vez, estudou a performance de revestimentos Co-Cu e Co-Cu-Re sobre aço carbono frente à corrosão em meio de NaCl 3,5 %. Eles reportaram que o revestimento Co-Cu-Re apresentou uma densidade de corrente de corrosão de 3,2 x 10^{-6} A cm^{-2}, o que foi 3,4 vezes menor do que o do substrato de aço carbono e 2,4 vezes menor do que o do revestimento Co-Cu. A resistência à transferência de carga (Rct) para o revestimento Co-Cu-Re foi de 4512 Ω cm^2, 6 vezes maior do que a do substrato de aço carbono e 1,1 vezes maior do que a do revestimento de Co-Cu. Assim, concluíram que a adição do elemento rênio pode aumentar a resistência à corrosão do revestimento Co-Cu. (15)

Por outro lado, a utilização do meio aquoso para eletrodeposição apresenta desvantagens, como pequeno intervalo eletroquímico, volatilidade e, principalmente, a necessidade do uso de cianetos como complexantes, que são tóxicos. Nesse contexto, emergem solventes de melhor desempenho, como os líquidos iônicos (LI) e os solventes (profundamente) eutéticos, do inglês *deep eutectic solventes* (DES).

O termo LI tem sido aplicado a compostos iônicos com baixos pontos de fusão, especialmente abaixo de 100 ºC. Eles possuem uma ampla gama de diversidade química devido às diferentes combinações de ânions e cátions, além de elevadas estabilidades química e

térmica, notável poder de solvatação e entalpias de vaporização extremamente altas, o que os torna efetivamente não voláteis. Além disso, o intervalo eletroquímico de alguns LI é muito amplo (até 6 V em alguns casos), tornando-os indicados para a eletrodeposição de metais ativos e semicondutores. (16)

Já os DES, por definição, são misturas eutéticas formadas por um haleto de um cátion volumoso, como os haletos de amônio quaternário, e um doador de ligação de hidrogênio. Entre os sais de amônio quaternário utilizados na produção de DES, pode-se citar cloreto de etilamônio, acetato de colina, nitrato de colina e o mais comumente visto nos trabalhos de aplicações eletroquímicas de DES, cloreto de colina (ChCl). Já entre os doadores de ligação de hidrogênio, pode-se citar 1-metilureia, acetamida, glicerol, 1,4-butanodiol, ureia (U) e etilenoglicol (EG), sendo estes últimos aqueles mais amplamente reportados como solventes em trabalhos da área de Eletroquímica. (17-20) Por conta de suas propriedades semelhantes às dos LI, alguns autores consideram os DES como uma classe de LI.

1.2 Eletrodeposição em DES

Entre as suas muitas aplicações, os DES têm sido utilizados como solventes para eletropolimento (em tradução livre do inglês *eletropolishing*), bem como para reações eletroquímicas diversas e para o preparo de soluções eletrolíticas para eletrodeposição. (13) Neste último caso, os DES apresentam uma série de vantagens sobre a água, que tem sido, ao longo dos anos, o principal solvente empregado em banhos eletrolíticos. A primeira dessas vantagens é o aumento da janela de potencial de trabalho devido à ausência da RDH, o que possibilita a eletrodeposição de um número maior de metais e ligas. Isso porque, em meio aquoso, a presença da RDH como reação paralela na eletrodeposição de revestimentos não é desejável, uma vez que esta leva à diminuição da eficiência catódica, à restrição da janela de potencial de trabalho e pode resultar na formação de filmes pouco aderentes. Essa é a principal desvantagem da utilização da água como solvente na eletrodeposição de metais e suas ligas. Além disso, há uma restrição das temperaturas de trabalho por conta da volatilidade da água e uma frequente necessidade de aditivos no banho eletrolítico, que podem ser poluentes e acrescentar uma etapa extensa de tratamento da solução antes de seu descarte. (17, 21)

Além disso, os DES apresentam alta condutividade, alta solubilidade de sais metálicos, além de não serem inflamáveis, terem uma ampla faixa de temperaturas de trabalho, serem biodegradáveis e poderem ser produzidos de forma simples e com baixo custo. (6, 19) Em trabalhos de eletrodeposição de metais e ligas, DES têm sido utilizados com grande sucesso.

(22-26). Na Figura 1, é apresentado um diagrama qualitativo das principais propriedades dos DES.

Para exemplificar a utilização de DES na eletrodeposição de metais isolados, pode-se citar o trabalho de Urcezino e colaboradores, em que eles estudaram a eletrodeposição de revestimentos de Ni sobre substrato de Cu a utilizando os solventes eutéticos ChCl:2U (1 mol de ChCl: 2 mol de U) e ChCl:2EG (1 mol de ChCl: 2 mol de EG). Avaliou-se tanto a influência da temperatura quanto a do DES nos revestimentos obtidos, sendo observado que os coeficientes de difusão do íon Ni^{2+} variaram de $2{,}2 \times 10^{-9}$ cm^2 s^{-1} a $3{,}7 \times 10^{-8}$ cm^2 s^{-1} em meio de ChCl:2U e de $1{,}3 \times 10^{-8}$ cm^2 s^{-1} a $5{,}8 \times 10^{-8}$ cm^2 s^{-1} em meio de ChCl:2EG. Além disso, estudou-se o mecanismo de nucleação dos filmes segundo o modelo de Scharifker e Hills. Desse modo, foi constatado que, em meio de ChCl:2EG, a nucleação era instantânea, enquanto em meio de ChCl:2U, era progressiva. As imagens obtidas por microscopia eletrônica de varredura (MEV) mostraram que o aumento da temperatura levou à obtenção de revestimentos mais compactos. Além disso, os revestimentos foram avaliados como protetores frente à corrosão em meio de NaCl 3,5 %, em que foi observado que os revestimentos mais protetores foram aqueles obtidos a temperaturas mais altas, corroborando com os resultados de MEV. (22)

Figura 1 – Representação das vantagens de se usar DES como solvente

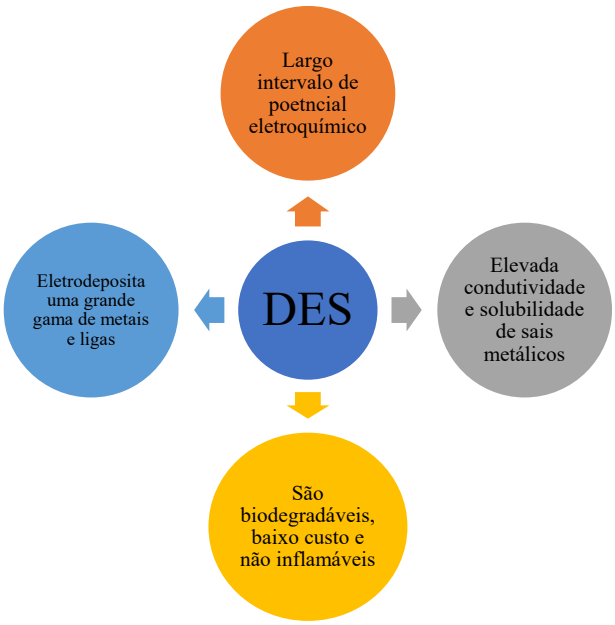

Fonte: Elaborada pelo autor (2023).

Pereira e colaboradores, por sua vez, estudaram os efeitos dos parâmetros de eletrodeposição na resistência à corrosão de revestimentos Zn-Sn sobre aço carbono, obtidos a partir de ChCl:2EG. Esses autores observaram que a resistência à corrosão dos revestimentos em meio de NaCl 3,5% era maior quando a deposição de Zn era favorecida, fosse pelo aumento da temperatura da solução eletrolítica, fosse pelo aumento do potencial de deposição. Ademais, notaram que o aumento da concentração de Sn na solução eletrolítica levava a um aumento da quantidade deste metal nos revestimentos, fato que associaram a um regime de deposição normal. Por outro lado, os padrões obtidos por difração de raios-X (DRX) obtidos mostraram que a eletrodeposição de Zn e Sn ocorreu sem a formação de fase intermetálica, enquanto as micrografias obtidas por MEV mostraram forte dependência da morfologia dos revestimentos com a presença de Sn^{2+} e com a temperatura. (23)

Além disso, DES também podem ser usados para a eletrodeposição de revestimentos contendo mais de dois metais, como no trabalho em que Pereira e colaboradores avaliaram a corrosão eletroquímica de revestimentos Zn-Sn-In em meio de ChCl:2EG. Eles constataram que o aumento da concentração de In^{3+} na solução eletrolítica promoveu aumento na porcentagem de In no revestimento, assim como levou à obtenção de grãos mais refinados. Em contrapartida, o aumento do potencial de deposição até −1,3 V levou à obtenção de revestimentos mais densos e compactos, bem como ricos em Zn. Ademais, em meio de NaCl 3,5 %, o aumento da quantidade de In nos depósitos levou à maior resistência à corrosão. (24)

Esses e outros tantos trabalhos mostram a utilidade e a versatilidade dos DES frente à eletrodeposição de revestimentos metálicos de diversas composições. (3, 25-28) A escolha dos metais a serem depositados depende, principalmente, da aplicação que se fará dos eletrodepósitos. Zn, por exemplo, por seu potencial de corrosão, comporta-se como metal de sacrifício frente ao Fe presente nos aços carbono. Além disso, como um metal abundante na crosta terrestre, tem o potencial de ser uma alternativa à Fe na catálise da RDH. Já Co, enquanto revestimento, pode tanto oferecer proteção à corrosão, devido à suas características intrínsecas, bem como pode atuar em eletrocatálise, já que eletrocatalisadores à base de Co têm demonstrado excelente condutividade elétrica, alta atividade e durabilidade em meio alcalino, além de serem de baixo custo. (6, 29)

1.3 Eletrodeposição de revestimentos contendo Zn e Co

Com relação à produção de revestimentos de Co por via eletroquímica, Li, Wang e Reddy estudaram a eletrodeposição de Co em meio de solvente produzido a partir de U e ChCl. O mecanismo de redução dos íons Co^{2+} foi avaliado por voltametria cíclica (VC), cujos experimentos foram conduzidos em sistema de três eletrodos, com um fio de W como eletrodo de trabalho (0,157 cm^2 de área), um fio de Pt como eletrodo auxiliar e um fio de Ag como eletrodo pseudo-referência. O intervalo de potencial foi de 0,30 a −0,90 V e a velocidade de varredura variou de 40 mV s^{-1} a 100 mV s^{-1}, a 373,15 K, com $CoCl_2$ 0,05 mol L^{-1} em solução. Esses autores observaram um processo de redução em potencial de aproximadamente −0,78 V e um processo de oxidação em 0,16 V, atribuindo o processo de redução à reação $CoCl_x^{2-x} + 2e^- \rightarrow Co + xCl^-$ e o de oxidação, à reação inversa, $Co + xCl^- \rightarrow CoCl_x^{2-x} + 2e^-$. Eles argumentaram que, como a diferença de potencial entre o processo de redução e o de oxidação é maior que 900 mV e há um deslocamento do potencial de pico do processo de redução para valores mais negativos, a redução do Co^{2+} é irreversível e ocorre em uma etapa única, que envolve a transferência de dois elétrons. A obtenção dos revestimentos foi feita utilizando sistema de três eletrodos, sendo o eletrodo de trabalho feito de Cu e tendo 0,5 cm^2 de área (formato não especificado), o eletrodo auxiliar, um fio de Pt e um fio de Ag utilizado como eletrodo pseudo-referência. Os depósitos foram obtidos em modo potenciostático, aplicando diferentes potenciais, −0,80 V, −0,85 V, −0,90 V e −0,95 V, variando a temperatura de 353,15 K a 383, 15 K. A aplicação de diferentes potenciais de deposição a 373,15 K levou à obtenção de diferentes morfologias nos revestimentos, de acordo com as imagens de MEV. Sob potencial de −0,80 V, o eletrodepósito apresentou morfologia uniforme, densa e compacta. Ao se aumentar o potencial de deposição para −0,85 V, observou-se a formação de algumas partículas poligonais na superfície do revestimento. Já aplicando um potencial de −0,90 V, o revestimento obtido apresentou morfologia nodular e, por fim, quando o potencial aplicado foi de −0,95 V, foi observada a formação de dendritos. (30)

Diferentemente do que ocorre para Ni e Co, nos últimos 10 anos, houve um número diminuto de publicações relativas à utilização de revestimentos em que o Zn é o componente majoritário para eletrocatálise, em especial da RDH. Essa escassez de publicações representa uma lacuna no conhecimento dos eletrocatalisadores à base de Zn frente à RDH e desperta o interesse no estudo deste tipo de filme. Utilizando a metodologia de busca (base de dados *Web of Science*®), averiguou-se ainda os artigos publicados nos últimos 10 anos, utilizando a palavra-chave “eletrodeposição”, “eletrodeposição cobalto”, seguido simultaneamente de

“eletrodeposição de cobalto-zinco” em seguida “eletrodeposição de cobalto e zinco em DES”, com os dados indicados na Figura 2.

No que concerne à eletrodeposição de revestimentos à base de Zn, Alesary e colaboradores estudaram a influência da utilização de ácido nicotínico, de ácido bórico e de benzoquinona como aditivos na obtenção de eletrodepósitos de Zn em meio de solvente eutético formado por ChCl e EG. As soluções utilizadas para eletrodeposição continham $ZnCl_2$ 0,4 mol L^{-1}, na ausência e na presença de aditivos. Os eletrodepósitos foram produzidos sobre substrato de Cu (área não informada), que foi previamente tratado por imersão em solução de $(NH_4)_2S_2O_8$ 0,87 mol L^{-1}, seguida de imersão em H_2SO_4 0,2 mol L^{-1}, com posterior lavagem com água (não especificada) e secagem (não detalhada). Utilizou-se uma rede de Ti como eletrodo auxiliar, e os eletrodepósitos foram obtidos sob densidade de corrente de 3,3 mA cm^{-2} por 2 h a 80 ºC (353,15 K). A caracterização eletroquímica foi realizada utilizando célula de três eletrodos, sendo o eletrodo de trabalho um disco de Pt de 1 mm de diâmetro – previamente polido com pasta de alumina de 0,05 μm, lavado com água deionizada e, em seguida, com acetona – o auxiliar, uma placa de Pt (dimensões não informadas) e o de referência, Ag/AgCl. Obteve-se voltamogramas cíclicos utilizando solução de $ZnCl_2$ 0,4 mol L^{-1} em intervalo de potencial de 0,0 V a −1,5 V, com velocidade de varredura de 30 mV s^{-1}, a temperatura ambiente (não especificada, na ausência de aditivos) e a 353 K, na ausência e na presença de aditivos (0,03 mol L^{-1} a 0,1 mol L^{-1} de ácido nicotínico; 0,05 mol L^{-1} a 0,15 mol L^{-1} de ácido bórico e 0,03 mol L^{-1} a 0,1 mol L^{-1} de benzoquinona). (31)

De acordo com esses autores, os voltamogramas cíclicos obtidos a 353,15 K na ausência de aditivos diferem significativamente dos obtidos a temperatura ambiente, mostrando aumento considerável nas correntes de deposição e de dissolução de Zn. Eles apresentaram várias razões para este resultado. Primeiro, eles argumentaram que o aumento de temperatura leva à diminuição na viscosidade da solução eletrolítica, aumentando a velocidade do transporte de massa em direção à superfície eletródica. Depois, afirmaram que a solução continha alta concentração de íons Cl^-, que adsorveram nesta superfície e impediram a aproximação da espécie $(ZnCl_4)^{2-}$, forma atribuída aos íons Zn^{2+} com sua esfera de coordenação em solução contendo Cl^-, para ser reduzida. A elevação da temperatura fez com que diminuísse a quantidade de íons Cl^- adsorvidos na superfície eletródica, o que aumentou a quantidade de sítios disponíveis para a redução de $(ZnCl_4)^{2-}$ na superfície do substrato. Além disso, foram obsrvados dois processos sobrepostos de redução em torno de −1,2 V e −1,3 V; e dois processos de oxidação de Zn, em potenciais próximos a −0,95 V e −0,85 V. A existência

de dois processos de redução foi atribuída à formação e à dissolução de fases microcristalinas energeticamente discretas do depósito de Zn. (31)

Figura 2 – Análise quantitativa da produção científica internacional relativa aos materiais depositados de Zn e Co. Os dados foram obtidos por meio da base de dados científicos *Web of Science*®, utilizando simultaneamente o refinamento por: palavras-chave, interstício de 2013 a 2023 e apenas artigos científicos.

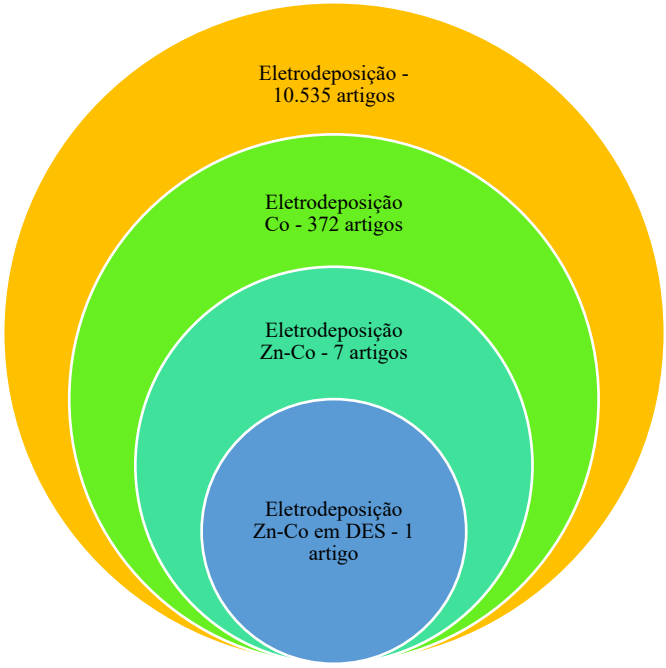

Fonte: Elaborada pelo autor (2023).

Com relação aos aditivos analisados, esses autores observaram que a presença de ácido nicotínico (0,03 mol L^{-1}) levou à diminuição nas correntes de redução, além de deslocamento de potencial de cerca de −30 mV, o que atribuíram à necessidade de maior quantidade de energia para a redução devido à ocupação de sítios do substrato pelas moléculas do ácido nicotínico. Contudo, o aumento da concentração de 0,03 mol L^{-1} para 0,05 mol L^{-1} levou ao aumento nas correntes de redução em relação ao sistema contendo 0,03 mol L^{-1} do aditivo e, por fim, ao adicionar 0,1 mol L^{-1} de ácido nicotínico ao sistema, houve diminuição das correntes e redução. Os autores atribuíram essas variações nas correntes a mudanças na posição que as moléculas de ácido nicotínico assumem sobre a superfície eletródica com a variação de sua concentração na solução. Para baixa concentração (0,03 mol L^{-1}), eles admitiram adsorção e posição paralela à superfície, bloqueando vasta área de sítios ativos; para concentração de 0,05 mol L^{-1}, eles consideraram adsorção perpendicular à superfície, deixando mais sítios livres que com 0,03 mol L^{-1}; por fim, para a concentração de 0,1 mol L^{-1}, admitiram a

agregação das moléculas de ácido nicotínico sobre a superfície do eletrodo, bloqueando uma grande quantidade de sítios, levando a nova diminuição das correntes. Para os aditivos ácido bórico e benzoquinona, houve diminuição consistente das correntes de redução com o aumento da concentração destes em solução. (31)

Além disso, Alesary e colaboradores caracterizaram, por MEV, a morfologia dos eletrodepósitos produzidos. Para o revestimento de Zn obtido a partir de solução de $ZnCl_2$ 0,4 mol L^{-1} na ausência de aditivos, eles observaram partículas de Zn de diferentes tamanhos, levando a uma morfologia rugosa e policristalina. Em contrapartida, a utilização de aditivos levou à produção de revestimentos menos rugosos e com tamanhos de grãos mais refinados. (31)

Chu, Liang e Hao, por sua vez, estudaram a eletrodeposição de ligas Zn-Co em meio de solvente preparado a partir de ChCl e U na proporção molar 1:2 (ChCl:2U). A concentração de Zn^{2+} e Co^{2+} foi fixa, sendo a fonte daquele $ZnCl_2$ (0,11 mol L^{-1}) e a deste, $CoCl_2$ (0,01 mol L^{-1}). A eletrodeposição foi realizada em modo potenciostático, utilizando diferentes potenciais de deposição (não foram especificados na parte experimental, mas ao longo do texto tem-se 0,06 V, −0,25 V, −0,30 V, −0,35 V, −0,37 V, −0,40 V, −0,45 V e −0,50 V) sobre substrato de Cu (área superficial de 126 mm^2), com contra-eletrodo e eletrodo de referência, ambos, de placa de Zn (100 mm^2 de área geométrica). O potencial foi mantido constante por 20 min a 353,15 K. (32)

A caracterização eletroquímica foi feita por VC, utilizando sistema de três eletrodos, com eletrodo de trabalho de Pt (disco de 1,0 mm de diâmetro), eletrodo de referência e eletrodo auxiliar de placa de Zn (100 mm^2 de área geométrica), a 353,15 K, com velocidade de varredura de 50 mV s^{-1}. Observou-se dois processos de redução, um em 0,06 V, atribuído à redução de Co^{2+} e outro em −0,37 V, atribuído à redução de Zn^{2+}. Já na varredura anódica, os autores relataram três processos, os quais atribuíram à dissolução dos metais de diferentes fases da liga eletrodepositada durante a varredura catódica. Os processos observados em potenciais menos positivos (0,24 V e em aproximadamente 0,50 V) foram atribuídos à dissolução de Zn e o processo observado em torno de 0,82 V foi atribuído à dissolução de Co. (32)

A morfologia e a composição química dos eletrodepósitos foram estudadas por MEV e espectroscopia de energia dispersiva de raios-X (EDS, do inglês *energy-dispersive X-ray spectroscopy*). As imagens de MEV mostraram que o revestimento Zn-Co obtido sob potencial de −0,3 V apresentou aglomerados esféricos com diâmetro variando de 1 a 2 μm que se distribuíam independentemente uns dos outros, tornando a superfície do depósito muito porosa. Quando se aplicou potencial mais negativo (−0,40 V), foram observados aglomerados de grãos

com tamanho de 2 a 3 μ na superfície do revestimento; e, para potencial de −0,5 V, o diâmetro dos aglomerados de grãos aumentou para 3 a 4 μm. Esse crescimento dos grãos foi atribuído, pelos autores, a uma maior taxa de crescimento com o aumento do potencial (em módulo). Os resultados de EDS, por sua vez, evidenciaram que houve uma diminuição na quantidade de Co depositado quando o potencial foi se tornando mais negativo, atribuindo esse fato a um aumento da taxa de deposição de Zn nessas condições. Esses autores estabeleceram uma linha de referência de composição dos eletrodepósitos, correspondente à percentagem de Co nos revestimentos iguais à sua quantidade em solução. Todos os depósitos apresentaram sempre porcentagem maior de Co que a solução de partida, o que levou esses autores a afirmarem que ocorreu codeposição normal de Zn-Co. (32) Rosen e colaboradores, por sua vez, propuseram a utilização de Zn eletrodepositado sobre folha de Zn para a redução eletrocatalítica de CO_2. (33)

1.4 Aplicações

1.4.1 Eletrocatálise

A eletrocatálise pode ser entendida como o tipo de processo catalítico que envolve reações tanto de oxidação quanto de redução por meio da transferência direta de elétrons entre as espécies reagentes em uma interface eletroquímica. (34) O termo eletrocatálise foi cunhado originalmente por Kobosev e Monblanowa em 1934, quando faziam estudos de eletrodifusão, e utilizado mais tarde por Grub, quando este estabeleceu uma correlação entre resultados cinéticos da RDH sobre superfícies de vários metais e parâmetros como a energia de ligação metal-hidrogênio em um trabalho pioneiro neste campo. (35)

Os processos eletrocatalíticos são fortemente dependentes da natureza do substrato, isto é, da superfície do eletrodo de trabalho. Assim, eles são influenciados por fatores como i) a estrutura eletrônica do substrato, que está relacionada à atividade eletrocatalítica deste; ii) as interações substrato-adsorbato; iii) a distribuição das partículas catalisadoras ao longo da superfície do substrato, bem como iv) o número de coordenação médio dos átomos da superfície. (35)

O avanço tecnológico crescente que tem se desencadeado desde a Primeira Revolução Industrial levou a uma grande demanda por energia, não só para o setor de indústrias, mas, sobretudo, para os mais variados meios de transporte e, ainda, para utilização doméstica. Toda essa necessidade gerou uma utilização massiva de combustíveis fósseis, tais como óleo diesel, gasolina e gás natural, que apresentam excelente rendimento energético, mas são susceptíveis ao esgotamento, já que sua fonte, o petróleo, não é renovável. (36)

Além disso, a utilização em larga escala dos combustíveis fósseis tem sido relacionada ao agravamento do efeito estufa, devido principalmente à produção de óxidos de carbono, nitrogênio e enxofre, o que tem levado à procura por fontes de energia que sejam limpas ou verdes, isto é, ecologicamente corretas, e renováveis.

Nesse âmbito, o hidrogênio molecular ($H_{2(g)}$) tem surgido como uma alternativa viável aos combustíveis fósseis. Isso porque tem um conteúdo energético de cerca de $143 \cdot 10^6$ J kg^{-1}, o que chega a ser até três vezes maior que dos combustíveis fósseis líquidos, além de não ser tóxico, ter uma perspectiva de disponibilidade praticamente sem limites, sua queima não produzir gases tóxicos e não apresentar riscos operacionais adicionais, comparando-se com outros combustíveis largamente utilizados. (37)

O $H_{2(g)}$ pode ser produzido por diversos métodos, porém a eletrólise da água tem se mostrado a via mais promissora, em se tratando da proposta de um combustível renovável e ecologicamente correto, já que é um processo limpo e que produz hidrogênio com elevada pureza. (36-37)

A eletrólise da água envolve duas semi-reações: RDH e a reação de desprendimento de oxigênio (RDO). (38)

Em meio ácido, tem-se:

$$2H^+_{(aq)} + 2e^- \rightarrow H_{2(g)} \quad (1)$$

$$2H_2O_{(l)} \rightarrow O_{2(g)} + 4H^+_{(aq)} + 4e^- \quad (2)$$

Já em meio alcalino, tem-se:

$$2H_2O_{(l)} + 2e^- \rightarrow H_{2(g)} + 2OH^-_{(aq)} \quad (3)$$

$$4OH^-_{(aq)} \rightarrow O_{2(g)} + 2H_2O_{(l)} + 4e^- \quad (4)$$

As equações 1 e 3 referem-se à RDH e as equações 2 e 4 referem-se à RDO.

Apesar de suas vantagens, a grande desvantagem da eletrólise da água é que sua cinética eleva o sobrepotencial necessário para que a reação global ocorra, chegando a valores que podem variar de 1,8 V a 2,4 V *v.s.* ERH (eletrodo reversível de hidrogênio), muito maiores que o valor de 1,23 V *v.s.* ERH, que é o termodinamicamente previsto. (4) Assim, as semi-reações da eletrólise da água são de grande interesse no campo da eletrocatálise, pois a utilização de eletrocatalisadores adequados é capaz de reduzir o sobrepotencial necessário, tornando a via

eletroquímica de produção de hidrogênio, além de atrativa do ponto de vista ambiental, mais interessante do ponto de vista econômico. (36)

1.4.1.1 Reação de Desprendimento de Hidrogênio

A RDH consiste na redução eletroquímica do íon H^+ (em meio ácido) ou da molécula de H_2O (meio alcalino) para formar hidrogênio gasoso, que se desprende da superfície eletródica, fato que dá nome ao fenômeno. A RDH ocorre em duas etapas, e o seu mecanismo pode ser do tipo Volmer-Heyrovsky ou Volmer-Tafel. (39, 40)

A primeira etapa, denominada etapa de Volmer, que consiste na quebra heterolítica da molécula de água e na adsorção de hidrogênio atômico à superfície eletródica (H_{ads}), pode ser escrita na forma da Equação 5 em meio alcalino. (41)

$$2H_2O_{(l)} + 2e^- \rightarrow 2H_{ads} + 2OH^-_{(aq)} \quad (5)$$

Uma segunda etapa do tipo Heyrovsky ocorre, em meio alcalino, segundo a equação (37):

$$H_2O_{(l)} + H_{ads} + e^- \rightarrow H_{2(g)} + OH^-_{(aq)} \quad (6)$$

Já quando a segunda etapa é do tipo Tafel, ocorre da seguinte maneira (25-27):

$$H_{ads} + H_{ads} \rightarrow H_{2(g)} \quad (7)$$

Assim, em meio alcalino, a RDH se processa de forma que, inicialmente, uma molécula de água é reduzida eletroquimicamente para formar H_{ads} e o íon hidroxila (reação de Volmer). Em seguida, H_{ads} é reduzido eletroquimicamente, com a participação de uma molécula de água e a formação de $H_{2(g)}$ (reação de Heyrovsky) ou combina-se quimicamente com outro H_{ads} para formar hidrogênio, que abandona a superfície eletródica (dessorção química, reação de Tafel). (41)

Tanto em meio alcalino quanto em meio ácido, a segunda etapa depende da concentração de H_{ads} na superfície eletródica. Se a concentração de H_{ads} for baixa, o mecanismo favorecido é do tipo Volmer-Heyrovsky. Mas, se a concentração de H_{ads} for alta, há um

favorecimento da combinação com outro H_{ads} e, consequentemente do mecanismo Volmer-Tafel. (42)

1.4.1.2 Eletrocatalisadores

Um eletrocatalisador é um catalisador de reações eletroquímicas. Ele pode ser o próprio eletrodo (*bulk*, como um eletrodo de Pt) ou estar depositado sobre um determinado substrato (como metais e ligas eletrodepositadas). Geralmente, um eletrocatalisador atua de forma a auxiliar a transferência de elétrons entre o eletrodo e os reagentes presentes em solução e/ou a facilitar uma etapa intermediária. Como as velocidades das reações eletroquímicas dependem, além de fatores como concentração e temperatura, da estrutura da dupla camada elétrica e do campo elétrico formado na interface eletrodo/solução, esses processos podem ser controlados por meio da modificação da superfície eletródica. (43)

Neste contexto, a reação de eletrólise da água em meio alcalino merece especial atenção devido ao fato de ser um processo industrial bem estabelecido e produzir hidrogênio de alta pureza (99,9%) por meio da RDH. (44) Contudo, para que esta, em especial, tenha rendimento satisfatório do ponto de vista tecnológico, a utilização de eletrocatalisadores adequados é fundamental para diminuir o sobrepotencial de trabalho e aumentar a densidade de corrente produzida, o que leva tanto à redução do custo operacional quanto ao aumento da eficiência do processo. (45-46)

Existe uma certa variedade quanto aos métodos de síntese dos eletrocatalisadores. Entre eles, pode-se destacar a deposição química a partir de vapor (CVD, do inglês *chemical vapor deposition*), e a deposição física a partir de vapor (PVD, também derivada do nome em língua inglesa, *physical vapor deposition*). Ambas CVD e PVD são processos complexos que demandam altas temperaturas de trabalho, especialmente na deposição de metais e ligas. (47)

Um método alternativo que tem sido utilizado com sucesso para a produção de eletrocatalisadores é a eletrodeposição, que consiste na utilização de energia elétrica como força motriz para a deposição de determinada espécie, inicialmente em solução, sobre uma superfície eletródica. (36) Entre as principais vantagens deste método de síntese frente aos demais, tem-se o fato de tanto a termodinâmica quanto a cinética de crescimento dos filmes, bem como suas características físicas destes poderem ser controladas por ajustes simples na metodologia, como potencial e/ou densidade de corrente aplicada ou concentração da solução de partida; além de apresentar baixo custo e baixo impacto ambiental. (43,47-48)

1.4.1.3 Eletrocatalisadores produzidos via eletrodeposição

Nos últimos anos, os trabalhos voltados para a síntese de eletrocatalisadores via eletrodeposição têm se multiplicado na literatura, especialmente no que diz respeito àqueles projetados para atuarem nas semirreações da eletrólise da água. Entre as razões para tal busca desse tipo de material, tem-se a necessidade de aumentar a eficiência dos processos eletroquímicos de produção de $H_{2(g)}$, cujo principal é a RDH, e dos dispositivos que se utilizam de reações eletroquímicas, como as células a combustível e as baterias metal-ar, para atender à urgente demanda pela utilização em larga escala de combustíveis verdes. (6,44,47,49)

É sabido que a Pt metálica é um excelente eletrocatalisador para a RDH, contudo, a escassez deste metal e seu alto custo o tornam inviável para aplicação em larga escala. (50, 51) Por isso, é mister a busca por eletrocatalisadores de baixo custo para a RDH e, nesse âmbito, diversos materiais têm sido propostos para tal fim, como materiais compósitos e metais não-nobres e suas ligas. (41,48,52-56)

Entre os materiais compósitos, pode-se dizer genericamente que os eletrocatalisadores são formados ou por materiais carbonáceos nanoestruturados, como nanotubos, nanofolhas, grafeno; ou não, como carbetos; e um material metálico, que pode ser um óxido e/ou hidróxido, nanopartículas, ligas metálicas; ou uma liga metálica e um óxido, entre outras diversas possibilidades de combinações. (48, 57-68)

Contudo, os metais de transição não-nobres apresentam como vantagens sua distribuição eletrônica única e sua abundância na natureza, os que os torna promissores substitutos da Pt na eletrocatálise. (47, 69) Mas, frequentemente, é necessário que sejam formadas ligas metálicas para que a eficiência desses metais na eletrocatálise, especialmente da RDH, seja comparável à da Pt, devido à diferença da variação de energia livre do processo de adsorção de hidrogênio às superfícies catalíticas desses metais em relação à Pt. (57)

1.4.2 Corrosão

A definição IUPAC de corrosão é

> Uma reação interfacial irreversível de um material (metal, cerâmica, polímero) com seu ambiente, resultando no consumo do material ou na dissolução no material de um componente do ambiente. Frequentemente, mas não necessariamente, a corrosão resulta em efeitos prejudiciais ao uso do material em questão. Processos exclusivamente físicos ou mecânicos, como fusão ou evaporação, abrasão ou fratura mecânica, não estão incluídos no termo corrosão. (70)

Dentre os materiais susceptíveis à corrosão, destacam-se os materiais metálicos, que são de grande interesse para a indústria química, petroquímica, automobilística, naval, entre outras. Desse modo, o estudo da corrosão dos metais nas condições de suas aplicações, bem como de métodos para mitigar esse processo, é de suma importância. (10)

Nesse âmbito, há três fatores principais envolvidos, sendo eles economia, segurança e conservação. (10) No que se refere à economia, a *NACE (National Association of Corrosion Engineers) International* relata que o custo global da corrosão é estimado em US$ 2,5 trilhões, sem contar gastos com segurança pessoal ou com remediação de impactos ambientais causados pela corrosão. (71) No que diz respeito à conservação e à segurança, pode-se citar acidentes ocasionados pela corrosão de estruturas metálicas, como o que ocorreu em 10 de julho de 2022, em um parque de diversões em Minas Gerais, que deixou oito pessoas feridas. (72)

Há diversos métodos de proteção à corrosão dos materiais metálicos. Nesse contexto, existem métodos baseados na modificação do processo, como projeto de estrutura, condições da superfície e proteção catódica; métodos baseados na modificação do meio corrosivo, entre eles, desaeração da solução, purificação ou diminuição da umidade do ar e adição de inibidores de corrosão; métodos baseados na modificação do metal, como adição de elementos-liga e tratamento térmico; e métodos baseados em revestimentos protetores, como tratamento químico ou eletroquímico da superfície metálica; revestimentos orgânicos – tintas, resinas ou polímeros etc; revestimentos inorgânicos – esmaltes, cimentos; e revestimentos metálicos. (10)

No âmbito da síntese de revestimentos metálicos para a proteção à corrosão, assim como para outras aplicações, a eletrodeposição se destaca por ser um método simples e de baixo custo. Nesse caso, evidencia-se o fato de que é possível conseguir uma resistência à corrosão adequada, mesmo com espessuras de filmes eletrodepositados da ordem de micrômetros. (10)

Entre os metais aplicados industrialmente, destaca-se o Zn, cujo processo de galvanização é utilizado em diversos setores industriais para proteger ligas ferrosas durante o processo de corrosão. A eletrodeposição de Zn tem um custo relativamente baixo comparado a outros materiais de revestimento para a mesma finalidade; no entanto, a sua resistência à corrosão é inferior à da maioria dos depósitos protetivos, sugerindo que haja necessidade da produção de revestimentos contendo Zn e outros metais para uma elevação da resistência à corrosão do filme obtido. (73-74)

De fato, muitos trabalhos têm reportado a eletrodeposição de revestimentos de Zn e de Zn com outros metais para proteção à corrosão. (73, 75-78) Almeida e colaboradores estudaram o efeito do glicerol na resistência à corrosão e nas condições de eletrodeposição de Zn sobre

aço carbono AISI 1020, com uma densidade de corrente de 10 mA cm^{-2}. O banho eletrolítico continha $ZnCl_2$, KCl e H_3BO_3, na ausência e na presença de glicerol. O tempo de eletrodeposição foi de 17,56 minutos, resultando em um revestimento de 5 μm de espessura. Os autores reportaram que a presença de glicerol no banho diminuiu a eficiência da deposição, mas levou a um aumento da resistência à corrosão do revestimento, além de promover a formação de revestimentos mais compactos e refinados. (73)

Onkarappa e colaboradores, por outro lado, propuseram a utilização da combinação dos aditivos brometo de cetiltrimetilamônio (CTAB), ácido benzóico (BA) e 2-bromo-3-cloro-5,5-dimetilciclo-hex-2-enona (BCD) para o desenvolvimento de um eletrodepósito de Zn brilhante sobre aço carbono. A combinação desses aditivos teve um efeito sinérgico na melhoria da eficiência faradaica, bem como na capacidade de cobertura do banho otimizado. Além disso, os autores reportaram que presença dos três aditivos, CTAB, BA e BCD, no banho de revestimento levou à formação de um revestimento de Zn nanocristalino e brilhante, com orientação preferencial (100), (110), menor rugosidade superficial e propriedade anticorrosiva superior. (75)

Já Burliaev, Kozaderov e Volovithv elaboraram uma revisão acerca da cinética de eletrodeposição, da corrosão e da dissolução seletiva de revestimentos de Zn-Ni. Segundo esses autores, os revestimentos contendo 18 % de Ni na composição, eletrodepositados sobre aço carbono, apresentaram maior resistência à corrosão entre os trabalhos analisados. Eles também perceberam que a eletrodeposição de Zn-Ni apresenta mecanismo de co-deposição anômalo, em que, portanto, a redução predominante é de Zn. Além disso, observaram que a eletrodeposição de ligas de Zn-Ni pode ser realizada a partir de vários eletrólitos, tanto ácidos quanto alcalinos e que o uso de aditivos permite regular certas propriedades dos revestimentos, como composição química e/ou de fase, morfologia e características anticorrosivas. (76)

Pereira e colaboradores, por sua vez, estudaram a eletrodeposição de Zn em meio de solvente eutético ChCl:2EG na ausência e na presença de aditivos (acetamida, dimetiacetamida e dimetilsulfóxido), bem como o comportamento dos revestimentos obtidos frente à corrosão em meio de NaCl 3% aquoso. Os autores observaram alterações na morfologia dos depósitos pela presença dos aditivos. Desse modo, na ausência de aditivos, a morfologia obtida foi de lâminas dispostas perpendicularmente à superfície eletródica, enquanto na presença de acetamida observaram morfologia de couve-flor; na presença de dimetilacetamida, obtiveram lâminas menores com formato hexagonal e, na presença de dimetilsulfóxido, reportaram a formação de lâminas finas. Com relação à corrosão em meio de NaCl 3%, observaram que o

revestimento obtido na presença de dimetilsulfóxido apresentou maior resistência à corrosão dentre os avaliados. (77)

Yavuz e colaboradores, ainda, estudaram a eletrodeposição de Zn, Co e Zn-Co em meio de solvente eutético ChCl:2EG sobre substrato de Cu e avaliaram a resistência à corrosão dos revestimentos em meio de NaCl 3,5 % aquoso. Eles observaram que o revestimento Zn-Co apresentou resistência à corrosão cerca de 30 vezes a do substrato de Cu, visto que a corrente de corrosão para este foi de 40,7 μA cm^{-2} enquanto a daquele foi de 1,26 μA cm^{-2}. (78)

Diante do exposto, o objetivo deste trabalho foi o de eletrodepositar revestimentos de Zn, Co e Zn-Co em meio de ChCl:2EG, sobre substrato de Cu e de aço carbono, variando a proporção molar Zn:Co e a temperatura do experimento para avaliar a performance dos revestimentos obtidos frente à RDH em meio de KOH 1 mol L^{-1} e frente à corrosão em meio de NaCl 3,5 %.

2 MANUSCRITO 1

$Zn_xCo_{(1-x)}$ coatings from choline chloride-ethylene glycol deep eutectic solvent as electrocatalysts for hydrogen evolution reaction

Deomar N. Rodrigues-Júnior[a], Natalia G. Sousa[a], F. Murilo T. Luna[b], Thiago M.B.F. Oliveira[c], Dieric[d], Walther Schwarzacher[e], Pedro de Lima-Neto[a], Adriana N. Correia[a,*]

[a] Grupo de Eletroquímica e Corrosão, Departamento de Química Analítica e Físico-Química, Centro de Ciências, Universidade Federal do Ceará, Campus do Pici, Fortaleza, CE 60440-900, Brazil

[b] Grupo de Pesquisa em Separações por Adsorção, Departamento de Engenharia Química, Centro de Tecnologia, Universidade Federal do Ceará, Campus do Pici, Fortaleza, CE 60455-760, Brazil

[c] Laboratório de Química Aplicada, Centro de Ciência e Tecnologia, Universidade Federal do Cariri, Juazeiro do Norte - CE, 63048-080, Brazil

[d] Grupo de

[e] H. H. Wills Physics Laboratory,

University of Bristol, Tyndall Avenue, Bristol, BS8 1TL, United Kingdom

* Corresponding author: Prof. Dr. Adriana Nunes Correia
Telephone: +55 85 3366 9050
E-mail address: adriana@ufc.br

ABSTRACT

Hydrogen has emerged as a clean and renewable energy and its production by water splitting is a promising production route. However, to meet the demand on a commercial scale, research focusing on more efficient electrocatalysts is necessary. In this work, new findings on Zn, Co and Zn-Co coatings produced in deep eutectic solvent based on choline chloride (ChCl) and ethylene glycol (EG) are reported. Varying the concentrations of Zn^{2+} and Co^{2+} ions in 1ChCl:2EG, crystalline electrodeposits with fine control of composition and morphology were obtained, and which present different reactivity to electrocatalyze the hydrogen evolution reaction (HER) in alkaline medium. The performance of metallic coatings is influenced by temperature, due to changes in viscosity, ionic diffusion coefficient and charge transport in the electrolyte. The results also revealed that increasing the Co content in the coatings, changes occur in the morphological organization, stability, and electrode area, which positively influence the hydrogen production. Among the different coatings tested (Zn, Co, Zn_{96}-Co_4 and Zn_3-Co_{97}), Zn_3-Co_{97} was the most promising in terms of Tafel coefficient (108 mV dec^{-1}), exchange current density (8.57×10^{-6} A cm^{-2}) and overpotential estimated for HER (333 mV at 10 mA cm^{-2}) in 1 mol L^{-1} KOH at 298.15 K, although the other materials also showed electrochemical advantages over the unmodified Cu substrate. The reported data also reiterate the great electrochemical potential of metallic coatings for water splitting and complement the growing energy demand for hydrogen gas.

Keywords: Water splitting; Hydrogen production; Metallic coatings; Deep eutectic solvents; Electrocatalysis.

1. INTRODUCTION

The deleterious effects caused to the environment from non-renewable energy sources, such as fossil fuels, coal, and petroleum, require urgent and more sustainable alternatives to reduce greenhouse gas emissions and, consequently, the disastrous effects of global warming. (1) Today, hydrogen stands out among the most promising alternatives, since it can be produced from renewable sources and has a highly attractive energy density per mass (≈ 140 MJ kg^{-1}) and volume (≈ 0.011 MJ kg^{-1}) at room temperature, compared to more traditional fuels. (1-4) One of the great challenges is that there is not freely available and ready-to-use hydrogen, requiring appropriate methods and systems to extract it from energetically stable precursors, such as water and hydrocarbons. Water splitting is simpler and easier to accomplish, and the type of electrocatalyst employed has a significant impact on the HER yield in terms of reaction overpotential, corrosion resistance and resulting current density. (1, 2, 5-7)

It is known that noble metal (Pt, Ru and Ir)-based electrocatalysts are highly reactive toward HER, but their scarcity and high cost make them uneconomic for large-scale production and application. (8–13) Cobalt and its alloys have a better cost-benefit ratio, besides combine different electrochemical advantages (e.g., excellent electrical conductivity, high activity, and stability in alkaline medium) that arouse speculation regarding their efficiency in producing hydrogen by water splitting. (14-17) Such performance is linked to several parameters of synthesis and application of these materials, which must be meticulously studied and continuously improved. Fan et al. (18) studied cobalt-coated copper substrates as HER electrocatalysts in 30 wt% KOH. These authors identified remarkable changes in the structural arrangement, morphology, and reactivity of the electrodeposits according to the electrolytic medium, presence of oxygen and temperature of synthesis, so that the lowest overpotential and highest surface roughness factor for HER was obtained from an acetate-enriched solution, kept

at 25 ºC. Maurya et al. (19) also showed reactivity changes when HER was promoted in 1 mol L^{-1} KOH, using Ni-Co coatings immobilized onto copper and steel derived substrates as electroactive surfaces, suggesting a synergistic effect of intercalated materials in the electrode configuration. Kublanovsky and Yapontseva (20) found that electrodeposited Co-Mo alloys can have better electrocatalytic properties in alkaline medium (reduction in HER overpotential around 400 mV) than pure Co, especially when obtained from 10:1% (v/v) Co:Mo compositions. Ling et al. (21) also reported that doping CoO nanorods with Ni and Zn has an important electrocatalytic effect for HER in alkaline medium, Zn being responsible for modulating bulk electronic structure and boost electrical conduction. Other Zn-containing materials have been successfully applied as electrocatalysts for water splitting. Sumesh (22) prepared zinc oxide functionalized molybdenum disulfide heterostructures ($MoS_2 \cdot ZnO$) and tested them for HER electrocatalysis in acidic medium, without compromising their structural stability. Additionally, Cao et al. (23) worked with metal-dopped carbon nanotubes and found that Zn both reduced charge-transfer resistance and increased the proportion of reactive sites available to produce hydrogen.

Since Co and Zn have a positive effect on water splitting, coatings made with combinations of them can achieve superior performance and deserve more attention. Electrodeposition is a simple and low-cost way to produce Zn-Co electrocatalysts for HER, either by potentiostatic or galvanostatic mode. (24) However, the electrosynthesis of metallic coatings from aqueous solutions can compromise their stability due to the existence of parallel reduction reactions, including HER itself. There are also limitations regarding cathodic efficiency, working potential range, and electrodeposit adhesion. Water volatility also narrows the working temperature range, leading to frequent need for electrolyte bath additives and increased laboratory waste. (25, 26)

Deep eutectic solvents (DES) overcome the limitations and provide a wide range of working potential for electrodepositing various metals and alloys. They are non-ideal liquid mixtures of organic salts with hydrogen bond donors, such as amides, amines, alcohols and carboxylic acids. DES still have high electrical conductivity and solubility for metallic salts, are non-flammable even at relatively high temperatures, biodegradable, produced simply and cheaply. (25, 27-29) In the electrodeposition of metals and alloys, DES formed by choline chloride (ChCl) and ethylene glycol (EG) have been used with great success. (30-33) From this perspective, the main objective of this work was to produce coatings of Zn, Co, and Zn-Co from ChCl/EG-based DES, as well as to evaluate the physicochemical properties and effectiveness of these electrodeposits to promote HER in alkaline environment.

2. EXPERIMENTAL PROCEDURES

2.1 Chemicals and electrolytic solutions

ChCl, EG, zinc chloride ($ZnCl_2$) and cobalt chloride ($CoCl_2$) were purchased from Sigma-Aldrich and used as received. ChCl and EG were mixed in a 1:2 molar ration (1ChCl:2EG) and heated to 353 K until a colorless and homogeneous liquid was formed. (15) The electrodeposition solutions were obtained by dissolving $ZnCl_2$ (0.025 mol L^{-1} or 0.4 mol L^{-1} Zn^{2+}) and $CoCl_2$ (0.025 mol L^{-1} or 0.4 mol L^{-1} Co^{2+}) in 1ChCl:2EG, under constant agitation. Since the electric conductivity of the electrolytes strongly depends on the water content, this parameter was determined by Karl Fischer coulometric titration (899 coulometer, Metrohm) in freshly prepared DES mixtures. The water content in 1ChCl:2EG was 13.25 ± 0.06 ppm and ranged from 23.32 ± 0.13 to 57.87 ± 0.31 ppm after adding Zn^{2+} and Co^{2+}.

2.2 Electrochemical experiments

Electrochemical experiments were carried out using a glass electrochemical cell configured with three electrodes. The working electrode was a copper disc embedded in epoxy resin, with an exposed geometric area of approximately 0.023 cm^2. Before each experiment, the working electrode was mechanically polished with 100, 400 and 600-grain size sandpaper, following this sequence, and washed with Milli-Q® water (18.2 MΩ cm). A platinum plate (1 cm^2 geometric area; 99.5 % purity) and a silver wire covered with AgCl and immersed in 1ChCl:2EG, were used as auxiliary and reference electrodes, respectively. The tests were carried out in a potentiostat/galvanostat AUTOLAB PGSTAT30, Metrohm-Eco Chemie, controlled by NOVA 2.1 software.

Electrodeposition processes of metallic coatings were monitored by cyclic voltammetry (CV) at 5 mV s^{-1}, keeping the system at 343 K. The ion diffusion coefficients in the deep eutectic solvent were evaluated at different temperatures (303 − 343 K), using chronoamperometry data adapted to the Cottrell Equation. For these experiments, three electrochemical potentials (i.e., −0.4, −0.8 and −1.3 V) were evaluated for 60 s, chosen from cyclic voltammetry data registered with a Cu substrate (0.023 cm^2 geometric area) immersed in 1ChCl:2EG containing 0.4 mol L^{-1} $CoCl_2$ and 0.4 mol L^{-1} $ZnCl_2$.

The influence of metallic coatings and selected experimental conditions on HER were studied by linear sweep voltammetry (LSV) at 0.5 mV s^{-1}, using 1 mol L^{-1} KOH at 298 K as electrolyte and $Hg_{(s)}|HgO_{(s)}|OH^-_{(aq)}$ (1 mol L^{-1} KOH) as reference electrode (30). The measured potentials ($E_{Hg/HgO}$) were converted to those of the reversible hydrogen electrode (E_{RHE}), through the following equation:

$$E_{RHE}\ (\mathrm{V}) = E_{Hg/HgO}\ (\mathrm{V}) + 0.095 + 0.059pH \quad (1)$$

Coating stability tests were performed over 100 h in a two-electrode cell, applying an average operating potential of –1.8 V at 10 mA cm^{-2}, being repeated three times. Coatings

with a nominal thickness around 1.0 μm were immobilized on copper substrates (0.20 cm^2 geometric area), and the results were compared to those obtained with the same electrode without coating and with an AISI 304 stainless steel electrode (0.18 cm^2 geometric area). The electrical circuit was concluded with a stainless steel AISI 304 counter-electrode (0.69 cm^2 geometric area), immersed together with the working electrode in 1 mol L^{-1} KOH at 333 K. The current density was set at 10 mA cm^{-2}, taking into account the high HER yield and stability of the coatings, using a direct current power source monitored by a multimeter at fixed time intervals. Specific mass and viscosity measurements were performed with an Anton Paar's Stabinger viscometer, model SVM 3000.

2.3 Electrodeposition of metallic coatings

Zn and Co electrodeposits were obtained from 1ChCl:2EG electrolytes containing 0.4 mol L^{-1} Zn^{2+} and 0.4 mol L^{-1} Co^{2+}, without mechanical convection influence. Zn_x-$Co_{(1-x)}$ coatings were obtained from solutions with different Zn^{2+}:Co^{2+} molar ratios, i.e., (Zn^{2+}) = 0.4 mol L^{-1} and (Co^{2+}) = 0.025 mol L^{-1} or (Zn^{2+}) = 0.025 mol L^{-1} and (Co^{2+}) = 0.4 mol L^{-1}. Electrodeposits were obtained potentiostatically at −1.3 V and 343 K, with charge control to obtain coatings with a nominal thickness of 1 μm.

2.4 Complementary physicochemical characterizations

The surface morphology of the coatings was evaluated using a field emission scanning electron microscope (SEM; FEG-SEM FEI-Quanta 450), operating at 20 keV. The atomic percentages of Zn and Co in the coatings were determined by energy-dispersive X-ray spectroscopy (EDS), using a spectrometer coupled to the microscope. The crystallinity and composition of electrodeposits were also evaluated by X-ray diffraction (XRD) analyses, using a Rigaku DMAXB diffractometer, which operated with a 2kW X-ray generator and CuKα

copper radiation (λ = 0.154 nm). Crystalline phases were identified using the X-Pert HighScore Plus version 3.0.5 (PANalytical®) program, associating the results with the International Centre for Diffraction Data (ICDD)/Joint Committee on Powder Diffraction Standards (JCPDS) database.

3. RESULTS AND DISCUSSION

3.1 Electrochemical characterization

Initially, CV studies were performed with cooper substrates at 5 mV s^{-1} in pure ChCl/EG-based DES and after adding Zn^{2+} and Co^{2+}, to monitor and evaluate the efficiency of the electrodeposition conditions employed. The result illustrated in Fig. 1a demonstrated that no process was observed in 1ChCl:2EG, varying the potential between −0.4 V and −1.3V. Above this range, there was a sharp increase in the current density, due to the decomposition of the eutectic solvent caused by the reduction of hydroxyl groups present in ethylene glycol and choline ions. (32) In Fig. 1b, during the positive scan, three well-defined anodic processes with different intensities appeared between −1.1 and −0.6 V, related to the dissolution of zinc electrodeposits and possible Zn-Cu intermetallic entities. A similar profile was observed by Alesary et al. (34), using a Pt electrode polarized anodically in 1ChCl:2EG containing 0.4 mol L^{-1} Zn^{2+}, keeping the system at 353 K. There is also a crossover of cathodic and anodic currents around −1.1 V, which indicates self-organization of crystals by nucleation and electrodeposit growth.

FIGURE 1

In Fig. 1c, there is a small increase in cathodic current attributed to cobalt reduction around −0.9 V. Then, a significant increase in the cathodic current at −1.2 V begins, followed by a discrete current loop, resulting from the nucleation of zinc on cobalt. In the anodic scan, there are three well-defined processes related to the dissolution of metals, so that the first two

refer to zinc and the last to cobalt. Chu et al. (35) obtained analogous results for Zn-Co coatings, produced from 1ChCl:2U at 353 K, using cyclic voltammetry at 50 mV s^{-1}. They attributed the first two anodic processes (at less positive potentials) to zinc dissolution from different phases of the Zn-Co alloy, followed by dissolution of the cobalt electrodeposits as a third process. In Fig. 1d, there is only one process in the cathodic scan before solvent decomposition. This process results from the reduction of cobalt, as its concentration is 16 times higher than zinc. No process is observed in the anodic scan between −0.4 V and −1.3 V. The observed result is also very similar to that shown in Fig. 1e, whose voltammogram was recorded in the electrochemical cell containing only cobalt.

3.2 Relationship between coating stability, ionic diffusion, and temperature

Chronoamperometry experiments are very useful to examine the electrochemical activity and stability of metallic coatings, especially under temperature gradients. In this work, studying HER at –1.3 V in 1 mol L^{-1} KOH (previously optimized condition based on reaction yield and corrosion resistance), an increase in mass-transport-limited current densities was noticed as the temperature increased from 303 K to 343 K, both for Zn and Co-based coatings. This is related to the decrease in the viscosity of the solutions at higher temperatures, which allows faster ion diffusion and a consequent increase in current density. Issues related to mass- and charge-transport variations resulting from temperature changes and their influence on viscosity have also been reported by Fu et al. (36), based on studies on the electrochemical nucleation of copper in ChCl:EG. From the Cottrell Equation, (37) it is also possible to verify the impact of the temperature increase on the ionic diffusion coefficient (D), as shown in Table 1. For cobalt coatings, D values varied between $2.6\times10^{-7} \pm 0.7\times10^{-8}$ cm² s^{-1} and $4.4\times10^{-7} \pm 0.5\times10^{-7}$ cm² s^{-1}, while for zinc coatings the variation was from $8.9\times10^{-11} \pm 0.8\times10^{-11}$ cm² s^{-1}

to $4.5\times10^{-10} \pm 0.3\times10^{-10}$ cm² s^{-1}. The same trend was observed by Phuong et al. (38) for the nucleation of Co^{2+} ions in 1ChCl:2U, as the temperature increased from 313 K to 343 K.

TABLE 1

For comparison purposes, Table 1 also gathers other *D* values obtained for Co- and Zn-based coatings obtained in different solvents and temperatures. (38-44) For both cases, the values were equivalent to those obtained by other authors who studied coatings produced from the same deep eutectic solvent (7.1×10^{-10} cm² s^{-1} at 313 K for Zn^{2+} (43)) or from other compositions, such as ChCl:urea (8.1×10^{-8} – 1.1×10^{-7} cm² s^{-1} at 313 – 343 K for Co^{2+} (38); 7.8×10^{-9} cm² s^{-1} at 363 K for Zn^{2+} (41)), EG (2.3×10^{-8} cm² s^{-1} at 343 K for Co^{2+} (39)), 1-methylimidazolium trifluoromethylsulfonate (7.7×10^{-9} cm² s^{-1} at 373 K for Zn^{2+} (40)), urea:1-ethyl-3-methylimidazolium (5.5×10^{-9} cm² s^{-1} at 353 K for Zn^{2+} (42)), and hybrid eutectic sulfolane:water (5.0×10^{-12} cm² s^{-1} for Zn^{2+} (44)). However, *D* values for Co^{2+} ions in 1ChCl:2EG were higher than those for Zn^{2+} ions recorded under the same experimental conditions. This is due to the formation of a smaller solvation sphere for Co^{2+} ions, giving them greater mobility than Zn^{2+} ions. (31, 45) Regardless of the precursor, all coatings remained electrochemically stable at the different HER potentials evaluated, i.e., −0.4, −0.8 and −1.3 V.

3.3 Composition and morphology studies

Fig. 2 presents the percentage elemental composition of electrodeposits obtained by EDS, as well as surface morphological features observed by SEM micrographs, before and after immobilizing the coatings. According to Fig. 2a, the proportion of Zn and Co atoms present in the electrodeposits is very close to their molar concentration contained in the electrolytes: 94% Zn and 6% Co from 0.4 mol L^{-1} $ZnCl_2$ + 0.025 mol L^{-1} $CoCl_2$; and 97% Co and 3% Zn from 0.025 mol L^{-1} $ZnCl_2$ + 0.4 mol L^{-1} $CoCl_2$. This shows that the use of 1ChCl:2EG allows excellent control of the desired chemical composition for Zn-Co deposits.

FIGURE 2

As for morphology, Fig. 2b illustrates the copper substrate surface after mechanical grinding and polishing processes, where only the inherent grooves of metal erosion are observed. The results also indicated that all electrodeposits ensured a complete surface coating, proving the efficiency of the electrochemical conditions employed. For Zn coating (Fig. 2c), individual crystallites are seen, while the Co coating (Fig. 2d) exhibits dendritic shapes. The same characteristics are seen when any one of these cations is present as a major part of the electrolyte. Regardless of the proportion tested for each cation, observing at a higher magnification, the Zn-Co coatings (Fig. 2e and 2f) showed cracked morphological patterns, which have a high surface area and are considered excellent catalysts for electrochemical reactions. Table 2 shows the concentration of precursors tested in each electrolytic bath, in addition to the percentage of Zn, Co and Zn-Co measured by EDS in each coating.

TABLE 2

XRD analyses were conducted to evaluate the crystalline structure of Zn, Co, and Zn-Co films. Fig. 3 shows the diffraction patterns before and after modification of copper substrates in deep eutectic solvent. According to ICDD/JCPDS database, the XRD data obtained indicate characteristic peaks associated with Cu with a face-centered cubic structure (card 85-1326), hexagonal metallic forms of Zn (card 03-065-5973), Co (card 15-0806), $Zn_{96}Co_4$ and Zn_3Co_{97} alloys (card 23-1390), besides rhombohedral $Co_2(OH)_3Cl$ (space group R-3m #166). The presence of the coatings also denotes high quality of the modifications carried out on the electrode substrate. On the other hand, the presence of $Co_2(OH)_3Cl$ shows that when Co^{2+} is electroimmobilized individually, parallel equilibria can be formed, leading to the formation of soluble salts and loss of coating stability. Although the same trend has not been registered for Zn^{2+}, Zn-Co coatings tend to be more stable and suitable as electrocatalysts, as

will be demonstrated later. No peaks resulting from impurities were detected, reaffirming the success in the electrosynthesis of the different metallic materials.

FIGURE 3

3.4 HER electrocatalysis

The overall performance of metallic substrates and coatings towards HER electrocatalysis is summarized in Fig. 4. The steady state curves obtained by LSV at 5 mV s^{-1} (Fig. 4a), using 1 mol L^{-1} KOH at 333 K as electrolyte, indicate the following onset potential order: Zn_3Co_{97} < $Zn_{96}Co_4$ < Co < Zn < Cu. This result proves that Zn-Co alloys are more promising as HER electrocatalysts, in addition to providing higher hydrogen production yields at lower potentials. (46) Even so, it is important to point out that all tested coatings performed better than the unmodified copper substrate, used as one of the standard electrode materials in studies with hydrogen production by water splitting.

FIGURE 4

Under alkaline conditions, the Tafel diagrams (Fig. 4b) are concentrated in a narrow overpotential range (≈ 150–320 mV dec^{-1}), suggesting that the HER mechanism for all the films is not affected by their thickness. (47) However, observing the Tafel fits, there are changes in slope values and, consequently, greater reaction rate on the Zn_3-Co_{97} coating (kinetic constant = 108.2 ± 0.74 mv dec^{-1}). About the surface stability, evaluated by potential variations at a current density of 10 mA cm^{-2} applied for 100 h of electrolysis (Fig. 4c), the greatest stability trend is seen for coatings that work at lower overpotentials (Co- and Zn_3Co_{97}-based coatings), possibly because they are less exposed to corrosion conditions and/or surface fouling by reaction by-products, which lead to variations in ohmic resistance. The electrochemical behaviour demonstrated by the Cu substrate, Cu/Zn and Cu/$Zn_{96}Co_4$ is like that registered for AISI 304 stainless steel (overpotential variation from 100 mV to 300 mV during electrolysis), requiring higher potentials to promote HER and showing that the presence

of cobalt contributes positively to catalyze this electrochemical reaction, including as an additive in metallic alloys. Zn_3Co_{97} coatings had the lowest overpotential variation among all the analyzed materials.

Values of electrochemical active surface area (ECSA) for catalysts were estimated from them electric double layer capacitance (C_{dl}). Cyclic voltammetric profiles of Zn, $Zn_{96}Co_4$, Zn_3Co_{97} and Co electrodes were recorded in a non-Faradic region (±0.05V vs. reversible hydrogen electrode (RHE) in relation on E_{OCP} (t = 180 s)) at different scan rates (2.5, 5, 10 and 15 mV s^{-1}) in 1 mol L^{-1} KOH (Figures S1 and S2 in the Supplementary Material). For comparison purposes, Table 3 presents Tafel coefficients (–*b*), exchange current densities (i_0) and estimated overpotentials (|η|) for HER on each catalyst, obtained from fitting LSV data at 5 mV s^{-1} and using 1 mol L^{-1} KOH at 298.15 K. Now the values were normalized by geometric area and ECSA, as can be seen in Figure S2 and Table S1 (in the Supplementary Material). These results corroborate the SEM images obtained in Figure 3: the coating with the highest electroactive area ($Zn_{96}Co_4$) showed higher roughness, accompanied by Zn_3Co_{97}, which showed cracks.

TABLE 3

As already stated earlier, the Cu substrate requires a highest |η| value (546 mV) to achieve a current density of 10 mA cm^{-2} during HER, followed by Zn (509 mV), Co (372 mV), $Zn_{96}Co_4$ (355 mV) and Zn_3Co_{97} (333 mV), reiterating the better electrocatalytic effect of the latter. (48) This sequence does not change even working at 10 times higher current densities. In addition, according to Banoth, Kandula and Kollu, it is desirable that an electrocatalytic material presents low values of Tafel slope accompanied by high values of exchange current. (49) When this occurs, high operating current densities can be achieved without a significant increase in overvoltage, which leads to lower operating costs. (49) Thus, the –*b* and i_0 values

presented by the Zn_3Co_{97} and Co coatings are also indicative of their higher electrocatalytic activity compared to the others.

For Zn_3Co_{97}, comparing the Tafel parameters obtained in this study with previously published ones (Table 3), the values of $-b$ and $|\eta|$ were higher than those reported with Zn-Co-S, CoZn, NiCoZn e $Zn_{85}Ni$ coatings, but i_0 values were lower. (46, 48, 50-52) Since water molecules are precursors of HER by electrolysis, variations in the Tafel parameters may be due to uncompensated ohmic drop, so that small stoichiometric changes are sufficient to cause significant influences on the electrochemical reaction. Therefore, even more satisfactory results than those obtained in this work can be achieved from more detailed studies about the reaction mechanism and surface reactivity of the coatings.

4. CONCLUSIONS

Zn, Co, and Zn-Co alloys, produced electrochemically from 1ChCl:2EG DES, are functional materials to produce hydrogen in an alkaline medium, achieving remarkable electrocatalytic effect. The potentiostatic electrodeposition of these coatings allows a good stoichiometric control of the metallic constituents, and these materials achieved a better performance at higher temperatures, due to the reduction in electrolyte viscosity, charge-transfer resistance and increase in the diffusion coefficient of the precursor cations. Increasing Co content in coatings leads to morphological organization changes, resulting in cracked surfaces that have high surface area and directly contribute to HER electrocatalysis. Among the coatings studied, Zn_3Co_{97} was the one that showed the best performance in terms of $-b$, i_0 and $|\eta|$, therefore it is the most promising to produce hydrogen by water splitting.

Acknowledgments

This study was financed in part by the Coordenação de Aperfeiçoamento de Pessoal de Nível Superior - Brasil (CAPES) – Finance Code 001. The authors thank the financial support given by the following Brazilian funding agencies: Coordenação de Aperfeiçoamento de Pessoal de Nível Superior (CAPES), Conselho Nacional de Desenvolvimento Científico e Tecnológico (CNPq) and Fundação Cearense de Apoio ao Desenvolvimento Científico e Tecnológica (FUNCAP). A.N. Correia gratefully acknowledges funding provided by CNPq (proc. 405596/2018-9 and 305136/2018-6). P. de Lima-Neto thanks the financial support received from CNPq (proc. 408626/2018-6 and 304152/2018-8). N. G. Sousa thanks CNPq for her grant (proc. 141171/2021-9). The authors would like to thank the Central Analítica-UFC/CT-INFRA/MCTI-SISANO/Pró-Equipamentos CAPES for the support.

REFERENCES

(1) R. Shilpa, K. S. Sibi, S. R. Sarath Kumar, R. K. Pai, and R.B. Rakhi, Electrocatalysts for hydrogen evolution reaction, in: *Mater. Hydrog. Prod. Conversion, Storage*, Wiley, 2023: p. 115-146. https://doi.org/10.1002/9781119829584.ch5.

(2) C. Pi, Z. Zhao, X. Zhang, B. Gao, Y. Zheng, P. K. Chu, L. Yang, and K. Huo, In situ construction of γ-MoC/VN heterostructured electrocatalysts with strong electron coupling for highly efficient hydrogen evolution reaction, *Chem. Eng. J.*, vol. 416, p. 129130, 2021, https://doi.org/10.1016/j.cej.2021.129130.

(3) C. Feng, B. Xin, H. Li, Z. Jia, X. Zhang, and B. Geng, Agaric-like cobalt diselenide supported by carbon nanofiber as an efficient catalyst for hydrogen evolution reaction, *J. Colloid Interface Sci.*, vol. 610, p. 854-862, 2022, https://doi.org/10.1016/j.jcis.2021.11.130.

(4) X. Wang, R. Su, H. Aslan, J. Kibsgaard, S. Wendt, L. Meng, M. Dong, Y. Huang, and F. Besenbacher, Tweaking the composition of NiMoZn alloy electrocatalyst for enhanced

hydrogen evolution reaction performance, *Nano Energy*, vol. 12, p. 9-18, 2015, https://doi.org/10.1016/j.nanoen.2014.12.007.

(5) Z. Xu, Q. Zhu, X. Xi, M. Xing, J. Zhang, Z-scheme CdS/WO_3 on a carbon cloth enabling effective hydrogen evolution, *Front. Energy*, vol. 15, p. 678-686, 2021, https://doi.org/10.1007/s11708-021-0768-6.

(6) L. Chang, Z. Sun, Y. H. Hu, 1T phase transition metal dichalcogenides for hydrogen evolution reaction, *Electrochem. Energy Rev.*, v. 4, p. 194-218, 2021, https://doi.org/10.1007/s41918-020-00087-y.

(7) H. Wu, C. Feng, L. Zhang, J. Zhang, D. P. Wilkinson, Non-noble metal electrocatalysts for the hydrogen evolution reaction in water electrolysis, *Electrochem. Energy Rev.*, v. 4, p. 473-507, 2021, https://doi.org/10.1007/s41918-020-00086-z.

(8) M. Plevová, J. Hnát, and K. Bouzek, Electrocatalysts for the oxygen evolution reaction in alkaline and neutral media. A comparative review, *J. Power Sources*, vol. 507 p. 230072, 2021, https://doi.org/10.1016/j.jpowsour.2021.230072.

(9) T. Lim and S.-K. Kim, Non-precious hydrogen evolution reaction catalysts: Stepping forward to practical polymer electrolyte membrane-based zero-gap water electrolyzers, *Chem. Eng. J.*, vol. 433, p. 133681, 2022, https://doi.org/10.1016/j.cej.2021.133681.

(10) M. Nemiwal, T. C. Zhang, and D. Kumar, Graphene-based electrocatalysts: Hydrogen evolution reactions and overall water splitting, *Int. J. Hydrog. Energy*, vol. 46, p. 21401-21418, 2021, https://doi.org/10.1016/j.ijhydene.2021.04.008.

(11) V. D. Nithya, Recent advances in CoSe2 electrocatalysts for hydrogen evolution reaction, *Int. J. Hydrog. Energy*, vol. 46, p. 36080-36102, 2021, https://doi.org/10.1016/j.ijhydene.2021.08.157.

(12) S. Zhang, X. Zhang, Y. Rui, R. Wang, and X. Li, Recent advances in non-precious metal electrocatalysts for pH-universal hydrogen evolution reaction, *Green Energy Environ.*, vol. 6,

p. 458-478, 2021, https://doi.org/10.1016/j.gee.2020.10.013.

(13) A. Ali, F. Long, P. K. Shen, Innovative strategies for overall water splitting using nanostructured transition metal electrocatalysts, *Electrochem. Energy Rev.*, v. 5, p. 1, 2022, https://doi.org/10.1007/s41918-022-00136-8.

(14) R. Zahra, E. Pervaiz, M. Yang, O. Rabi, Z. Saleem, M. Ali, and S. Farrukh, A review on nickel cobalt sulphide and their hybrids: Earth abundant, pH stable electro-catalyst for hydrogen evolution reaction, *Int. J. Hydrogen Energy*, vol. 45, p. 24518-24543, 2020, https://doi.org/10.1016/j.ijhydene.2020.06.236.

(15) M. Ďurovič, J. Hnát, and K. Bouzek, Electrocatalysts for the hydrogen evolution reaction in alkaline and neutral media. A comparative review, *J. Power Sources*, vol. 493, p. 229708, 2021, https://doi.org/10.1016/j.jpowsour.2021.229708.

(16) G. Gao, W. Wang, Y. Wang, Z. Fu, L. Liu, Y. Du, Z. Li, Y. Liu, L. Wang, Synergistic coupling of NiCoS nanorods with NiCo-LDH nanosheets towards highly efficient hydrogen evolution reaction in alkaline media, *J. Electroanal. Chem,* vol. 943, p. 117622, 2023, https://doi.org/10.1016/j.jelechem.2023.117622.

(17) Z. Zhai, H. Li, C. Zhou, H. Zheng, Y. Liu, W. Yan, J. Zhang, Anisotropic Strain Boosted Hydrogen Evolution Reaction Activity of F-NiCoMo LDH for Overall Water Splitting, *J. Electrochem. Soc.* v. 170, p. 036509, 2023, https://doi.org/10.1149/1945-7111/acc555.

(18) C. L. Fan, D. L. Piron, H. J. Miao, and M. Rojas, Hydrogen evolution in alkaline water on cobalt electrodeposits prepared from baths containing different anions, *J. Appl. Electrochem.*, vol. 23, p. 985-990, 1993, https://doi.org/10.1007/BF00266119.

(19) A. Maurya, S. Suman, A. Bhardwaj, L. Mohapatra, and A. K. Kushwaha, Substrate dependent electrodeposition of Ni–Co alloy for efficient hydrogen evolution reaction, *Electrocatalysis*, vol. 14, p. 68-77, 2023, https://doi.org/10.1007/s12678-022-00773-z.

(20) V. S Kublanovsky and Y. S. Yapontseva, Electrocatalytic properties of Co-Mo alloys

electrodeposited from a citrate-pyrophosphate electrolyte, *Electrocatalysis*, vol. 5, p. 372-378, 2014, https://doi.org/10.1007/s12678-014-0197-y.

(21) T. Ling, T. Zhang, B. Ge, L. Han, L. Zheng, F. Lin, Z. Xu, W.-B. Hu, X.-W. Du, K. Davey, and S.-Z. Qiao, Well-dispersed nickel- and zinc-tailored electronic structure of a transition metal oxide for highly active alkaline hydrogen evolution reaction, *Adv. Mater.*, vol. 31, p.1807771, 2019, https://doi.org/10.1002/adma.201807771.

(22) C. K. Sumesh, Zinc oxide functionalized molybdenum disulfide heterostructures as efficient electrocatalysts for hydrogen evolution reaction, *Int. J. Hydrog. Energy*, vol. 45, p. 619-628, 2020, https://doi.org/10.1016/j.ijhydene.2019.10.235.

(23) Q. Cao, Z. Cheng, J. Dai, T. Sun, G. Li, L. Zhao, J. Yu, W. Zhou and J. Lin, Enhanced hydrogen evolution reaction over co nanoparticles embedded n-doped carbon nanotubes electrocatalyst with Zn as an accelerant, *Small*, vol. 18, p. 2204827, 2022, https://doi.org/10.1002/smll.202204827.

(24) S. S. V. Tatiparti and F. Ebrhimi, Potentiostatic versus galvanostatic electrodeposition of nanocrystalline Al–Mg alloy powders, *J. Solid State Electrochem.*, vol. 16, p. 1255-1261, 2012, https://doi.org/10.1007/s10008-011-1522-5.

(25) F. Endres, D. MacFarlane, and A. Abbott, Electrodeposition from ionic liquids, *Electrodeposition from Ionic Liquids*. p. 1-387, 2008, https://doi.org/10.1002/9783527622917.

(26) K. Li, T. Ren, Z. Y. Yuan and T. J. Bandosz, Electrodeposited P-Co nanoparticles in deep eutectic solvents and their performance in water splitting, *Int. J. Hydrog. Energy*, vol. 43, p. 10448-10457, 2018, https://doi.org/10.1016/j.ijhydene.2018.04.136.

(27) C. Lei, H. F. Alesary, F. Khan, A. P. Abbott, and K. S. Ryder, Gamma-phase Zn-Ni alloy deposition by pulse-electroplating from a modified deep eutectic solution, *Surf. Coat. Technol.*, vol. 403, p. 126434, 2020, https://doi.org/10.1016/j.surfcoat.2020.126434.

(28) A. P. Abbott, D. Boothby, G. Capper, D. L. Davies, and R. K. Rasheed, Deep eutectic

solvents formed between choline chloride and carboxylic acids: versatile alternatives to ionic liquids, *J. Am. Chem. Soc.*, vol. 126, p. 9142-9147, 2004, https://doi.org/10.1021/ja048266j.

(29) A. Srivastava, P. Sahu, M. S. Murali, Sk. M. Ali, M. Sahu, J. S. Pillai, and N. Rawat, New deep eutectic solvents based on imidazolium cation: Probing redox speciation of uranium oxides by electrochemical and theoretical simulations, *J. Electroanal. Chem.* vol. 901, p. 115752, 2021.

(30) A. S. C. Urcezino, L. P. M. Dos Santos, P. N. S. Casciano, A. N. Correia, and P. De Lima-Neto, Electrodeposition study of Ni coatings on copper from choline chloride-based deep eutectic solvents, *J. Braz. Chem. Soc.*, vol. 28, p. 1193-1203, 2017, https://doi.org/10.21577/0103-5053.20160278.

(31) J. C. Pereira, L. P. M. Santos, A. A. C. Alcanfor, H. B. de Sant'Ana, F. X. Feitosa, O. S. Campos, A. N. Correia, Paulo N.S. Casciano, and P. de Lima-Neto, Effects of electrodeposition parameters on corrosion resistance of ZnSn coatings on carbon steel obtained from eutectic mixture based on choline chloride and ethylene glycol, *J. Alloys Compd.*, vol. 886, p. 161159, 2021, https://doi.org/10.1016/j.jallcom.2021.161159.

(32) J. C. Pereira, L. P. M. Santos, A. A. C. Alcanfor, O. S. Campos, P. N. S. Casciano, A. N. Correia, and P. de Lima-Neto, Electrochemical corrosion evaluation of new Zn-Sn-In coatings electrodeposited in a eutectic mixture containing choline chloride and ethylene glycol, *Electrochim. Acta*, vol. 407, p. 139647, 2022, https://doi.org/10.1016/j.electacta.2021.139647.

(33) L. P. M. Santos, R. M. Freire, S. Michea, J. C. Denardin, D. B. Araújo, E. B. Barros, A. N. Correia, and Pedro de Lima-Neto, Electrodeposition of 1-D tellurium nanostructure on gold surface from choline chloride-urea and choline chloride-ethylene glycol mixtures, *J. Mol. Liq.*, vol. 288, p. 111038, 2019, https://doi.org/10.1016/j.molliq.2019.111038.

(34) H. F. Alesary, S. Cihangir, A. D. Ballantyne, R. C. Harris, D. P. Weston, A. P. Abbott, and K. S. Ryder, Influence of additives on the electrodeposition of zinc from a deep eutectic

solvent, *Electrochim. Acta*, vol. 304, p. 118-130, 2019, https://doi.org/10.1016/j.electacta.2019.02.090.

(35) Q. Chu, J. Liang, and J. Hao, Electrodeposition of zinc-cobalt alloys from choline chloride–urea ionic liquid, *Electrochim. Acta*, vol. 115, p. 499-503, 2014, https://doi.org/10.1016/j.electacta.2013.10.204.

(36) X. Fu, C. Zhan, R. Zhang, B. Wang, H. Sun and J. Sun, Effect of temperature on mechanism and kinetics of electrochemical nucleation of copper in ChCl-based deep eutectic solvents, *J. Solid State Electrochem.*, vol. 26, p. 2713-2722, 2022, https://doi.org/10.1007/s10008-022-05282-z.

(37) M. V. Tesakova, S. M. Kuzmin, and V. I. Parfenyuk, Electrodeposition of films of individual 5,10,15,20-tetrakis(3-aminophenyl)porphyrin metal complexes and their composite for electrocatalytic oxygen reduction, *Inorg. Chem. Commun.*, vol. 135, p. 109106, 2022, https://doi.org/10.1016/j.inoche.2021.109106.

(38) T. D. V. Phuong, L. M. Quynh, N. N. Viet, L. V. Thong, N. T. Son, V.-H. Pham, P. D. Tam, V. H. Nguyen, and T. L. Manh, Effect of temperature on the mechanisms and kinetics of cobalt electronucleation and growth onto glassy carbon electrode using reline deep eutectic solvent, *J. Electroanal. Chem.*, vol. 880, p. 114823, 2021, https://doi.org/10.1016/j.jelechem.2020.114823.

(39) G. Panzeri, A. Accogli, E. Gibertini, S. Varotto, C. Rinaldi, L. Nobili, L. Magagnin, Electrodeposition of cobalt thin films and nanowires from ethylene glycol-based solution, *Electrochem. Commun.*, vol. 103, p. 31-36, 2019, https://doi.org/10.1016/j.elecom.2019.04.012.

(40) M. Li and Y. Li, Electrodeposition of zinc from zinc oxide and zinc chloride in 1-methylimidazolium trifluoromethylsulfonate ionic liquid, *Prot. Met. Phys. Chem. Surfaces*, vol. 56, p. 180-188, 2020, https://doi.org/10.1134/S2070205120010141.

(41) H. Yang and R. G. Reddy, Electrochemical kinetics of reduction of zinc oxide to zinc using 2:1 urea/ChCl ionic liquid, *Electrochim. Acta*, vol. 178, p. 617-623, 2015, https://doi.org/10.1016/j.electacta.2015.08.050.

(42) W. He, L. Shen, Z. Shi, B. Gao, X. Hu, J. Xu, and Z. Wang, Zinc electrodeposition from zinc oxide in the urea/1-ethyl-3-methylimidazolium chloride at 353 K, *Electrochemistry*, vol. 84, p. 872-877, 2016, https://doi.org/10.5796/electrochemistry.84.872.

(43) K. Wang, J. Phelps, R. Abdolvand, J. Carter, and H. A. Hamedani, Zinc nanoparticles electrodeposited on TiO2 nanotube arrays using deep eutectic solvents for implantable electrochemical sensors. *ACS Appl. Nano Mater.*, vol. 6, p. 8238-8249, 2023, https://doi.org/10.1021/acsanm.3c00511.

(44) C. Li, R. Kingsbury, A. S. Thind, A. Shyamsunder, T. T. Fister, R. F. Klie, K. A. Persson, and L. F. Nazar, Enabling selective zinc-ion intercalation by a eutectic electrolyte for practical anodeless zinc batteries. *Nat. Commun.*, vol. 14, p. 3067, 2023, https://doi.org/10.1038/s41467-023-38460-2.

(45) T. K. Dang, N. V. Toan, C. M. Hung, N. V. Duy, N. N. Viet, L. V. Thong, N. T. Son, N. V. Hieu, and T. L. Manh, Investigation of zinc electronucleation and growth mechanisms onto platinum electrode from a deep eutectic solvent for gas sensing applications, *J. Appl. Electrochem.*, vol. 52, p. 229, 2002, https://doi.org/10.1007/s10800-021-01635-0.

(46) G. Sheela, Zinc–nickel alloy electrodeposits for water electrolysis, *Int. J. Hydrog. Energy*, vol. 27, p. 627–633, 2002, https://doi.org/10.1016/S0360-3199(01)00170-7.

(47) F. Bao, E. Kemppainen, I. Dorbandt, R. Bors, F. Xi, R. Schlatmann, R. van de Krol, and S. Calnan, Understanding the hydrogen evolution reaction kinetics of electrodeposited nickel-molybdenum in acidic, near-neutral, and alkaline conditions, *ChemElectroChem*, vol. 8, p. 195-208, 2021, https://doi.org/10.1002/celc.202001436.

(48) H. Ren, L. Yu, L. Yang, Z. H. Huang, F. Kang, and R. Lv, Efficient electrocatalytic overall

water splitting and structural evolution of cobalt iron selenide by one-step electrodeposition, *J. Energy Chem.*, vol. 60, p. 194-201, 2021, https://doi.org/10.1016/j.jechem.2021.01.002.

(49) P. Banoth, C. Kandula, and P. Kollu, Introduction to electrocatalysis, In: Noble metal-free electrocatalysts: new trends in electrocatalysts for energy applications, vol. 2, ch. 1, p. 1-37, 2022, https://doi.org/10.1021/bk-2022-1432.ch001.

(50) B. Zhang, G. Yang, C. Li, K. Huang, J. Wu, S. Hao, J. Feng, D. Peng, and Y. Huang, Phase controllable fabrication of zinc cobalt sulfide hollow polyhedra as high-performance electrocatalysts for the hydrogen evolution reaction, *Nanoscale*, vol. 10, p. 1774-1778, 2018, https://doi.org/10.1039/C7NR08097B.

(51) A. Döner, R. Solmaz, and G. Kardaş, Enhancement of hydrogen evolution at cobalt–zinc deposited graphite electrode in alkaline solution, *Int. J. Hydrog. Energy*, vol. 36, p. 7391-7397, 2011, https://doi.org/10.1016/j.ijhydene.2011.03.083.

(52) R. Solmaz and G. Kardaş, Fabrication and characterization of NiCoZn–M (M: Ag, Pd and Pt) electrocatalysts as cathode materials for electrochemical hydrogen production, *Int. J. Hydrog. Energy*, vol. 36, p. 12079-12087, 2011, https://doi.org/10.1016/j.ijhydene.2011.06.101.

TABLES

Table 1. Comparison of diffusion coefficients obtained for Co^{2+} and Zn^{2+} ions at different temperatures and electrolytes.

Temperature / K	Electrolyte	D / cm² s^{-1}	Reference
	Co^{2+}		
303	1ChCl:2EG	$2.6 \times 10^{-7} \pm 0.7 \times 10^{-8}$	This work
313	1ChCl:2EG	$3.0 \times 10^{-7} \pm 0.8 \times 10^{-8}$	This work
323	1ChCl:2EG	$3.4 \times 10^{-7} \pm 0.5 \times 10^{-7}$	This work
343	1ChCl:2EG	$4.4 \times 10^{-7} \pm 0.5 \times 10^{-7}$	This work
313	1ChCl:2U	8.1×10^{-8}	(32)
323	1ChCl:2U	1.1×10^{-7}	(32)
333	1ChCl:2U	1.1×10^{-7}	(32)
343	1ChCl:2U	1.5×10^{-7}	(32)
343	Ethylene glycol	2.3×10^{-8}	(33)
	Zn^{2+}		
303	1ChCl:2EG	$8.9 \times 10^{-11} \pm 0.8 \times 10^{-11}$	This work
313	1ChCl:2EG	$1.4 \times 10^{-10} \pm 0.1 \times 10^{-10}$	This work
323	1ChCl:2EG	$2.9 \times 10^{-10} \pm 0.5 \times 10^{-11}$	This work
343	1ChCl:2EG	$4.5 \times 10^{-10} \pm 0.3 \times 10^{-10}$	This work
373	1-methylimidazolium trifluoromethylsulfonate	7.7×10^{-9}	(34)
363	1ChCl:2U	7.8×10^{-9}	(35)
353	urea / 1-ethyl-3-methylimidazolium	5.5×10^{-9}	(36)
313	1ChCl:2EG	7.1×10^{-10}	(37)
——	hybrid eutectic sulfolane/water	5.0×10^{-12}	(38)

Table 2. Composition of metallic coatings estimated by energy dispersive X-ray spectroscopy.

Bath	Precursor concentration (mol L^{-1})		Coatings composition (%)		Sample label
	$ZnCl_2$	$CoCl_2$	Zn	Co	
I	0.4	-	100	0	Zn
II	0.4	0.025	96	4	$Zn_{96}Co_4$
III	0.025	0.4	3	97	Zn_3Co_{97}
IV	-	0.4	0	100	Co

Table 3. Electrochemical parameters obtained with different metallic coatings developed to produce hydrogen in 1 mol L^{-1} KOH at 298.15 K.

Catalyst	$-b$ mV dec^{-1}	i_0 A cm^{-2}	$i_{0\ ECSA}$ A cm^{-2}	$\lvert\eta\rvert$ (10 mA cm–2) mV	$\lvert\eta\rvert$ (100 mA cm–2) mV	Reference
Copper	622.2 ± 2.04	$2.27\times 10^{-4} \pm 1.80\times 10^{-5}$	-	546	-	this work
Zn	233.1 ± 64.3	$1.20\times 10^{-4} \pm 2.86 \times 10^{-5}$	$1.09\times 10^{-6} \pm 2.60\times 10^{-7}$	509	-	this work
$Zn_{96}Co_4$	247.6 ± 15.5	$1.24\times 10^{-4} \pm 5.33 \times 10^{-5}$	$9.63\times 10^{-8} \pm 5.42\times 10^{-8}$	355	600	this work
Zn_3Co_{97}	108.2 ± 0.74	$8.57\times 10^{-6} \pm 3.28 \times 10^{-7}$	$2.12\times 10^{-8} \pm 8.12\times 10^{-10}$	333	524	this work
Co	191.4 ± 3.20	$2.52\times 10^{-5} \pm 2.56 \times 10^{-6}$	$8.42\times 10^{-8} \pm 8.53\times 10^{-9}$	372	578	this work
Zn-Co-S	86.3	-	-	176	-	(56)
CoZn	96	3.80×10^{-3}	-	-	240	(57)
NiCoZn	81	1.62×10^{-3}	-	-	140	(58)
$Zn_{85}Ni$	-	0.30×10^{-4}	-	95*	-	(50)

*not mentioned

FIGURE CAPTIONS

Fig. 1. Cyclic voltammograms obtained at 5 mV s^{-1} in (a) 1ChCl:EG and after adding (b) 0.4 mol L^{-1} $ZnCl_2$, (c) 0.4 mol L^{-1} $ZnCl_2$ + 0.025 mol L^{-1} $CoCl_2$, (d) 0.025 mol L^{-1} $ZnCl_2$ + 0.4 mol L^{-1} $CoCl_2$, (e) 0.4 mol L^{-1} $CoCl_2$.

Fig. 2. (a) Metallic composition, along with the SEM images of (b) Cu substrate, (c) Cu/Zn, (d) Cu/Co, (e) Cu/$Zn_{96}Co_4$ and (f) Cu/Zn_3Co_{97}. The micrographs illustrated in b-d and e-f were recorded with 500- and 1000-times magnification, respectively.

Fig. 3. XRD pattern of Zn, Co, and Zn-Co coatings, electrodeposited on Cu substrate.

Fig. 4. (a) Polarization curves carried out with different catalysts at 0.5 mV s^{-1}. (b) The corresponding Tafel slopes. (c) Electrochemical stability tests of the catalysts, evaluated at 10 mA cm^{-2} and 333 K for 100 h. Supporting electrolyte: 1 mol L^{-1} KOH.

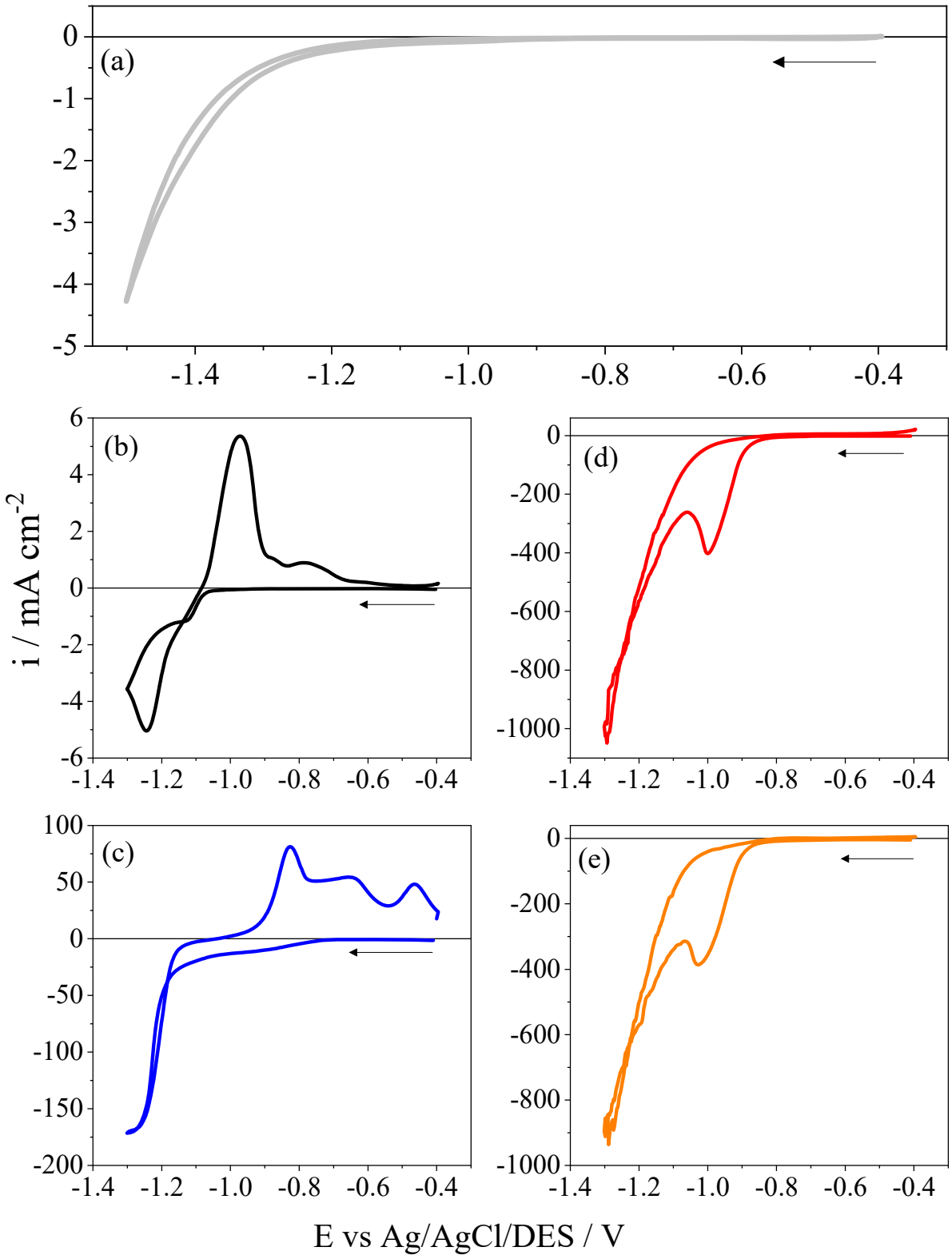

Figure 1. Rodrigues-Júnior *et al*.

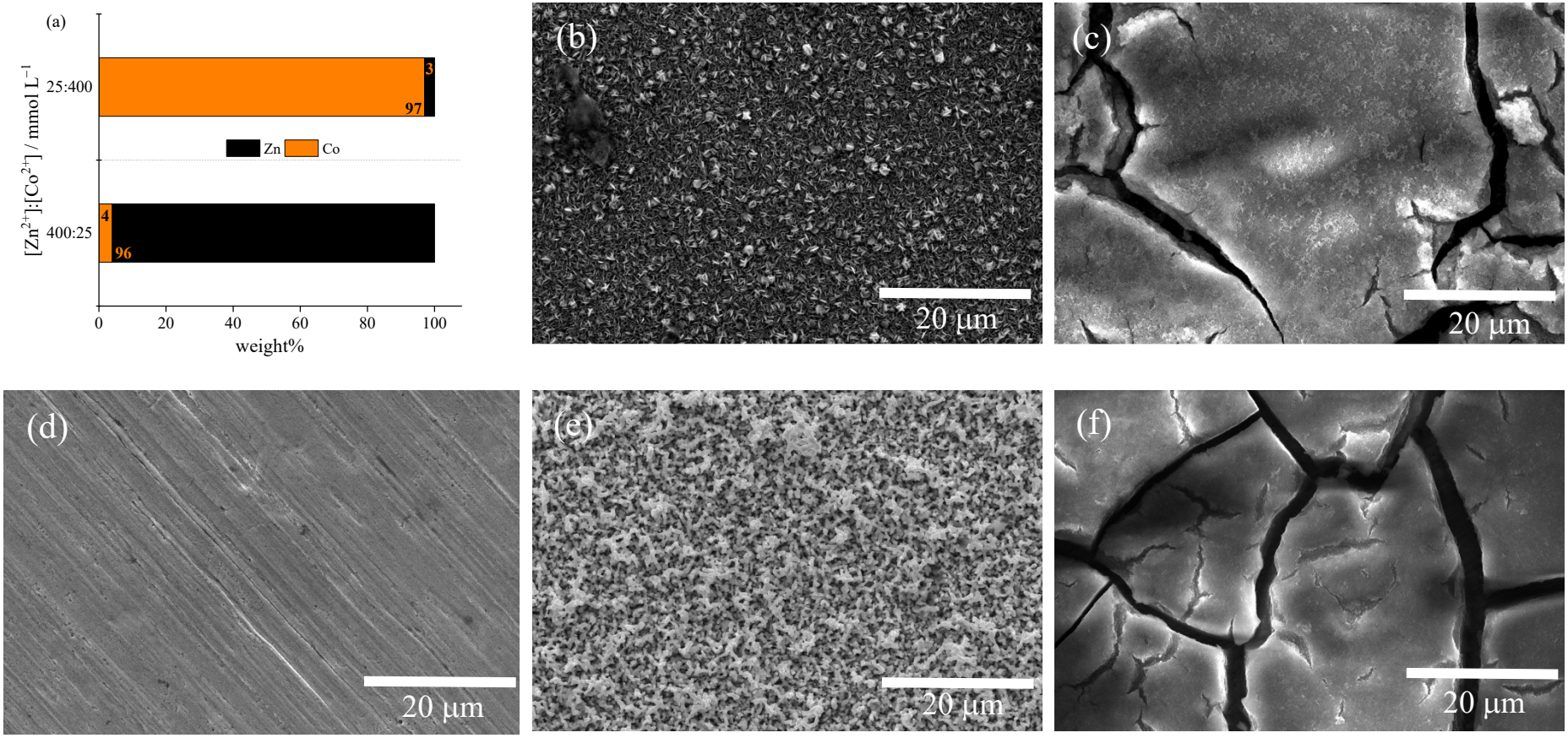

Figure 2. Rodrigues-Júnior *et al*.

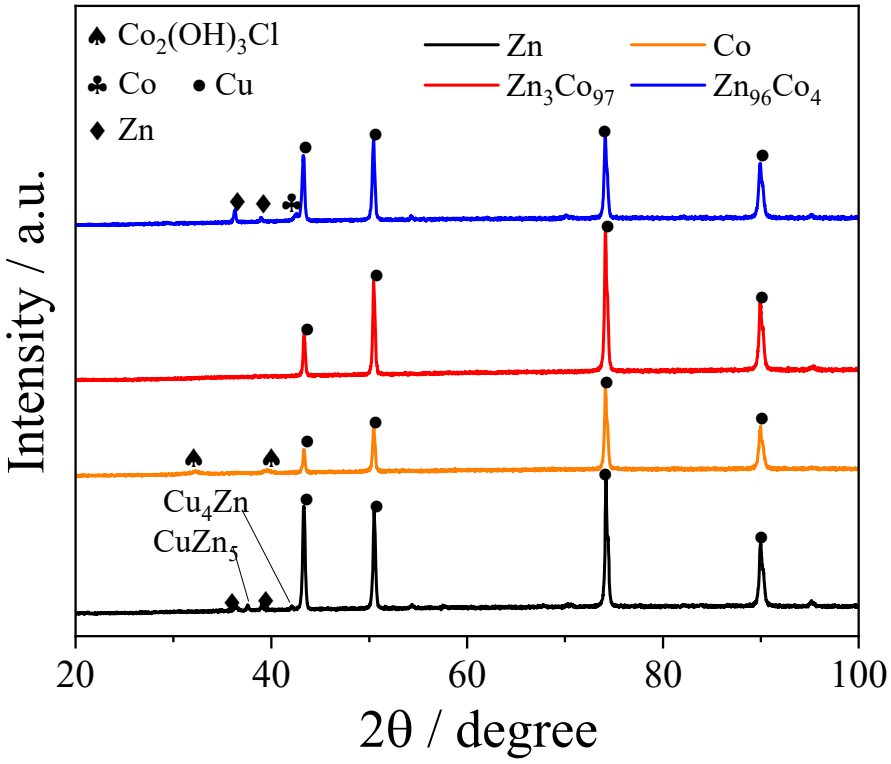

Figure 3. Rodrigues-Júnior *et al*.

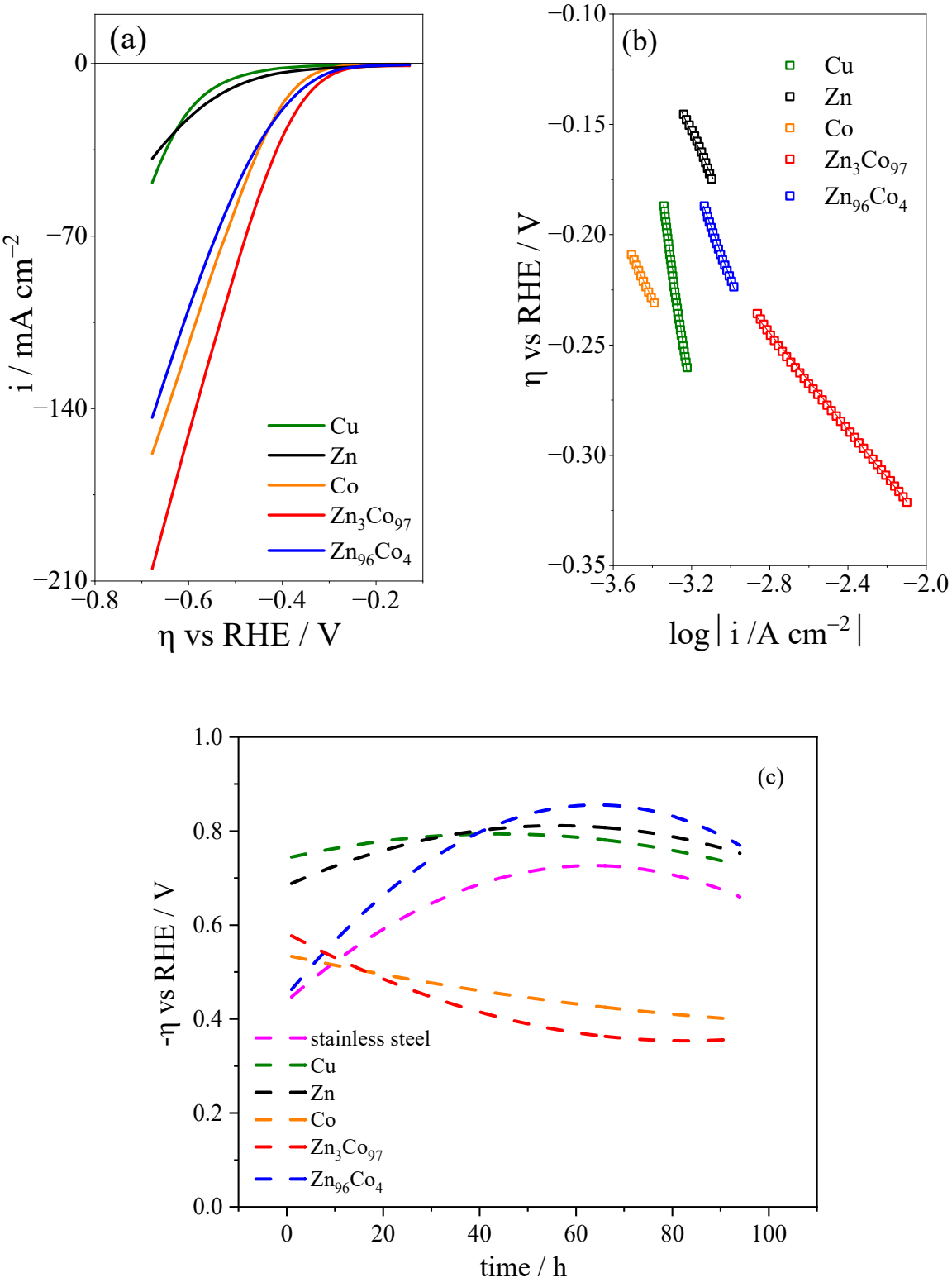

Figure 4. Rodrigues-Júnior *et al.*

Supplementary Material

$Zn_xCo_{(1-x)}$ coatings from choline chloride-ethylene glycol deep eutectic solvent as electrocatalysts for hydrogen evolution reaction

Deomar N. Rodrigues-Júnior[a], Natalia G. Sousa[a], F. Murilo T. Luna[b], Thiago M.B.F. Oliveira[c], Dieric S. Abreu[d], Walther Schwarzacher[e], Pedro de Lima-Neto[a], Adriana N. Correia[a,*]

[a] Grupo de Eletroquímica e Corrosão, Departamento de Química Analítica e Físico-Química, Centro de Ciências, Universidade Federal do Ceará, Campus do Pici, Fortaleza - CE, 60440-900, Brazil

[b] Grupo de Pesquisa em Separações por Adsorção, Departamento de Engenharia Química, Centro de Tecnologia, Universidade Federal do Ceará, Campus do Pici, Fortaleza - CE, 60455-760, Brazil

[c] Laboratório de Química Aplicada, Centro de Ciência e Tecnologia, Universidade Federal do Cariri, Juazeiro do Norte - CE, 63048-080, Brazil

[d] Laboratório de Materiais e Dispositivos, Departamento de Química Analítica e Físico-Química, Centro de Ciências, Universidade Federal do Ceará, Campus do Pici, Fortaleza, CE 60440-900, Brazil

[e] H. H. Wills Physics Laboratory,
University of Bristol, Tyndall Avenue, Bristol, BS8 1TL, United Kingdom

Figure S1. Cyclic voltammetry curves for effective electrochemical active surface area tests (ECSA) in 1 mol L^{-1} KOH for (a) Zn, (b) $Zn_{96}Co_4$, (c) Zn_3Co_{97} and (d) Co. The capacitive currents are collected at ±0.05 V (from the open circuit potential) from 2.5 up to 15 mV s^{-1}.

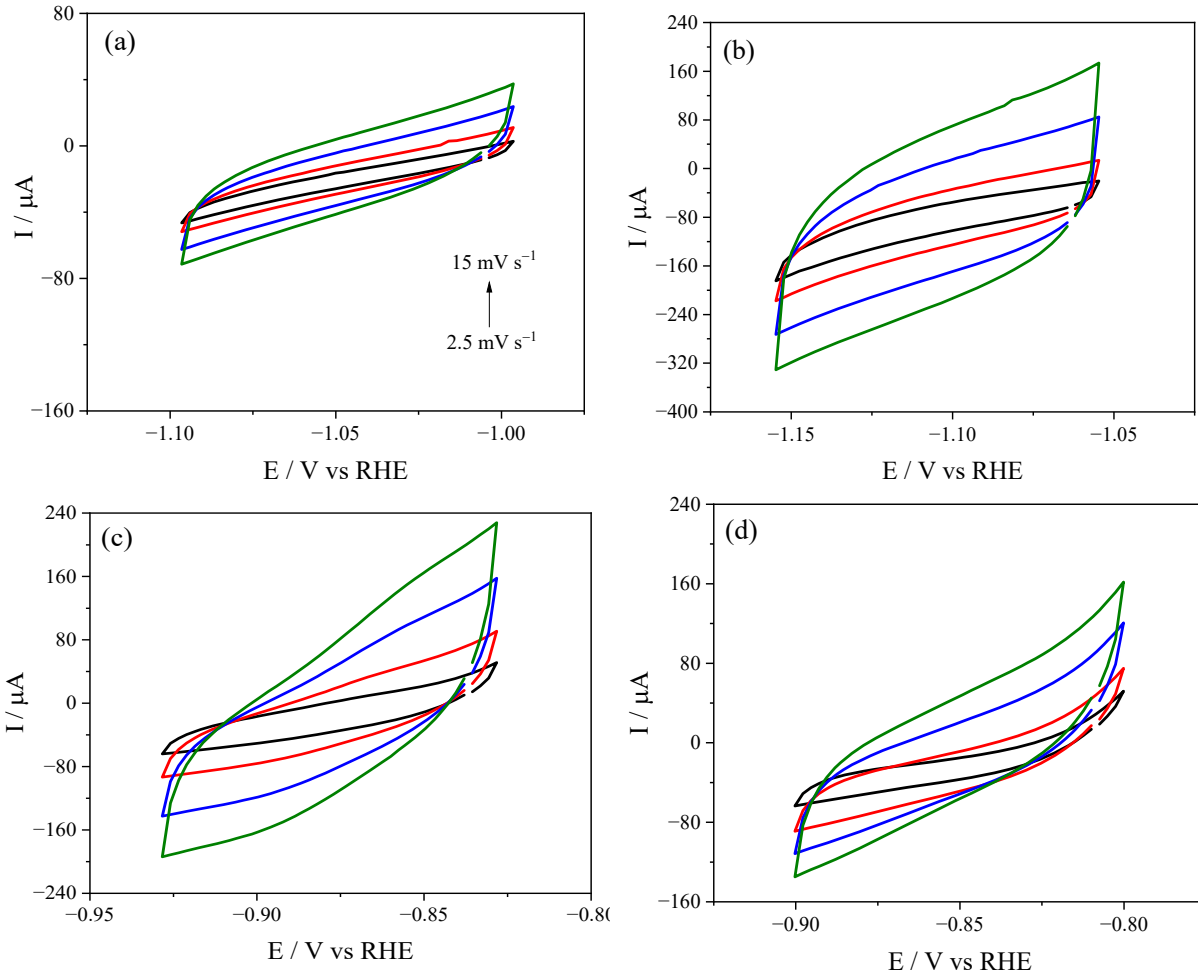

Figure S2. The charging current density differences plotted against scan rates of Zn, Co, Zn_3Co_{97}, and $Zn_{96}Co_4$ electrodes.

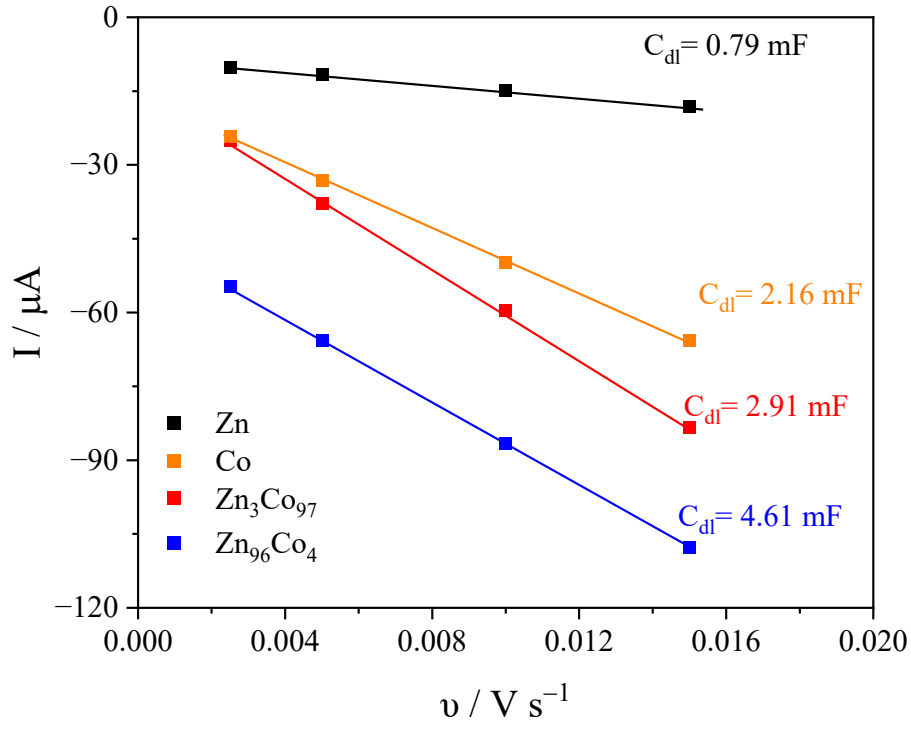

For these calculations, the value of the C_s used was 0.040 mF cm^{-2}. (R1 and R2) Considering these relative surface areas, it was possible to normalize the electrochemical data to determine the values of Tafel slope and exchange current density and the results are summarized in Table 3.

References

(R1) P. Mukherjee, K. Sathiyan, R. S. Vishwanatha and T. Zidki, Anchoring MoS2 on an ethanol-etched Prussian blue analog for enhanced electrocatalytic efficiency for the oxygen evolution reaction, *Mater. Chem. Front.*, vol. 6, p. 1770-1778, 2022, https://doi.org/10.1039/D2QM00183G.

(R2) H. Liang, D. Jiang, S. Wei, X. Cao, T. Chen, B. Huo, Z. Peng, C. Li and J. Liu, 3D cellular CoS1.097/nitrogen doped graphene foam: a durable and self-supported bifunctional electrode for overall water splitting, *J. Mater. Chem. A*, vol. 6, p. 16235-16245, 2018, https://doi.org/10.1039/C8TA05407J.

Table S1. Benchmarking parameters for catalysts studied in 1 mol L^{-1} KOH.

Catalyst	$C_{dl}=\frac{(\text{anodic slope} - \text{cathodic slope})}{2}$	$\text{ECSA}=\frac{C_{dl}}{C_s}$
Zn	0.79 mF	19.8 ± 4.2
$Zn_{96}Co_4$	4.61 mF	115.2 ± 51.6
Zn_3Co_{97}	2.91 mF	72.8 ± 23.6
Co	2.16 mF	53.9 ± 2.7

Fig.S3. (a) Polarization curves performed at 0.5 mV s^{-1} at 298 K and (b) Tafel slopes with linear fittings, considering normalized ECSA in 1 mol L^{-1} KOH for Zn (black line or symbol), Co (orange line or symbol), Zn_3Co_{97} (red line or symbol) and $Zn_{96}Co_4$ (blue line or symbol).

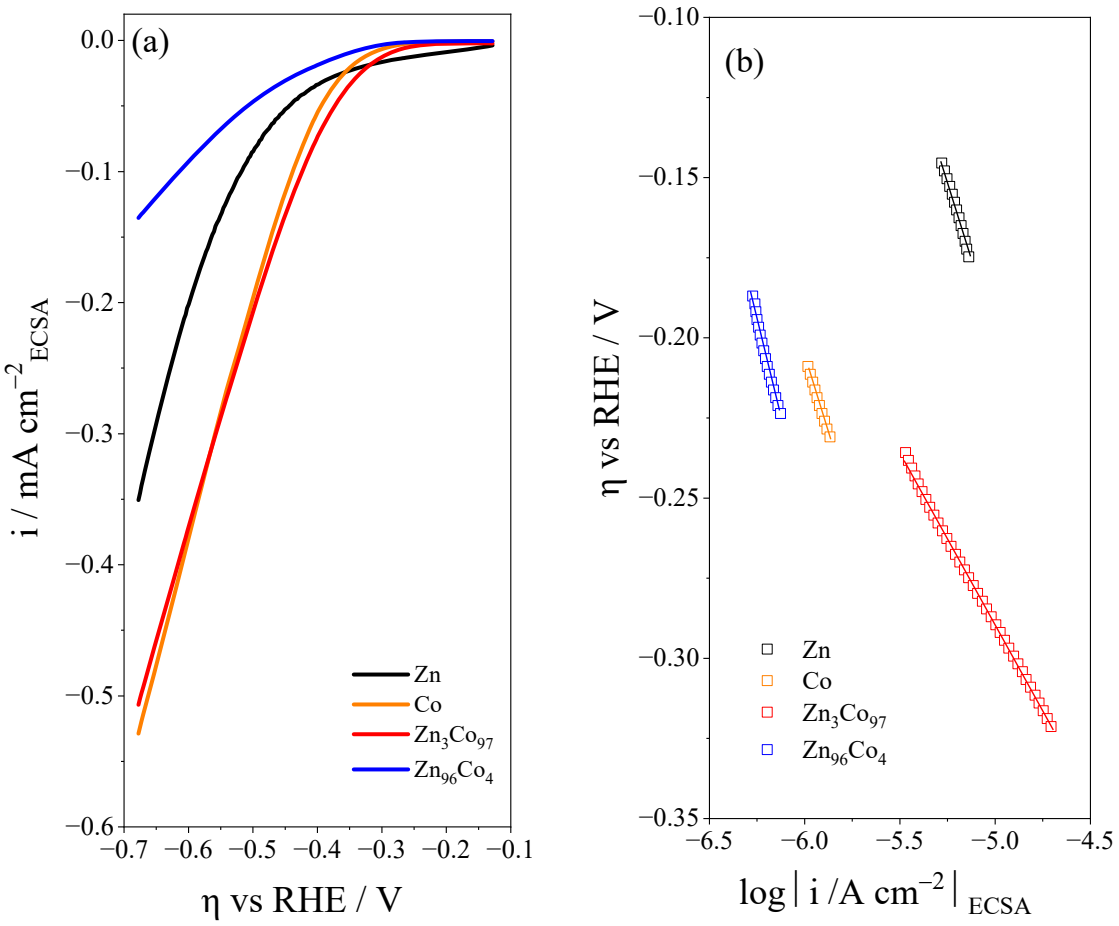

Surface Plasmon Resonance (SPR)

SPR experiments of Zn-Co metal coatings was performed on MP-SPR Navi™ 200 OTSO (Bionavis, Sweden) equipped with two laser channels (670nm and 785 nm) in angular scan mode on two separate spots on the surface. The SPR curves were taken first in air and later in water with a flow rate of 100 µL/min during a measure of 60 minutes. The thin film Zn-Co metal coatings were characterized in terms of layer thickness (d), using dedicated MP-SPR Navi™ LayerSolver™ software. Zn and Co were electrodeposited on a SPR Au-substrate (2 nm Cr adhesion layer and 50 nm Au layer). Prior to electrodeposition, the SPR Au-substrate were cleaned in Piranha solution (H_2SO_4: H_2O_2, 3:1 v/v) for 2 min and rinsed with Milli-Q water. Then, clean SPR Au-slide were placed in electrochemical cell as work electrode to perform electrodeposition of metallic coatings (see *Section 2.3*). The resultant SPR Au-substrate with Zn-Co coatings (Au-substrate + Zn, Au-substrate + Co, Au-substrate + $Zn_{96}Co_4$, and Au-substrate + Zn_3Co_{97}) was promptly washed with water and isopropanol and dried under nitrogen prior to use in SPR. The results are presented in Figure S4.

The SPR curves in Figure S4 show the peak minimum intensity shifted upwards and the peak showed significant broadening with respect to gold due to presence of absorbing layers of Zn-Co metal coatings with optical constants very different from those of gold substrate. Also, due to the nom-plasmonic metallic nature of Zn and Co coatings on gold in the 670 nm and 785 nm wavelengths region and the high values of extinction coefficient for Co (k = 6.5355), (SPR#1) the SPR curves vanishes for those coatings with high composition of Co (i.e., Co and Zn_3Co_{97}). That behaviour indicates a high ordered and dense thin film,(SPR#2) corroborating with powder DRX results (see *Section 3.3*). In addition, SPR curves obtained with water flux for 1h (Figure S4. (b) and (d)) indicate no change in optics properties of coatings, also confirming their stabilities.

Figure S4. SPR curves for the Co, Zn, Zn_3Co_{97} and $Zn_{96}Co_4$ metal coatings on Au-substrate. Measurements were performed with 785 nm wavelength in (a) air and (b) water, and with 670 nm wavelength in air (c) and (d) water.

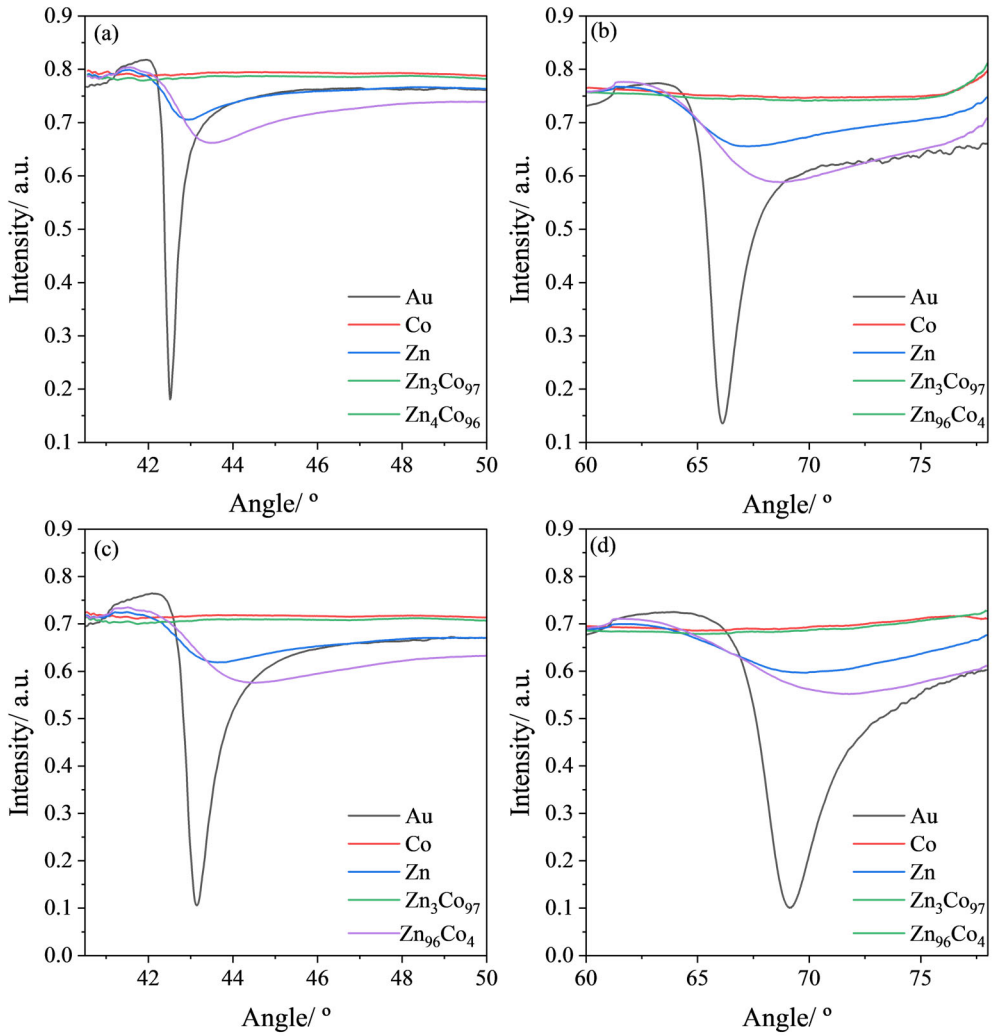

References

(SPR#1) Wolfgang S. M. Werner, Kathrin Glantschnig, Claudia Ambrosch-Draxl; Optical Constants and Inelastic Electron-Scattering Data for 17 Elemental Metals. *Journal of Physical and Chemical Reference*, vol. 4, p. 1013–1092, 2009, https://doi.org/10.1063/1.3243762.

(SPR#2) Popov, K. I., Djokić, S. S., Nikolić, N. D., & Jović, V. D.. Electrodeposition of Metals with Hydrogen Evolution. *Morphology of electrochemically and chemically deposited metals,* p. 171-203. Switzerland: Springer. 2016. https://doi.org/10.1007/978-3-319-26073-0_5.

3 MANUSCRITO 2

Study of the anticorrosive behaviour of $Zn_xCo_{(1-x)}$ coatings obtained by mixing choline chloride-ethylene glycol

Deomar N. Rodrigues-Júnior, Adriana N. Correia*

Grupo de Eletroquímica e Corrosão, Departamento de Química Analítica e Físico-Química, Centro de Ciências, Universidade Federal do Ceará, Campus do Pici, Fortaleza, CE 60440-900, Brazil

* Corresponding author: Prof. Dr. Adriana Nunes Correia
Telephone: +55 85 3366 9050
E-mail address: adriana@ufc.br

Abstract

The corrosion behaviour of electrodeposited $Zn_xCo_{(1-x)}$ coatings in 3.5% NaCl aqueous solutions was investigated using cyclic voltammetry (CV), scanning electron microscopy (SEM), energy-dispersive X-ray (EDS), and potentiodynamic polarization curves (PP). All coatings were electrodeposited on mild steel. The percentages of Zn and Co were determined through EDS analysis with reference to SEM images of potentiostatically electrodeposited $Zn_xCo_{(1-x)}$ coatings (-1.4 V), having a theoretical thickness of 1 μm, from solutions with varying concentrations of $ZnCl_2$ and $CoCl_2$. All curves displayed active dissolution behaviour of the materials in the anode branch, but the curves of the 0.4 mol L^{-1} Zn, 0.4 mol L^{-1}: 0.025 mol L^{-1} Zn^{2+}:Co^{2+} exhibited evidence of diffusional control in the coating oxidation reaction, with a more pronounced effect observed in the electrodeposition of 0.4 mol L^{-1}: 0.025 mol L^{-1} Zn^{2+}:Co^{2+}. The corrosion current value of the 0.025 mol L^{-1} Co^{2+} coating, 1.21×10^{-5} A cm^{-2}, was significantly higher than that of all other coatings. This increase may be associated with the presence of cracks on the surface, leading to an expansion of the electroactive area of the coating. Conversely, this electrodeposit presented lower Tafel coefficients (η_a = 67 mV dec^{-1}; $|\eta_c|$ = 57 mV dec^{-1}) than the 0.025 mol L^{-1}:0.4 mol L^{-1} Zn^{2+}:Co^{2+} coating (η_a = 73 mV dec^{-1}; $|\eta_c|$ = 68 mV dec^{-1}).

Keywords: Electrodeposition; corrosion; ZnCo; DES

1 INTRODUCTION

According to NACE (National Association of Corrosion Engineers) International, the global cost of corrosion is estimated at US$2.5 trillion, excluding expenses related to personal safety or the remediation of environmental impacts caused by corrosion. This figure corresponds to 3.4% of the global gross domestic product (GDP) and could be reduced by approximately 15 to 35% per year if corrosion protection measures were more consistently and assertively implemented. (1)

The effects of corrosion, particularly on buildings and monuments, are evident, and it is estimated that they account for 42% of failures in aircraft structures, pipelines, ships, and other infrastructure. Noteworthy incidents resulting from corrosion include the 2015 leak of 540 m^3 of crude oil off the coast of Santa Barbara, California. This incident was caused by the propagation of cracks in the lower quadrant of a pipeline, which experienced a 45% reduction in thickness due to corrosion. Another notable event occurred in 2013 when a fire broke out in a turbine of an Airbus A330 at Manchester airport, traveling at a speed of 190 km h^{-1}. Investigation revealed that a fracture in the turbine blades was initiated by pitting corrosion-induced cyclic fatigue. Additionally, in the 1980s, the Union Carbide India Limited pesticide plant in Bhopal experienced the release of toxic gases into the atmosphere due to corrosion in the structures, resulting in the death of more than 2,000 people, according to official figures. (2)

So, it is necessary to develop corrosion-resistant materials, whether to better manage financial resources, to avoid environmental catastrophes, and, above all, to avoid loss of human life. Industrially, carbon steel is one of the most widely used materials due to its versatility. However, its low corrosion resistance leads to the need for corrosion protection methods in

carbon steel applications. This includes, for example, the use of protective metallic coatings for steel. (3)

In this context, Cr coatings have found wide application due to their resistance to heat, corrosion, and erosion and the high hardness and attractive appearance of this metal. However, most electrolytic baths to obtain these coatings use Cr^{6+} as a source of Cr, an ion that poses environmental and health risks. This has led to the research for other materials that can replace Cr, providing protection without the severe environmental impacts it causes. (4, 5)

Among the metals proposed to replace Cr, Zn can be highlighted, which, due to its anodic electrochemical behaviour against Fe, corrodes preferentially to the carbon steel substrate. Zinc electrodeposition is an economical Zn coating process compared to the conventional galvanic process. The galvanizing process is used in several industrial sectors to protect ferrous alloys during the corrosion process. Zn electrodeposition is relatively cheap compared to other coating materials for the same purpose. (6,7)

Zn is commonly considered an effective material for coating reactive metal surfaces and the electroplating of Zn coatings has received great attention due to its corrosion resistance. (8) In recent years, several researchers have carried out investigations into Zn electrodeposition using deep eutectic solvents (DES) as the solvent. Jiang et al. performed metallic Zn coating in a medium of choline chloride (ChCl) and ethylene glycol (EG) on a Cu substrate using $ZnCl_2$ as the source of Zn. The results showed that the Zn coating obtained had good adherence to the surface of the Cu substrate, with a corrosion current density of 7,99 μA cm^{-2} and a corrosion potential of −1.97 V at 40 mA cm^{-2} in 3.5 % NaCl. (9)

Chen et al. developed a method to improve the electrodeposition rate of Zn in ChCl-based DES and investigated the effects of the electrodeposition temperature and of the current density on Zn coating properties. A high electrodeposition rate was observed for the DES mixture containing 2 mol L^{-1} $ZnCl_2$. When the current density was 12 mA cm^{-2}, only 5 min

were required to deposit almost 15 μm of the Zn coating. Regarding the dependence between the electrodeposition temperature and the density of the Zn coating, it was found that in a specific temperature range of 28 to 60 °C, the higher the temperature, the denser the Zn coating. When the temperature was elevated (e.g., 80 °C), the specific mass of the Zn coating decreased. (10, 11)

However, due to environmental conditions, the use of solely Zn coatings sometimes does not provide the desired protection. Therefore, attempts have been made to increase the corrosion resistance of pure Zn coatings through the co-deposition of other metals, such as Co. (12, 13)

Nakano et al. used a bath containing ZnO, $CoSO_4 \cdot 7H_2O$, NaOH, and, as a complexing agent, triethanolamine in deionized water to electrodeposit Zn-Co coatings on Cu substrate. The deposits were obtained in both coulostatic (5×10^4 C m^{-2}) and galvanostatic (2 to 500 A m^{-2}) mode at 308 K. They observed that for current densities below 3 A m^{-2}, codeposition of Zn and Co was normal. For current densities above 6 A m^{-2}, there was an anomalous codeposition. Furthermore, these authors noticed a drastic increase in deposition efficiency for the current density of 6 A m^{-2}, which they attributed to the observed potential of −1.27 V vs RHE, which corresponds to the equilibrium potential for Zn deposition, according to them. The morphology of the deposits, observed by scanning electron microscopy (SEM), changed from laminar crystals to aggregates of granular crystals (with diameters less than 1 μm) when the current density varied from 5 A m^{-2} to 20 A m^{-2}. (14)

Garcia et al. studied the electrodeposition of Co-rich Zn-Co coatings on a graphite substrate using aqueous solutions containing $ZnSO_4 \cdot 6H_2O$, $CoSO_4 \cdot 5H_2O$ and $Na_3C_5H_6O_7$. The percentages of Co obtained in the Zn-Co coatings ranged from 30.25% m/m to 92.38% m/m. The increase in the percentage of Co in the coatings led to a decrease in grains and a more homogeneous distribution of them in the micrographs obtained by SEM. The polarization

curves obtained by linear voltammetry in 0.5 mol L^{-1} NaCl medium showed that, for the coating containing 92.38% m/m of Co, the corrosion current was 7.0 μA cm^{-2} and the corrosion potential was −1.1190 V *vs* SCE. (15)

Bhat et al. electrodeposited Zn-Co coatings on carbon steel from a bath containing $ZnCl_2 \cdot 6H_2O$, $CoCl_2 \cdot 6H_2O$, NH_4Cl, KCl, and the additives sulfanilic acid ($C_6H_7NO_3S$) and gelatin ($C_6H_8O_6$), in demineralized water (pH 3.0). The deposition mode used was galvanostatic, and according to these authors, the optimized current was 20 mA cm^{-2}. They obtained coatings whose amount of Co varied from 0.78% (m/m) to 3.75% (m/m) and observed that the coating containing 1.74% (m/m) of Co presented more excellent resistance to corrosion in 3.5% NaCl medium. The thickness of this film was 10.5 μm, while its corrosion potential was −1.081 vs SCE, and its corrosion current was 9.021 μA cm^{-2}. (16)

Pandiyarajan et al. studied the electrodeposition of Zn-Co using supercritical CO_2 from an electrolyte containing $CoSO_4$ and $ZnSO_4$ in a 1:1 molar ratio and 0.3 mol L^{-1} H_3BO_3. The films were prepared at high pressure to create a supercritical atmosphere and atmospheric pressure for comparison. The substrate was steel, and the deposition mode was galvanostatic (3 A dm^{-2}, 30 min) at 50 ºC. The coatings were evaluated against corrosion in 3.5% NaCl. From the polarization curves, the corrosion current and the corrosion potential were determined, which were 191.7 μA cm^{-2} and 138.7 μA cm^{-2} and −900.1 mV and −887.3 mV vs Ag/AgCl (unspecified concentration) for deposits obtained at atmospheric pressure and in a supercritical atmosphere, respectively. From electrochemical impedance spectroscopy (EIS) experiments, the coatings obtained in a supercritical atmosphere obtained polarization resistance (Rp) of 251.3 Ω cm^2 and those obtained under atmospheric pressure of 61.3 Ω cm^2. (17)

As can be seen, water has been widely used as a solvent for the electrodeposition of Zn-Co alloys due to the versatility and availability of this solvent. However, the hydrogen evolution reaction (HER) strongly influences electrodeposition in aqueous medium, which reduces

deposition efficiency. Furthermore, additives such as complexing agents and surfactants are frequently used to reduce the production of gaseous H_2 and stabilize metal ions in solution. In this context, DES have stood out as a viable alternative for the electrodeposition of metals and alloys, including Zn-Co. (18-22)

Chu et al. electrodeposited nanocrystalline Zn-Co coatings from electrolyte containing $ZnCl_2$ and $CoCl_2 \cdot 6H_2O$ in choline chloride (ChCl) and urea (U) medium in 1:2 molar ratio (ChCl:2U) on AMB60B magnesium alloy. An alternating current of an average density of 3.5 mA cm^{-2} was imposed for 2 h to obtain the coatings. They observed that the concentration of Co^{2+} ions in the bath strongly influenced the amount of Co present in the coatings and the morphology of these. (23)

Yavuz et al. electrodeposited Zn, Co and Zn-Co coatings from ChCl and ethylene glycol (EG) in a 1:2 molar ratio (ChCl:2EG) containing $ZnCl_2$ and/or $CoCl_2$. The substrate was Cu, and the deposition mode was potentiostatic, applying −1.5 V vs Pt for 300 s at 55 ºC. The pure Zn and Co electrodeposits presented homogeneously distributed nanometric structures, while the Zn-Co presented agglomerates of different sizes. The corrosion currents obtained from the polarization curves for the electrodeposits in 3.5% NaCl medium were 3.89 μA cm^{-2} for the Co coating, 8.91 μA cm^{-2} for the Zn coating and 1.26 μA cm^{-2} for the Zn-Co coating. (24)

So, it was observed that Zn-Co coatings can be successfully obtained from electrolyte solutions of salts of these metals in DES. However, there still needs to be more to be filled in the study of these electrodeposits. Therefore, this work aims to obtain $Zn_xCo_{(1-x)}$ coatings in a ChCl:2EG medium for corrosion protection of carbon steel in a 3.5% NaCl medium.

2 EXPERIMENTAL

2.1 Chemicals

Choline chloride, ChCl (Sigma-Aldrich®, 99%), ethylene glycol, EG (Sigma-Aldrich®), zinc chloride, $ZnCl_2$ (Sigma-Aldrich®), cobalt chloride, $CoCl_2$ (Sigma-Aldrich®) and sodium chloride, NaCl (VETEC®), were used as received.

To prepare the eutectic solvent, ChCl and EG were mixed in a beaker at a molar ratio of 1:2 (1ChCl:2EG) and heated at 353 K until a colorless and homogeneous liquid was formed (21). The electrodeposition solutions were formulated by dissolving $ZnCl_2$ and $CoCl_2$ in 1ChCl:2EG, under constant stirring. The concentrations of the electroactive species used in these solutions were (Zn^{2+}) = 0.025 mol L^{-1}, (Co^{2+}) = 0.025 mol L^{-1}, (Zn^{2+}) = 0.4 mol L^{-1} and (Co^{2+}) = 0.4 mol L^{-1}. The electrolyte solution utilized in the potentiodynamic polarization curve (PP) tests was 3.5% NaCl dissolved in distilled water.

2.2 Measurements

The electrochemical experiments were conducted utilizing a glass electrochemical cell with a 20 mL capacity and a conventional three-electrode system. The working electrode was an AISI 1020 mild steel disc embedded in epoxy resin, with an exposed geometric area of approximately

0.0314 cm^2 for cyclic voltammetry tests and 0.17 cm^2 for polarization curve tests. Before each electrochemical experiment, the working electrode was mechanically polished with 100, 400 and 600 grit sandpaper consecutively; then, the mild steel electrodes were washed with Milli-Q® water (18.2 MΩ cm).

A platinum plate (99.5% purity) measuring 1 cm^2 and a silver wire covered with AgCl and immersed in saturated AgCl were used as auxiliary and reference electrodes, respectively. The acquisition and processing of electrochemical data were carried out by the AUTOLAB

PGSTAT30 potentiostat/galvanostat, Metrohm-Eco Chemie®, controlled by the NOVA version 2.1.

The voltammetric profiles of the AISI 1020 mild steel substrate in solutions containing the individual species Zn^{2+}, Co^{2+} and in solutions containing both Zn^{2+} and Co^{2+} ions in 1ChCl:2EG were obtained using the cyclic voltammetry technique at a temperature of 343 K, with scan rate of 4 mV s^{-1} and potential range from − 0.2 V to −1.4 V.

Zn electrodeposits were obtained from $[Zn^{2+}]$ = 0.4 mol L^{-1} colution, and Co coatings were electrodeposited from $[Co^{2+}]$ = 0.4 mol L^{-1} solution, both in 1ChCl:2EG. The Zn-Co coatings were obtained from solutions with different proportions Zn^{2+}:Co^{2+} in 1ChCl:2EG: $[Zn^{2+}]$ = 0.4 mol L^{-1} and $[Co^{2+}]$ = 0.025 mol L^{-1}; $[Zn^{2+}]$ = 0.025 mol L^{-1} and $[Co^{2+}]$ = 0.4 mol L^{-1}. Under all these conditions, Zn-Co electrodeposits on AISI 1020 mild steel were obtained potentiostatically at −1.4 V at 343 K, with charge control to obtain coatings with a theoretical thickness of 1 μm.

The surface morphology of the obtained coatings was evaluated using a field emission scanning electron microscope (FEG-SEM FEI-Quanta 450), operating at an accelerated voltage of 20 keV. The Zn and Co atomic percentages in the layers were determined by energy dispersive X-ray spectroscopy (EDS) coupled to SEM.

The corrosion behaviour of AISI 1020 mild steel and electrodeposited Zn, Co, and Zn-Co coatings on it in 3.5% NaCl was evaluated using potentiodynamic polarization (PP) tests. For this purpose, a potential window ranging from −0.2 V to −1.0 V was applied, with a prior stabilization of the open circuit potential (OCP) for 3600 s, and a scan rate of 1 mV s^{-1} at 343 K.

3 RESULTS AND DISCUSSION

Regarding the characterization of the electrochemical behaviour of the systems, Fig. 1a shows the cyclic voltammogram obtained for AISI 1020 mild steel in 1ChCl:2EG at 4 mV s^{-1} at 343 K. It is observed that there is no electrochemical process in the potential range of −0.3 V to −1.0 V, both in cathodic and in anodic scanning. However, at potentials below −1.0 V, an increase in current may be associated with the decomposition of DES, possibly involving the reduction of both the hydroxyl groups of ethylene glycol molecules and choline cations. (25) There is also an evident process at potentials around −0.2 V in the anodic scan.

Fig. 1b shows the cyclic voltammogram obtained for the AISI 1020 mild steel substrate in 1ChCl:2EG medium containing 0.4 mol L^{-1} $ZnCl_2$, with a scan rate of 4 mV s^{-1} at 343 K. In the cathodic scan, there is a loop around −1.1 V and a well-defined process around −1.3 V, attributed to the nucleation of the zinc film electrodeposited on the substrate. (26) In the anodic scan, an undefined process is observed around −1.0 V and two well-defined processes at potentials of −0.8 V and –0.7 V, which can be attributed to the dissolution of the film of Zn deposited in the cathodic scan. (26)

Fig. 1c presents the cyclic voltammogram relative to the system in which the AISI 1020 mild steel substrate is immersed in 1ChCl:2EG with 0.4 mol L^{-1} $ZnCl_2$ and 0.025 mol L^{-1} $CoCl_2$, obtained at 4 mV s^{-1} at a temperature of 343 K. In contrast to the voltammogram obtained only in the presence of $ZnCl_2$ (Fig. 1b), there is no evidence of nucleation in the voltammogram of Fig. 1c, but only an undefined reduction process around −1.0 V, possibly related to the reduction of Co^{2+} ions, and another well-defined peak around −1.3 V, already attributed to the reduction of Zn^{2+} ions on the substrate. (19,20) In the anodic scan, two well-defined processes were observed: one with a higher peak current, around −0.8 V, related to the

dissolution of the Zn film electrodeposited during the cathodic scanning, and another less pronounced, around −0.3 V, corresponding to the dissolution of the Co film. (26, 27)

Fig. 1d displays the cyclic voltammogram corresponding to the electrochemical behaviour of the system containing 0.4 mol L^{-1} $CoCl_2$ in 1ChCl:2EG, with a scan rate of 4 mV s^{-1} at 343 K. In the cathodic scan, a process around −0.95 V is observed, which can be related to the reduction of Co^{2+} ions on the surface of the AISI 1020 mild steel substrate. (20) In the anodic scan, there is the onset of a process around −0.3 V, attributed to the dissolution of the electrodeposited cobalt film during the cathodic scan. (27)

In Fig. 1e, the cyclic voltammogram corresponds to the AISI 1020 mild steel substrate in 1ChCl:2EG containing 0.025 mol L^{-1} $ZnCl_2$ and 0.4 mol L^{-1} $CoCl_2$, at 4 mV s–1 and 343 K. It is noticeable that this voltammogram closely resembles that in Fig. 1d, possibly because the molar ratio between the concentrations of $ZnCl_2$ and $CoCl_2$ in the electrolyte masked the processes related to Zn.

Fig. 2 presents the results of the physical characterization of the electrodeposited surfaces. In Fig. 2a, the percentages obtained by EDS referring to SEM images of potentiostatically electrodeposited $Zn_xCo_{(1-x)}$ coatings (–1.4 V), with a theoretical thickness of 1 μm, from solutions with different concentrations of $ZnCl_2$ and $CoCl_2$, are depicted. It is noticeable that the chemical composition of the coatings mirrors the proportion of Zn and Co salts present in the solutions used in the electrodeposition processes. This correlation arises from considering the molar concentrations of ions in the solution. For a total of 0.425 mol L^{-1} Zn^{2+} and Co^{2+} ions dissolved in 1ChCl:2EG, 0.4 mol L^{-1} of ions is equivalent to approximately 94% of the ions in solution, and 0.025 mol L^{-1} represents 6% of the total dissolved ions. Comparing this proportion of molar concentration of ions in solution with the proportion of the number of atoms present in electrodeposits, there is a close relationship between the concentration of electrolyte solutions and the relative number of metals present in the coatings.

In this context, the electrodeposit obtained from the solution of 0.4 mol L^{-1} $ZnCl_2$ + 0.025 mol L^{-1} $CoCl_2$, whose molar percentage of Zn is approximately 94%, contains 96% Zn atoms and 4% of Co; while the coating obtained from the solution of 0.025 mol L^{-1} $ZnCl_2$ + 0.4 mol L^{-1} $CoCl_2$ presents 3% Zn and 97% Co. This is an indication that the use of 1ChCl:2EG allows an excellent control of the desired chemical composition for $Zn_xCo_{(1-x)}$ deposits. On the other hand, Chu et al., when working with Zn-Co alloys electrodeposited from a solution containing a fixed concentration of 0.11 mol L^{-1} $ZnCl_2$ and 0.01 mol L^{-1} $CoCl_2$ in ChCl:2U, applying different potentials of deposition, observed that the percentage of Co present in their deposits was always more significant than that present in the electrolyte solution and that an increase in the deposition potential led to a deposition of a smaller relative quantity of Co and, consequently, a more significant amount of Zn. (28)

In the images in Figs. 2b – 2f, there are the micrographs obtained for the coatings obtained from solutions containing (b) 0.4 mol L^{-1} Zn^{2+}; (c) 0.4 mol L^{-1}: 0.025 mol L^{-1} Zn^{2+}:Co^{2+}; (d) 0.025 mol L^{-1}: 0.4 mol L^{-1} Zn^{2+}:Co^{2+}; (e) 0.4 mol L^{-1} Co^{2+}, electrodeposited on AISI 1020 mild steel substrate in 1ChCl:2EG medium at 343 K and for (f) AISI 1020 mild steel substrate without coating.

In Fig. 2b, a coating is observed distributed over the entire surface of the substrate, with the presence of nodules and multifaceted crystallites of varying sizes. In comparison, Alesary et al. electrodeposited Zn from a 0.4 mol L^{-1} $ZnCl_2$ solution in ChCl:2EG onto a Cu substrate in galvanostatic mode (i = 3.3 mA cm^{-2} for 2 h) at 353.15 K. These authors noted that SEM images revealed the presence of Zn particles of different sizes, resulting in a rough and polycrystalline morphology, like that obtained in the present work. In Fig. 2c, a change in morphology is observed, with the coating homogeneously distributed over the surface, with evidence of it being thinner due to the visualization of the grooves inherent to the sanding of the substrate.

In Figs. 2d and 2e, the electrodeposits showed cracks, possibly due to more remarkable film growth, generating tension in the material. Li et al., when electrodepositing Co on Cu substrate from a 0.05 mol L^{-1} $CoCl_2$ solution in 1ChCl:2U at 373.15 K, noticed changes in the morphology of the coatings with the change in deposition potential. Thus, their SEM images showed that, for a potential of −0.80 V, the electrodeposit presented a uniform, dense and compact morphology, like what was obtained in the present work, but without showing cracks. By varying the deposition potential to more negative values, they observed the formation of some polygonal particles on the coating surface, followed by the formation of nodules and, finally, when the applied potential was −0.95 V, the formation of dendrites. (30) In Fig. 2f, only the lines inherent to sanding are observed, as expected for the uncoated substrate.

Regarding the behaviour of materials against corrosion in 3.5% NaCl, Fig. 3 shows the polarization curves obtained at 343 K for the AISI 1020 mild steel substrate and for the Zn, $Zn_{96}Co_4$, Zn_3Co_{97} and Co electrodeposited films onto AISI 1020 mild steel substrate at 343 K. All curves exhibit active dissolution behaviour of the materials in the anode branch, but the curves of the Zn and $Zn_{96}Co_4$ coatings present evidence of diffusional control in the coating oxidation reaction, more pronounced in the $Zn_{96}Co_4$ coating.

Table 1 presents the parameters calculated from the polarization curves. For AISI 1020 mild steel, the corrosion potential was −0.63 V, and the corrosion current was 5.62×10^{-6} A cm^{-2}. The Tafel coefficients were 73 mV dec^{-1} for the anodic reaction and −171 mV dec^{-1} for the cathodic reaction. The Zn and $Zn_{96}Co_4$ coatings showed close corrosion potentials, −0.97 V and −0.91 V, respectively. The corrosion current of the Zn coating, 7.17×10^{-6} A cm^{-2}, was more than double the corrosion current of the $Zn_{96}Co_4$ coating, 3.27×10^{-6} A cm^{-2}. Comparing the Tafel coefficients, for the oxidation reaction, the $Zn_{96}Co_4$ coating presented a coefficient (33 mV dec^{-1}) slightly higher than the electrodeposited Zn (26 mV dec^{-1}). As for the reduction reaction, Zn coating presented a higher modulus coefficient

(115 mV dec^{-1}) than $Zn_{96}Co_4$coating (38 mV dec^{-1}). It is observable that, compared to AISI 1020 mild steel, Zn coating showed a higher corrosion current, possibly due to the sacrificial nature of Zn in relation to steel. Adding Co to the $Zn_{96}Co_4$ coating led to the lowest corrosion current.

On the other hand, Zn_3Co_{97} and Co coatings showed similar corrosion potentials, −0.57 V and −0.60 V, respectively. However, the corrosion current of the Co coating, 1.21×10^{-5} A cm^{-2}, was significantly higher than that of all coatings, which may be associated with the presence of cracks on the surface, as showed in Fig. 2e, increasing the electroactive area of the coating. On the other hand, this electrodeposit presented lower Tafel coefficients (η_a = 67 mV dec^{-1}; $|\eta_c|$ = 57 mV dec^{-1}) than the Zn_3Co_{97} coating (η_a = 73 mV dec^{-1}; $|\eta_c|$ = 68 mV dec^{-1}).

Gharahcheshmeh and Sohi obtained a corrosion potential of −1.120 V vs SCE for Zn coating and corrosion potentials from −1.124 V to −1.130 V vs. SCE for Zn-Co electrodeposits in which the percentage of Co varied from 0.52 to 3.34 %m/m. The corrosion current values were 6.76×10^{-4} A cm^{-2} for pure electroplated Zn and ranged from 1.298×10^{-3} A cm^{-2} to 3.880×10^{-3} A cm^{-2} for the coatings containing Co. (13) Bhat et al obtained corrosion potentials between −1.081 V and −1.129 V vs. SCE and corrosion currents ranging from 9.021×10^{-6} A cm^{-2} to 3.232×10^{-5} A cm^{-2} for Zn-Co coatings whose Co content was 0.78 % to 3.75 % m/m. (16)

Conclusions

$Zn_xCo_{(1-x)}$ coatings were successfully obtained by electrodeposition by potentiostatic mode at 343 K. The Co content in the films obtained by EDS data increased with the Co^{2+} ions concentration in the electrodeposition solution. SEM images showed the presence of cracks on the coating surface with an increase in the Co content. Finally, the corrosion current density of

the $Zn_{96}Co_4$ coating (3.27×10^{-6} A cm^{-2}) was almost half that of the mild steel substrate (5.62×10^{-6} A cm^{-2}), showing a promising protective behaviour of the $Zn_{96}Co_4$ coating against corrosion of the mild steel in a 3.5% NaCl medium.

Acknowledgments

This study was financed in part by the Coordenação de Aperfeiçoamento de Pessoal de Nível Superior - Brasil (CAPES) – Finance Code 001. The authors thank the financial support given by the following Brazilian funding agencies: Coordenação de Aperfeiçoamento de Pessoal de Nível Superior (CAPES), Conselho Nacional de Desenvolvimento Científico e Tecnológico (CNPq) and Fundação Cearense de Apoio ao Desenvolvimento Científico e Tecnológica (FUNCAP). A. N. Correia gratefully acknowledges funding provided by CNPq (proc. 405596/2018-9 and 305136/2018-6). The authors would like to thank the Central Analítica-UFC/CT-INFRA/MCTI-SISANO/Pró-Equipamentos CAPES for the support.

REFERÊNCIAS

[1]. G. Koch, J. Varney, N. Thompson, O. Moghissi, M. Gould, and J. Payer, *International Measures of Prevention, Application and Economics of Corrosion Technologies Study*. Houston: NACE International, 2016.

[2]. Z. Petrovic, “Catastrophes caused by corrosion,” *Vojnotehnicki glasnik*, vol. 64, no. 4, pp. 1048–1064, 2016, doi: 10.5937/vojtehg64-10388.

[3]. S. Zhang, Y. Li, C. Wang, and X. Zhao, “Preparation of a Cr coating on low-carbon steel by electrodeposition in a NaCl-KCl-NaF-Cr2O3 molten salt,” *Int J Electrochem Sci*, vol. 14, no. 1, pp. 91–101, Jan. 2019, doi: 10.20964/2019.01.07.

[4]. N. Imaz, M. Ostra, M. Vidal, J. A. Díez, M. Sarret, and E. García-Lecina, “Corrosion behaviour of chromium coatings obtained by direct and reverse pulse plating

electrodeposition in NaCl aqueous solution," *Corros Sci*, vol. 78, pp. 251–259, Jan. 2014, doi: 10.1016/j.corsci.2013.10.005.

[5]. V. Protsenko, L. Bobrova, and F. Danilov, "Trivalent chromium electrodeposition using a deep eutectic solvent," *Anti-Corrosion Methods and Materials*, vol. 65, no. 5, pp. 499–505, Oct. 2018, doi: 10.1108/ACMM-05-2018-1946.

[6]. Michele David de Jesus Almeida, Carlos Alberto Della Rovere, Luiz Rogério Pinho de Andrade Lima , Daniel Veras Ribeiro , Carlos Alberto Caldas de Souza, "Glycerol Effect on the Corrosion Resistance and Electrodeposition Conditions in a Zinc Electroplating Process", Materials Research. 2019; 22(4), DOI: http://dx.doi.org/10.1590/1980-5373-MR-2018-0480.

[7]. Zhongyu Cui ; Xiaogang Li; Kui Xiao ; Chaofang Dong ; Zhiyong Liu ; Li Wei Wang, "Corrosion Behaviour of Field-Exposed Zinc in a Tropical Marine Atmosphere", *CORROSION* (2014) 70 (7): 731–748.

[8]. Yasakau K A et al, "Influence of stripping and cooling atmospheres on surface properties and corrosion of zinc galvanizing coatings Appl". Surf. Sci. 389 144–56, 2016.

[9]. Fan Jiang, Ke Huang, Weifeng Shi, Xinye Yang e Yingchun Zhang, "Corrosion behaviour of zinc coating electroplated at high current from a deep eutectic solvent". Materials Research Express, June de 2019, 016402

[10]. Abdelhamid, HN; Georgouvelas, D.; Edlund, U.; Mathew, AP. CelloZIFPaper: Cellulose-ZIF hybrid paper for heavy metal removal and electrochemical sensing. **Chemical Enginnering Journal**, v. 446, p. 136614, 2022.

[11]. Jiayi Chen *et al,* "Rapid Electrodeposition and Corrosion Behaviour of Zn Coating from a Designed Deep Eutectic Solvent", *Metals,* Janeiro de 2023, doi.org/10.3390/met13010172.

[12]. J. Winiarski, W. Tylus, K. Winiarska, and B. Szczygieł, "The influence of molybdenum on the corrosion resistance of ternary Zn–Co–Mo alloy coatings deposited from

citrate–sulphate bath," *Corros Sci*, vol. 91, pp. 330–340, Feb. 2015, doi: 10.1016/j.corsci.2014.11.037.

[13]. M. H. Gharahcheshmeh and M. H. Sohi, "Study of the corrosion behaviour of zinc and Zn–Co alloy electrodeposits obtained from alkaline bath using direct current," *Mater Chem Phys*, vol. 117, no. 2–3, pp. 414–421, Oct. 2009, doi: 10.1016/j.matchemphys.2009.06.009.

[14]. H. Nakano, S. Shibata, S. Arakawa, S. Oue, and S. Kobayashi, "Electrodeposition Behaviour of Zn–Co Alloys from an Alkaline Zincate Solution Containing Triethanolamine," *ISIJ International*, vol. 53, no. 10, pp. 1858–1863, 2013, doi: 10.2355/isijinternational.53.1858.

[15]. J. R. Garcia, D. C. B. do Lago, and L. F. de Senna, "Electrodeposition of Cobalt Rich Zn-Co alloy Coatings from Citrate Bath," *Materials Research*, vol. 17, no. 4, pp. 947–957, Jul. 2014, doi: 10.1590/S1516-14392014005000096.

[16]. R. S. Bhat, K. B. Manjunatha, K. Venkatakrishna, and A. C. Hegde, "Electrodeposition of Zn–Co Coating and its Electrochemical Performance," *Protection of Metals and Physical Chemistry of Surfaces*, vol. 58, no. 1, pp. 99–108, Feb. 2022, doi: 10.1134/S207020512201004X.

[17]. S. Pandiyarajan, S. S. M. Manickaraj, A.-H. Liao, A. Ramachandran, K.-Y. Lee, and H.-C. Chuang, "Construction of zinc-cobalt alloy film by supercritical-CO2 electrodeposition pathway: Evaluation of electrochemical robustness," *Inorg Chem Commun*, vol. 144, p. 109858, Oct. 2022, doi: 10.1016/j.inoche.2022.109858.

[18]. A. S. C. Urcezino, L. P. M. Dos Santos, P. N. S. Casciano, A. N. Correia, and P. De Lima-Neto, "Electrodeposition study of Ni coatings on copper from choline chloride-based deep eutectic solvents," *J Braz Chem Soc*, vol. 28, no. 7, 2017, doi: 10.21577/0103-5053.20160278.

[19]. E. Gileadi and N. Eliaz, *Physical Electrochemistry - Fundamentals, Techniques and Applications*, 2nd ed. Weinheim: Wiley-VCH, 2019.

[20]. A. P. Abbott, "Deep eutectic solvents and their application in electrochemistry," *Curr Opin Green Sustain Chem*, vol. 36, p. 100649, Aug. 2022, doi: 10.1016/j.cogsc.2022.100649.

[21]. F. Endres, D. MacFarlane, and A. Abbott, "Electrodeposition from Ionic Liquids," *Electrodeposition from Ionic Liquids*. pp. 1–387, 2008. doi: 10.1002/9783527622917.

[22]. Anca Cojocaru, Mariana Lili Mares, Paula Prioteasa, Liana Anicai e Teodor Visan, "Study of electrode processes and deposition of cobalt thin films from ionic liquid analogues based on choline chloride", Journal of Solid State Electrochemistry, 19, pages1001–1014 (2015).

[23]. Q. Chu, W. Wang, J. Liang, J. Hao, and Z. Zhen, "Electrodeposition of high Co content nanocrystalline Zn–Co alloys from a choline chloride-based ionic liquid," *Mater Chem Phys*, vol. 142, no. 2–3, pp. 539–544, Nov. 2013, doi: 10.1016/j.matchemphys.2013.07.049.

[24]. A. Yavuz, P. Yilmaz Erdogan, H. Zengin, and G. Zengin, "Electrodeposition and Characterisation of Zn-Co Alloys from Ionic Liquids on Copper," *J Electron Mater*, vol. 51, no. 9, pp. 5253–5261, Sep. 2022, doi: 10.1007/s11664-022-09756-8.

[25]. J. C. Pereira *et al.*, "Electrochemical corrosion evaluation of new Zn-Sn-In coatings electrodeposited in a eutectic mixture containing choline chloride and ethylene glycol," *Electrochim Acta*, vol. 407, p. 139647, Mar. 2022, doi: 10.1016/j.electacta.2021.139647.

[26]. R. Asseli, M. Benaicha, S. Derbal, M. Allam, and O. Dilmi, "Electrochemical nucleation and growth of Zn-Ni alloys from chloride citrate-based electrolyte," *Journal of Electroanalytical Chemistry*, vol. 847, p. 113261, Aug. 2019, doi: 10.1016/j.jelechem.2019.113261.

[27]. G. Panzeri *et al.*, “Electrodeposition of cobalt thin films and nanowires from ethylene glycol-based solution,” *Electrochem commun*, vol. 103, pp. 31–36, Jun. 2019, doi: 10.1016/j.elecom.2019.04.012.

[28]. Q. Chu, J. Liang, and J. Hao, “Electrodeposition of zinc-cobalt alloys from choline chloride–urea ionic liquid,” *Electrochim Acta*, vol. 115, pp. 499–503, Jan. 2014, doi: 10.1016/j.electacta.2013.10.204.

[29]. H. F. Alesary *et al.*, “Influence of additives on the electrodeposition of zinc from a deep eutectic solvent,” *Electrochim Acta*, vol. 304, pp. 118–130, May 2019, doi: 10.1016/j.electacta.2019.02.090.

[30]. M. Li, Z. Wang, and R. G. Reddy, “Cobalt electrodeposition using urea and choline chloride,” *Electrochim Acta*, vol. 123, pp. 325–331, Mar. 2014, doi: 10.1016/j.electacta.2014.01.052.

TABLE

Table – Values of E_{corr}, i_0, η_a and η_c obtained from PPC experiments in 3.5 $\%_{m/m}$ NaCl

Material	**E_{corr} / V**	**i_0 / A cm^{-2}**	**η_a / mV dec^{-1}**	**η_c / mV dec^{-1}**
Mild steel	−0.63	5.62×10^{-6}	73	−171
Zn	−0.97	7.71×10^{-6}	26	−115
$Zn_{96}Co_4$	−0.91	3.27×10^{-6}	33	−38
Zn_3Co_{97}	−0.57	4.56×10^{-6}	73	−68
Co	−0.60	1.21×10^{-5}	67	−57

FIGURE CAPTIONS

Figure 1 – Cyclic voltammograms at 4 mV s^{-1} and 343 K in (a) 1ChCl:2EG DES and with addition of (b) 0.4 mol L^{-1} $ZnCl_2$, (c) 0.4 mol L^{-1} $ZnCl_2$ + 0.025 mol L^{-1} $CoCl_2$, (d) 0.4 mol L^{-1} $CoCl_2$, and 0.025 mol L^{-1} $ZnCl_2$ + 0.4 mol L^{-1} $CoCl_2$ to the DES.

Figure 2 – (a) Metallic composition by EDS, along with the SEM images of (b) Zn, (c) $Zn_{96}Co_4$, (d) Zn_3Co_{97}, (e) Co and (f) mild steel substrate.

Figure 3 – Potentiodynamic polarization curves obtained in 3.5 % NaCl solution at 343 K, and at 1 mV s^{-1} for Zn, $Zn_{96}Co_4$, Zn_3Co_{97} and Co coatings.

FIGURES

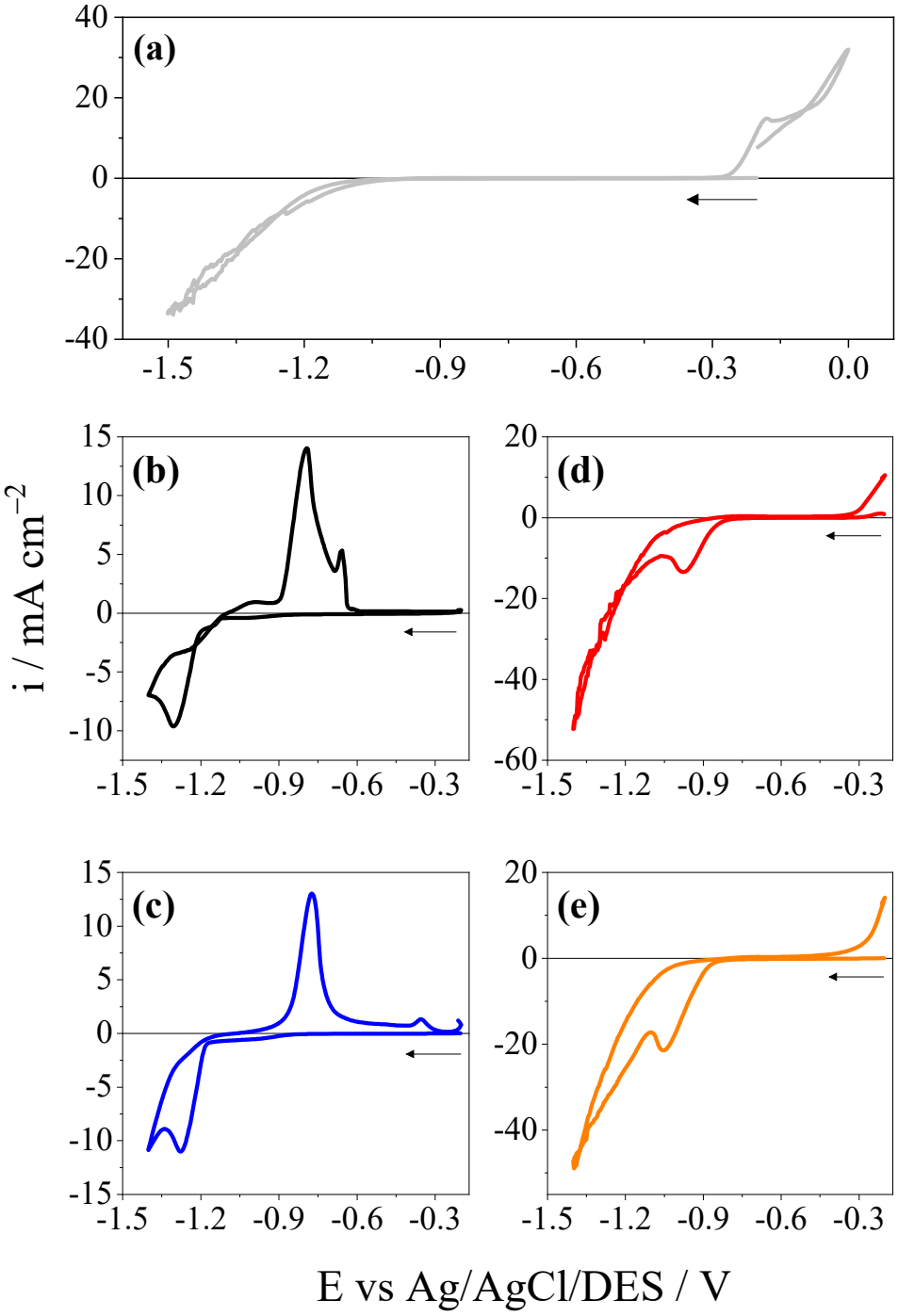

Figure 1 – Rodrigues-Júnior et al.

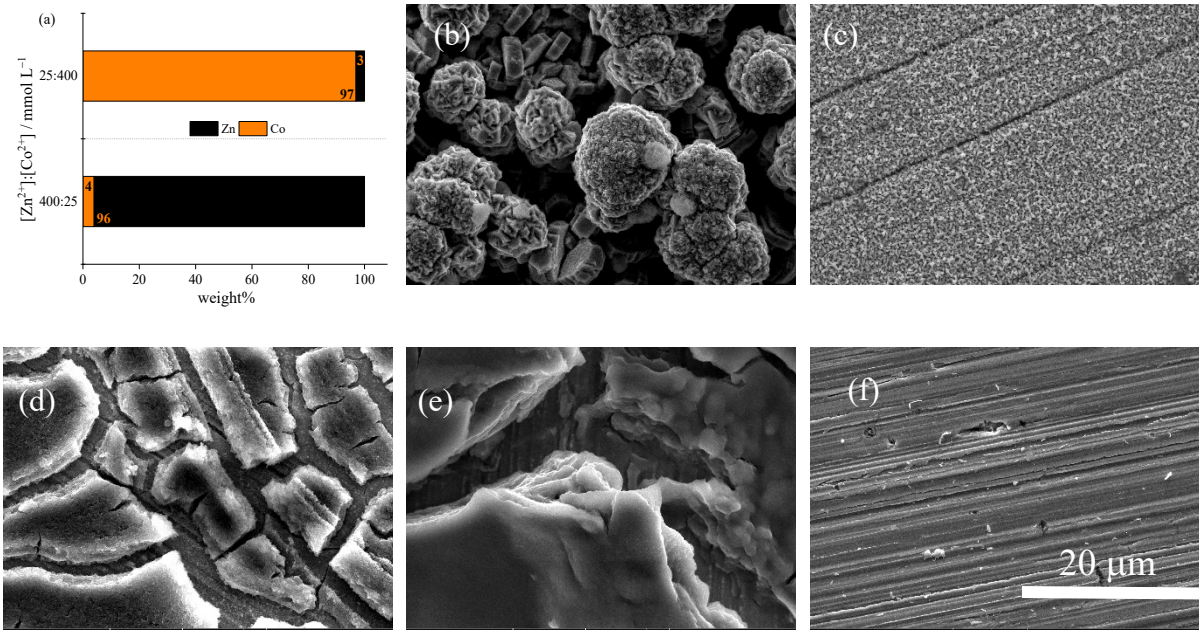

Figure 2 – Rodrigues-Júnior *et al*.

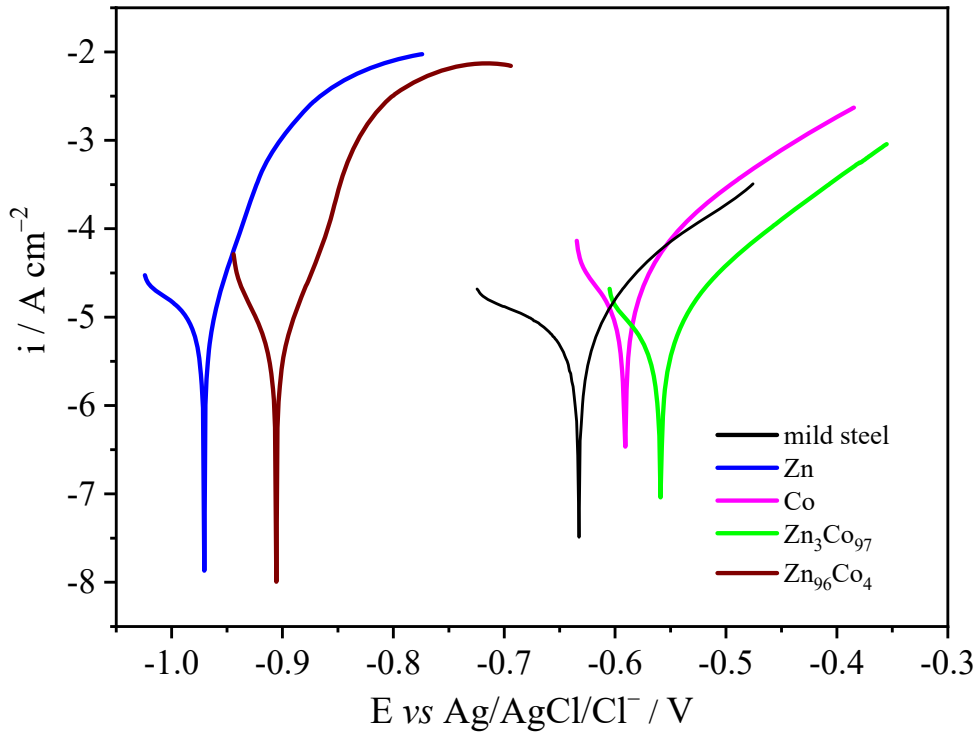

Figure 3 – Rodrigues-Júnior *et al*.

REFERÊNCIAS

1 EVERETT, D. H. Manual of Symbols and Terminology for Physicochemical Quantities and Units, Appendix II: Definitions, Terminology and Symbols in Colloid and Surface Chemistry. **Pure and Applied Chemistry**, v. 31, n. 4, p. 577-638, 1972.

2 PLETCHER, D. *et al*. **Instrumental methods in electrochemistry**. Philadelphia: Elsevier, 2001.

3 AJAYI-MAJEBI, J. *et al*. Review of electrodeposition perspectives towards anticorrosion mitigation of mild steel. **IOP Conference Series: Materials Science and Engineering**, p. 012082, 2021.

4 ELIAZ, NOAM; GILEADI, ELIEZER. **Physical electrochemistry: fundamentals, techniques, and applications**. Weinheim: Wiley-VCH, 2019.

5 LI, Y. *et al*. A review: Target-oriented transition metal phosphide design and synthesis for water splitting. **International Journal of Hydrogen Energy**, v. 46, n. 7, p. 5131-5149, 2021.

6 ĎUROVIČ, MARTIN; HNÁT, JAROMÍR; BOUZEK, KAREL. Electrocatalysts for the hydrogen evolution reaction in alkaline and neutral media. A comparative review. **Journal of Power Sources**, v. 493, p. 229708, 2021.

7 AGRAWAL, D. *et al*. Green hydrogen production pathways for sustainable future with net zero emissions, **Fuel**, v. 359, p. 130131,
2024.

8 GODINHO, I. Energia limpa pode levar desenvolvimento verde ao Nordeste. **Folha de S. Paulo**, São Paulo, 29 jun. 2023. Disponível em: https://www1.folha.uol.com.br/seminariosfolha/2023/06/energia-limpa-pode-levar-desenvolvimento-verde-ao-nordeste.shtml. Acesso em: 05 jan. 2024.

9 COMPLEXO INDUSTRIAL E PORTUÁRIO DO PECÉM. **HUB de hidrogênio verde do complexo do Pecém**. Pecém: CIPP, 2024. Disponível em: https://www.complexodopecem.com.br/hubh2v/. Acesso em: 05 jan. 2024.

10 GENTIL, V. **Corrosão**. 6. ed. Rio de Janeiro: LTC, 2017.

11 UNIVERSIDADE FEDERAL DO CEARÁ et al. **Estudo da agressividade do ar em Fortaleza/CE**. 2016.

12 CARIM, A. I. *et al*. Electrocatalysis of the hydrogen-evolution reaction by electrodeposited amorphous cobalt selenide films. **Journal of Materials Chemistry A**, v. 2, n. 34, p. 13835-13839, 2014.

13 KUBLANOVSKY, V. S.; YAPONTSEVA, Y. S. Electrocatalytic properties of Co-Mo alloys electrodeposited from a citrate-pyrophosphate electrolyte. **Electrocatalysis**, v. 5, n. 4, p. 372-378, 2014.

14 BHAT, R.S. *et al*. Electrochemical Studies of Zn-Ni-Fe Alloy Coatings for Better Corrosion Resistance Applications. **J. of Materi Eng and Perform**, v. 31, pp. 6819–6826, 2022.

15 LIN, Y. *et al*. Effect of rhenium on corrosion behaviour of electrodeposited Co-Cu alloy coating at room temperature and high temperature. **Materials Today Communications**, v. 35, p. 105579, 2023.

16 CLARE, B.; SIRWARDANA, A.; MacFARLANE, D. R. Synthesis, purification and characterization of ionic liquids. **Topics in Current Chemistry**, v. 290, p. 1-40, 2009.

17 ENDRES, FRANK; ABBOTT, ANDREW; MACFARLANE, DOUGLAS R. (ed.). **Electrodeposition from ionic liquids**. Weinheim: Wiley-VCH, 2017.

18 LEI, C. *et al*. Gamma-phase Zn-Ni alloy deposition by pulse-electroplating from a modified deep eutectic solution. **Surface and Coatings Technology**, v. 403, p. 126434, 2020.

19 ABBOTT, A. P. *et al*. Deep eutectic solvents formed between choline chloride and carboxylic acids: versatile alternatives to ionic liquids. **Journal of the American Chemical Society**, v. 126, n. 29, p. 9142-9147, 2004.

20 WAZEER, IRFAN; HAYYAN, MAAN; HADJ-KALI, MOHAMED K. Deep eutectic solvents: designer fluids for chemical processes. **Journal of Chemical Technology & Biotechnology**, v. 93, n. 4, p. 945-958, 2018.

21 URCEZINO, A. S. C. **Eletrodeposição de Níquel e Ligas Níquel-Ferro em Solventes Eutéticos Baseados em Cloreto de Colina**. Orientador: Pedro de Lima Neto. 2017. Tese (Doutorado em Química) – Centro de Ciências, Universidade Federal do Ceará, Fortaleza, 2017.

22 URCEZINO, A. S. C. *et al*, Electrodeposition study of Ni coatings on copper from choline chloride-based deep eutectic solvents. **Journal of the Brazilian Chemical Society**, v. 28, p. 1193-1203, 2017.

23 PEREIRA, J. C. *et al*. Effects of electrodeposition parameters on corrosion resistance of ZnSn coatings on carbon steel obtained from eutectic mixture based on choline chloride and ethylene glycol. **Journal of Alloys and Compounds**, v. 886, p. 161159, 2021.

24 PEREIRA, J. C. *et al*. Electrochemical corrosion evaluation of new Zn-Sn-In coatings electrodeposited in a eutectic mixture containing choline chloride and ethylene glycol. **Electrochimica Acta**, v. 407, p. 139647, 2022.

25 SANTOS, L. P. *et al*. Electrodeposition of 1-D tellurium nanostructure on gold surface from choline chloride-urea and choline chloride-ethylene glycol mixtures. **Journal of Molecular Liquids**, v. 288, p. 111038, 2019.

26 PRABHUNE, A.; DEY, R. Green and sustainable solvents of the future: Deep eutectic solvents. **Journal of Molecular Liquids**, v. 379, p. 121676, 2023.

27 RUDNEV, A. V. Electrodeposition of lanthanides from ionic liquids and deep eutectic solvents. **Russian Chemical Reviews**, v. 89, n. 12, p. 1463, 2020.

28 ABBOTT, A. P. Deep eutectic solvents and their application in electrochemistry. **Current Opinion in Green and Sustainable Chemistry**, v. 36, p. 100649, 2022.

29 ZAHRA, R. *et al*. A review on nickel cobalt sulphide and their hybrids: Earth abundant, pH stable electro-catalyst for hydrogen evolution reaction. **International Journal of Hydrogen Energy**, v. 45, n. 46, p. 24518-24543, 2020.

30 LI, M.;WANG, Z.; REDDY, R. G. Cobalt electrodeposition using urea and choline chloride. **Electrochimica Acta**, v. 123, p. 325-331, 2014.

31 ALESARY, H. F. *et al*. Influence of additives on the electrodeposition of zinc from a deep eutectic solvent. **Electrochimica Acta**, v. 304, p. 118-130, 2019.

32 CHU, Q.; LIANG, J.; HAO, J. Electrodeposition of zinc-cobalt alloys from choline chloride–urea ionic liquid. **Electrochimica Acta**, v. 115, p. 499-503, 2014.

33 ROSEN, J. *et al*. Electrodeposited Zn dendrites with enhanced CO selectivity for electrocatalytic CO2 reduction. **Acs Catalysis**, v. 5, n. 8, p. 4586-4591, 2015.

34 ANWAR, S. *et al*. Recent development in electrocatalysts for hydrogen production through water electrolysis. **International Journal of Hydrogen Energy**, v. 46, n. 63, p. 32284-32317, 2021.

35 ARVIA, A. J.; BOLZÁN, A. E.; PASQUALE, M. A. Electrocatalysis: a survey of fundamental concepts. *In:* **Catalysis in electrochemistry**: from fundamentals to strategies for fuel cell development. Hoboken: John Wiley & Sons, 2011. p. 17-65.

36 JOKAR, A. *et al*. Facile electrochemical synthesis of Ni-Co-B film on Cu sheet for dual-electrocatalysis of hydrogen and oxygen evolution reactions. **Electrochimica Acta**, v. 389, p. 138691, 2021.

37 MAZLOOMI, KAVEH; GOMES, CHANDIMA. Hydrogen as an energy carrier: Prospects and challenges. **Renewable and Sustainable Energy Reviews**, v. 16, n. 5, p. 3024-3033, 2012.

38 WU, LIHENG; XI, ZHENG; SUN, SHOUHENG. Well-defined metal nanoparticles for electrocatalysis. In: **Studies in Surface Science and Catalysis**. Elsevier, 2017. p. 123-148.

39 GROSS, AXEL; SCHNUR, SEBASTIAN. Computational chemistry applied to reactions in electrocatalysis. **Catalysis in Electrochemistry**, p. 165-196, 2011.

40 LIM, TAEHO; KIM, SOO-KIL. Non-precious hydrogen evolution reaction catalysts: Stepping forward to practical polymer electrolyte membrane-based zero-gap water electrolyzers. **Chemical Engineering Journal**, v. 433, p. 133681, 2022.

41 PAUL, S. C. *et al*. Nanomaterials as electrocatalyst for hydrogen and oxygen evolution reaction: Exploitation of challenges and current progressions. **Polyhedron**, v. 193, p. 114871, 2021.

42 FU, H. Q. *et al*. Hydrogen spillover-bridged Volmer/Tafel processes enabling ampere-level current density alkaline hydrogen evolution reaction under low overpotential. **Journal of the American Chemical Society**, v. 144, n. 13, p. 6028-6039, 2022.

43 WEI, L. *et al*. **Electrocatalyst Preparation by Electrodeposition**. Encyclopedia of Interfacial Chemistry, p. 507-520, 2018.

44 PLEVOVA, MICHAELA; HNAT, JAROMIR; BOUZEK, KAREL. Electrocatalysts for the oxygen evolution reaction in alkaline and neutral media. A comparative review. **Journal of Power Sources**, v. 507, p. 230072, 2021.

45 PI, C. *et al*. In situ construction of γ-MoC/VN heterostructured electrocatalysts with strong electron coupling for highly efficient hydrogen evolution reaction. **Chemical Engineering Journal**, v. 416, p. 129130, 2021.

46 SOUSA, J. B. **Estudo da influência dos parâmetros operacionais na eletrodeposição de camadas eletrocatalíticas de ligas de Ni-Fe**. 2007. Orientador: Pedro de Lima Neto. Dissertação (Mestrado em Ciências Química Inorgânica) – Centro de Ciências, Universidade Federal do Ceará, Fortaleza, 2007.

47 LI, R. *et al*. Electrodeposition: Synthesis of advanced transition metal-based catalyst for hydrogen production via electrolysis of water. **Journal of Energy Chemistry**, v. 57, p. 547-566, 2021.

48 LOPEZ, MIGUEL BERNAL; USTARROZ, JON. Electrodeposition of nanostructured catalysts for electrochemical energy conversion: Current trends and innovative strategies. **Current Opinion in Electrochemistry**, v. 27, p. 100688, 2021.

49 TAHIR, M. *et al*. Electrocatalytic oxygen evolution reaction for energy conversion and storage: a comprehensive review. **Nano Energy**, v. 37, p. 136-157, 2017.

50 ZHANG, S. *et al*. A kind of electro-catalyst with high efficiency for hydrogen evolution reaction: Platinum particles dispersed on multi-walled carbon nanotubes. **Materials Letters**, v. 312, p. 131704, 2022. *Materials Letters*, vol. 312, p. 131704, 2022.

51 LIU, W. *et al*. Electrodeposition of self–supported Ni–Mg–La electrocatalyst on Ni foam for efficient hydrogen evolution reaction. **Electrochimica Acta**, v. 411, p. 140058, 2022.

52 NEMIWAL, M.; ZHANG, T. C.; KUMAR, D. Graphene-based electrocatalysts: Hydrogen evolution reactions and overall water splitting. **International Journal of Hydrogen Energy**, v. 46, n. 41, p. 21401-21418, 2021.

53 NITHYA, V. D. Recent advances in CoSe2 electrocatalysts for hydrogen evolution reaction. **International Journal of Hydrogen Energy**, v. 46, n. 73, p. 36080-36102, 2021.

54 ZHANG, S. *et al*. Recent advances in non-precious metal electrocatalysts for pH-universal hydrogen evolution reaction. **Green Energy & Environment**, v. 6, n. 4, p. 458-478, 2021.

55 LIU, X. *et al*. Amorphous NiFe–OH/Ni–Cu–P supported on self-supporting expanded graphite sheet as efficient bifunctional electrocatalysts for overall water splitting. **International Journal of Hydrogen Energy**, v. 45, n. 55, p. 30387-30395, 2020.

56 GUO, MENGWEI; WEI, ZHUOMING; ZHANG, QIBO. Electrochemical construction of S-doped MnOx/Mn integrated film on carbon paper in a choline chloride based deep eutectic solvent for enhanced electrochemical water oxidation. **International Journal of Hydrogen Energy**, v. 47, n. 9, p. 6029-6043, 2022.

57 EFTEKHARI, ALI. Electrocatalysts for hydrogen evolution reaction. **International Journal of Hydrogen Energy**, v. 42, n. 16, p. 11053-11077, 2017.

58 KHAJEHSAEIDI, ZAHRA; SANGPOUR, PARVANEH; GHAFFARINEJAD, ALI. A novel co-electrodeposited Co/MoSe2/reduced graphene oxide nanocomposite as electrocatalyst for hydrogen evolution. **International Journal of Hydrogen Energy**, v. 44, n. 36, p. 19816-19826, 2019.

59 YANG, S. *et al*. One-step electrodeposition of carbon quantum dots and transition metal ions for N-doped carbon coupled with NiFe oxide clusters: A high-performance electrocatalyst for oxygen evolution. **Nano Energy**, v. 77, p. 105057, 2020.

60 YU, X. *et al*. Multi-walled carbon nanotubes supported porous nickel oxide as noble metal-free electrocatalysts for efficient water oxidation. **International journal of hydrogen energy**, v. 39, n. 20, p. 10467-10475, 2014.

61 SHENG, M. *et al*. Co-W/CeO2 composite coatings for highly active electrocatalysis of hydrogen evolution reaction. **Journal of Alloys and Compounds**, v. 743, p. 682-690, 2018.

62 YAO, Y. *et al*. Electrocatalytic degradation of methylene blue on PbO2-ZrO2 nanocomposite electrodes prepared by pulse electrodeposition. **Journal of hazardous materials**, v. 263, p. 726-734, 2013.

63 YANG, Y. *et al*. Electrocatalytic properties of porous Ni-Co-WC composite electrode toward hydrogen evolution reaction in acid medium. **International Journal of Hydrogen Energy**, v. 44, n. 36, p. 19771-19781, 2019.

64 AGRISUELAS, J. *et al*. Electrochemistry and electrocatalysis of a Pt@ poly (neutral red) hybrid nanocomposite. **Electrochimica Acta**, v. 171, p. 165-175, 2015.

65 HAN, H. *et al*. Fabrication of BN modified Ti/PbO2 electrodes with tunable hydrophobic characteristics and their electrocatalytic performance. **Journal of Alloys and Compounds**, v. 828, p. 154049, 2020.

66 PU, Z. *et al*. Graphene film-confined molybdenum sulfide nanoparticles: Facile one-step electrodeposition preparation and application as a highly active hydrogen evolution reaction electrocatalyst. **Journal of Power Sources**, v. 263, p. 181-185, 2014.

67 XIAO, X. *et al*. Hydrogen evolution at nanoporous gold/tungsten sulfide composite film and its optimization. **Electrochimica Acta**, v. 173, p. 393-398, 2015.

68 YIN, D. *et al*. In situ growth of copper/reduced graphene oxide on graphite surfaces for the electrocatalytic reduction of nitrate. **Electrochimica Acta**, v. 324, p. 134846, 2019.

69 JAMESH, MOHAMMED-IBRAHIM; SUN, XIAOMING. Recent progress on earth abundant electrocatalysts for oxygen evolution reaction (OER) in alkaline medium to achieve efficient water splitting–A review. **Journal of Power Sources**, v. 400, p. 31-68, 2018.

70 HEUSLER, K. E., LANDOLT, D., TRASATTI, S. Electrochemical corrosion nomenclature (Recommendations 1988). **Pure and Applied Chemistry**, v. 61, n. 1, 1989, p. 19-22.

71 VARNEY, J. *et al*. **International Measures of Prevention, Application, and Economics of Corrosion Technologies Study**, 2016.

72 BRINQUEDO que 'travou' e deixou 8 feridos em parque de diversões em MG tem sinais de corrosão e ferrugem, diz Corpo de Bombeiros. **G1 Triângulo e Alto Parnaíba**, Monte Carmelo, 11 jul. 2022. Disponível em: https://g1.globo.com/mg/triangulo-mineiro/noticia/2022/07/11/brinquedo-que-travou-e-deixou-8-feridos-em-parque-de-diversoes-em-mg-tem-sinais-de-corrosao-e-ferrugem-diz-corpo-de-bombeiros.ghtml. Acesso em: 17 dez. 2023.

73 ALMEIDA, M. D. D. J. *et al*. Glycerol effect on the corrosion resistance and electrodeposition conditions in a zinc electroplating process. **Materials Research**, v. 22, n. 4, p. e20180480, 2019.

74 YASAKAU, K. A. *et al*. Influence of stripping and cooling atmospheres on surface properties and corrosion of zinc galvanizing coatings. **Applied Surface Science**, v. 389, p. 144-156, 2016.

75 ONKARAPPA, N. K. *et al*. Influence of additives on morphology, orientation and anti-corrosion property of bright zinc electrodeposit. **Surface and Coatings Technology**, v. 397, p. 126062, 2020.

76 BURLIAEV, D. V.; KOZADEROV, O. A.; VOLOVITCH, P. Zinc-nickel alloy coatings: electrodeposition kinetics, corrosion, and selective dissolution. A review. **Condensed Matter and Interphases**, v. 23, n.1, p. 3-15, 2021.

77 PEREIRA, N. M. *et al*. Zinc Electrodeposition from deep eutectic solvent containing organic additives. **Journal of Electroanalytical Chemistry**, v. 801, p. 545-551, 2017.

78 YAVUZ, A. *et al*. Electrodeposition and Characterisation of Zn-Co Alloys from Ionic Liquids on Copper. **J. Electron. Mater.**, v. 51, p. 5253–5261, 2022.

APÊNDICE A – MANUSCRITO 1 - $Zn_xCo_{(1-x)}$ *COATINGS FROM CHOLINE CHLORIDE-ETHYLENE GLYCOL DEEP EUTECTIC SOLVENT AS ELECTROCATALYSTS FOR HYDROGEN EVOLUTION REACTION* - PUBLICADO NO PERIÓDICO *JOURNAL OF ELECTROANALYTICAL CHEMISTRY*

Journal of Electroanalytical Chemistry 947 (2023) 117785

Contents lists available at ScienceDirect

Journal of Electroanalytical Chemistry

journal homepage: www.elsevier.com/locate/jelechem

$Zn_xCo_{(1-x)}$ coatings from choline chloride-ethylene glycol deep eutectic solvent as electrocatalysts for hydrogen evolution reaction

Deomar N. Rodrigues-Júnior [a], Natalia G. Sousa [a], F. Murilo T. Luna [b], Thiago M.B.F. Oliveira [c], Dieric S. Abreu [d], Walther Schwarzacher [e], Pedro de Lima-Neto [a], Adriana N. Correia [a,*]

[a] Grupo de Eletroquímica e Corrosão, Departamento de Química Analítica e Físico-Química, Centro de Ciências, Universidade Federal do Ceará, Campus do Pici, Fortaleza, CE 60440-900, Brazil
[b] Grupo de Pesquisa em Separações por Adsorção, Departamento de Engenharia Química, Centro de Tecnologia, Universidade Federal do Ceará, Campus do Pici, Fortaleza, CE 60455-760, Brazil
[c] Laboratório de Química Aplicada, Centro de Ciência e Tecnologia, Universidade Federal do Cariri, Juazeiro do Norte, CE 63048-080, Brazil
[d] Laboratório de Materiais e Dispositivos, Departamento de Química Analítica e Físico-Química, Centro de Ciências, Universidade Federal do Ceará, Campus do Pici, Fortaleza, CE 60440-900, Brazil
[e] H. H. Wills Physics Laboratory, University of Bristol, Tyndall Avenue, Bristol, BS8 1TL, United Kingdom

ARTICLE INFO

Keywords:
Water splitting
Hydrogen production
Metallic coatings
Deep eutectic solvents
Electrocatalysis

ABSTRACT

Hydrogen has emerged as a clean and renewable energy and its production by water splitting is a promising production route. However, to meet the demand on a commercial scale, research focusing on more efficient electrocatalysts is necessary. In this work, new findings on Zn, Co and Zn-Co coatings produced in deep eutectic solvent based on choline chloride (ChCl) and ethylene glycol (EG) are reported. Varying the concentrations of Zn^{2+} and Co^{2+} ions in 1ChCl:2EG, crystalline electrodeposits with fine control of composition and morphology were obtained, and which present different reactivity to electrocatalyze the hydrogen evolution reaction (HER) in alkaline medium. The performance of metallic coatings is influenced by temperature, due to changes in viscosity, ionic diffusion coefficient and charge transport in the electrolyte. The results also revealed that increasing the Co content in the coatings, changes occur in the morphological organization, stability, and electrode area, which positively influence the hydrogen production. Among the different coatings tested (Zn, Co, Zn_{95}-Co_4 and Zn_3-Co_{97}), Zn_3-Co_{97} was the most promising in terms of Tafel coefficient (108 mV dec^{-1}), exchange current density (8.57×10^{-6} A cm^{-2}) and overpotential estimated for HER (333 mV at 10 mA cm^{-2}) in 1 mol L^{-1} KOH at 298.15 K, although the other materials also showed electrochemical advantages over the unmodified Cu substrate. The reported data also reiterate the great electrochemical potential of metallic coatings for water splitting and complement the growing energy demand for hydrogen gas.

1. Introduction

The deleterious effects caused to the environment from non-renewable energy sources, such as fossil fuels, coal, and petroleum, require urgent and more sustainable alternatives to reduce greenhouse gas emissions and, consequently, the disastrous effects of global warming [1]. Today, hydrogen stands out among the most promising alternatives, since it can be produced from renewable sources and has a highly attractive energy density per mass (≈ 140 MJ kg^{-1}) and volume (≈ 0.011 MJ kg^{-1}) at room temperature, compared to more traditional fuels [1–4]. One of the great challenges is that there is not freely available and ready-to-use hydrogen, requiring appropriate methods and systems to extract it from energetically stable precursors, such as water and hydrocarbons. Water splitting is simpler and easier to accomplish, and the type of electrocatalyst employed has a significant impact on the HER yield in terms of reaction overpotential, corrosion resistance and resulting current density [1,2,5–7].

It is known that noble metal (Pt, Ru and Ir)-based electrocatalysts are highly reactive toward HER, but their scarcity and high cost make them uneconomic for large-scale production and application [8–13]. Cobalt and its alloys have a better cost-benefit ratio, besides combine different electrochemical advantages (e.g., excellent electrical conductivity, high activity, and stability in alkaline medium) that arouse speculation regarding their efficiency in producing hydrogen by water splitting

* Corresponding author.
E-mail address: adriana@ufc.br (A.N. Correia).

https://doi.org/10.1016/j.jelechem.2023.117785
Received 25 July 2023; Received in revised form 29 August 2023; Accepted 7 September 2023
Available online 14 September 2023

[14–17]. Such performance is linked to several parameters of synthesis and application of these materials, which must be meticulously studied and continuously improved. Pan et al. [18] studied cobalt-coated copper substrates as HER electrocatalysts in 30 wt% KOH. These authors identified remarkable changes in the structural arrangement, morphology, and reactivity of the electrodeposits according to the electrolytic medium, presence of oxygen and temperature of synthesis, so that the lowest overpotential and highest surface roughness factor for HER was obtained from an acetate-enriched solution, kept at 25 °C. Maurya et al. [19] also showed reactivity changes when HER was promoted in 1 mol/L KOH, using Ni-Co coatings immobilized onto copper and steel derived substrates as electroactive surfaces, suggesting a synergistic effect of intercalated materials in the electrode configuration. Kublanovsky and Yapontseva [20] found that electrodeposited Co-Mo alloys can have better electrocatalytic properties in alkaline medium (reduction in HER overpotential around 400 mV) than pure Co, especially when obtained from 10:1% (v/v) Co:Mo compositions. Ling et al. [21] also reported that doping CoO nanorods with Ni and Zn has an important electrocatalytic effect for HER in alkaline medium, Zn being responsible for modulating bulk electronic structure and boost electrical conduction. Other Zn-containing materials have been successfully applied as electrocatalysts for water splitting. Sumesh [22] prepared zinc oxide functionalized molybdenum disulfide heterostructures (MoS_2-ZnO) and tested them for HER electrocatalysis in acidic medium, without compromising their structural stability. Additionally, Cao et al. [23] worked with metal-dopped carbon nanotubes and found that Zn both reduced charge-transfer resistance and increased the proportion of reactive sites available to produce hydrogen.

Since Co and Zn have a positive effect on water splitting, coatings made with combinations of them can achieve superior performance and deserve more attention. Electrodeposition is a simple and low-cost way to produce Zn-Co electrocatalysts for HER, either by potentiostatic or galvanostatic mode [24]. However, the electrosynthesis of metallic coatings from aqueous solutions can compromise their stability due to the existence of parallel reduction reactions, including HER itself. There are also limitations regarding cathodic efficiency, working potential range, and electrodeposit adhesion. Water volatility also narrows the working temperature range, leading to frequent need for electrolyte bath additives and increased laboratory waste [25,26].

Deep eutectic solvents (DES) overcome the limitations and provide a wide range of working potential for electrodepositing various metals and alloys. They are non-ideal liquid mixtures of organic salts with hydrogen bond donors, such as amides, amines, alcohols and carboxylic acids. DES still have high electrical conductivity and solubility for metallic salts, are non-flammable even at relatively high temperatures, biodegradable, produced simply and cheaply [25,27–29]. In the electrodeposition of metals and alloys, DES formed by choline chloride (ChCl) and ethylene glycol (EG) have been used with great success [30–33]. From this perspective, the main objective of this work was to produce coatings of Zn, Co, and Zn-Co from ChCl/EG-based DES, as well as to evaluate the physicochemical properties and effectiveness of these electrodeposits to promote HER in alkaline environment.

2. Experimental procedures

2.1. Chemicals and electrolytic solutions

ChCl, EG, zinc chloride ($ZnCl_2$) and cobalt chloride ($CoCl_2$) were purchased from Sigma-Aldrich and used as received. ChCl and EG were mixed in a 1:2 M ration (1ChCl:2EG) and heated to 353 K until a colorless and homogeneous liquid was formed [15]. The electrodeposition solutions were obtained by dissolving $ZnCl_2$ (0.025 mol/L or 0.4 mol/L Zn^{2+}) and $CoCl_2$ (0.025 mol/L or 0.4 mol/L Co^{2+}) in 1ChCl:2EG, under constant agitation. Since the electric conductivity of the electrolytes strongly depends on the water content, this parameter was determined by Karl Fischer coulometric titration (899 coulometer, Metrohm) in freshly prepared DES mixtures. The water content in 1ChCl:2EG was 13.25 ± 0.06 ppm and ranged from 23.32 ± 0.13 to 57.87 ± 0.31 ppm after adding Zn^{2+} and Co^{2+}.

2.2. Electrochemical experiments

Electrochemical experiments were carried out using a glass electrochemical cell configured with three electrodes. The working electrode was a copper disc embedded in epoxy resin, with an exposed geometric area of approximately 0.023 cm^2. Before each experiment, the working electrode was mechanically polished with 100, 400 and 600-grain size sandpaper, following this sequence, and washed with Milli-Q® water (18.2 MΩ cm). A platinum plate (1 cm^2 geometric area; 99.5% purity) and a silver wire covered with AgCl and immersed in 1ChCl:2EG, were used as auxiliary and reference electrodes, respectively. The tests were carried out in a potentiostat/galvanostat AUTOLAB PGSTAT30, Metrohm-Eco Chemie, controlled by NOVA 2.1 software.

Electrodeposition processes of metallic coatings were monitored by cyclic voltammetry (CV) at 5 mV s^{-1}, keeping the system at 343 K. The ion diffusion coefficients in the deep eutectic solvent were evaluated at different temperatures (303–343 K), using chronoamperometry data adapted to the Cottrell Equation. For these experiments, three electrochemical potentials (i.e., −0.4, −0.8 and −1.3 V) were evaluated for 60 s, chosen from cyclic voltammetry data registered with a Cu substrate (0.023 cm^2 geometric area) immersed in 1ChCl:2EG containing 0.4 mol/L $CoCl_2$ and 0.4 mol/L $ZnCl_2$.

The influence of metallic coatings and selected experimental conditions on HER were studied by linear sweep voltammetry (LSV) at 0.5 mV s^{-1}, using 1 mol/L KOH at 298 K as electrolyte and $Hg_{(s)}|HgO_{(s)}|OH^-_{(aq)}$ (1 mol/L KOH) as reference electrode [30]. The measured potentials (E_{H_2/H_2O}) were converted to those of the reversible hydrogen electrode (E_{RHE}), through the following equation:

$$E_{RHE}\,(\mathrm{V}) = E_{H_2/H_2O}\,(\mathrm{V}) + 0.095 + 0.059pH \quad (1)$$

Coating stability tests were performed over 100 h in a two-electrode cell, applying an average operating potential of −1.8 V at 10 mA cm^{-2}, being repeated three times. Coatings with a nominal thickness around 1.0 μm were immobilized on copper substrates (0.20 cm^2 geometric area), and the results were compared to those obtained with the same electrode without coating and with an AISI 304 stainless steel electrode (0.18 cm^2 geometric area). The electrical circuit was concluded with a stainless steel AISI 304 counter-electrode (0.69 cm^2 geometric area), immersed together with the working electrode in 1 mol/L KOH at 333 K. The current density was set at 10 mA cm^{-2}, taking into account the high HER yield and stability of the coatings, using a direct current power source monitored by a multimeter at fixed time intervals. Specific mass and viscosity measurements were performed with an Anton Paar's Stabinger viscometer, model SVM 3000.

2.3. Electrodeposition of metallic coatings

Zn and Co electrodeposits were obtained from 1ChCl:2EG electrolytes containing 0.4 mol/L Zn^{2+} and 0.4 mol/L Co^{2+}, without mechanical convection influence. Zn_x-$Co_{(1-x)}$ coatings were obtained from solutions with different Zn^{2+}:Co^{2+} molar ratios, i.e., $[Zn^{2+}]$ = 0.4 mol/L and $[Co^{2+}]$ = 0.025 mol/L or $[Zn^{2+}]$ = 0.025 mol/L and $[Co^{2+}]$ = 0.4 mol/L. Electrodeposits were obtained potentiostatically at −1.3 V and 343 K, with charge control to obtain coatings with a nominal thickness of 1 μm.

2.4. Complementary physicochemical characterisations

The surface morphology of the coatings was evaluated using a field emission scanning electron microscope (SEM; FEG-SEM FEI-Quanta 450), operating at 20 keV. The atomic percentages of Zn and Co in the

coatings were determined by energy-dispersive X-ray spectroscopy (EDS), using a spectrometer coupled to the microscope. The crystallinity and composition of electrodeposits were also evaluated by X-ray diffraction (XRD) analyses, using a Rigaku DMAXB diffractometer, which operated with a 2 kW X-ray generator and CuKα copper radiation (λ = 0.154 nm). Crystalline phases were identified using the X-Pert HighScore Plus version 3.0.5 (PANalytical®) program, associating the results with the International Centre for Diffraction Data (ICDD)/Joint Committee on Powder Diffraction Standards (JCPDS) database.

3. Results and discussion

3.1. Electrochemical characterisation

Initially, CV studies were performed with cooper substrates at 5 mV s^{-1} in pure ChCl/EG-based DES and after adding Zn^{2+} and Co^{2+}, to monitor and evaluate the efficiency of the electrodeposition conditions employed. The result illustrated in Fig. 1a demonstrated that no process was observed in 1ChCl:2EG, varying the potential between −0.4 V and −1.3 V. Above this range, there was a sharp increase in the current density, due to the decomposition of the eutectic solvent caused by the reduction of hydroxyl groups present in ethylene glycol and choline ions [32]. In Fig. 1b, during the positive scan, three well-defined anodic processes with different intensities appeared between −1.1 and −0.6 V, related to the dissolution of zinc electrodeposits and possible Zn-Cu intermetallic entities. A similar profile was observed by Alesary et al. [34], using a Pt electrode polarized anodically in 1ChCl:2EG containing 0.4 mol L^{-1} Zn^{2+}, keeping the system at 353 K. There is also a crossover of cathodic and anodic currents around −1.1 V, which indicates self-organization of crystals by nucleation and electrodeposit growth.

In Fig. 1c, there is a small increase in cathodic current attributed to cobalt reduction around −0.9 V. Then, a significant increase in the cathodic current at −1.2 V begins, followed by a discrete current loop, resulting from the nucleation of zinc on cobalt. In the anodic scan, there are three well-defined processes related to the dissolution of metals, so that the first two refer to zinc and the last to cobalt. Chu et al. [35] obtained analogous results for Zn-Co coatings, produced from 1ChCl:2U at 353 K, using cyclic voltammetry at 50 mV s^{-1}. They attributed the first two anodic processes (at less positive potentials) to zinc dissolution from different phases of the Zn-Co alloy, followed by dissolution of the cobalt electrodeposits as a third process. In Fig. 1d, there is only one process in the cathodic scan before solvent decomposition. This process results from the reduction of cobalt, as its concentration is 16 times higher than zinc. No process is observed in the anodic scan between −0.4 V and −1.3 V. The observed result is also very similar to that shown in Fig. 1e, whose voltammogram was recorded in the electrochemical cell containing only cobalt.

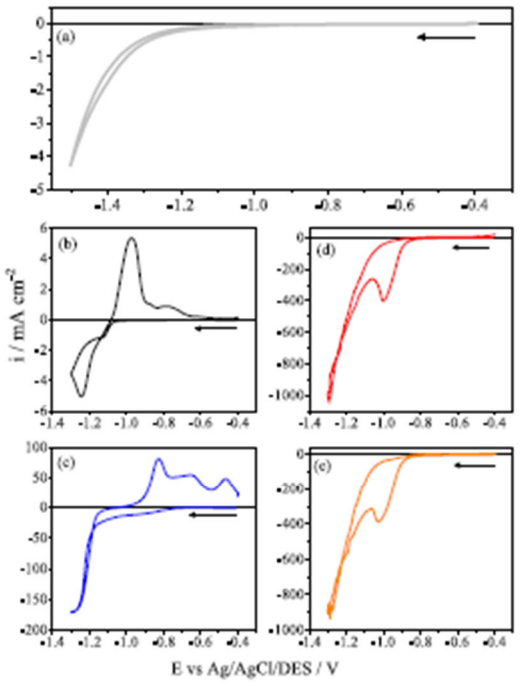

Fig. 1. Cyclic voltammograms obtained at 5 mV s^{-1} in (a) 1ChCl:EG and after adding (b) 0.4 mol L^{-1} $ZnCl_2$, (c) 0.4 mol L^{-1} $ZnCl_2$ + 0.025 mol L^{-1} $CoCl_2$, (d) 0.025 mol L^{-1} $ZnCl_2$ + 0.4 mol L^{-1} $CoCl_2$, (e) 0.4 mol L^{-1} $CoCl_2$.

3.2. Relationship between coating stability, ionic diffusion, and temperature

Chronoamperometric experiments are very useful to examine the electrochemical activity and stability of metallic coatings, especially under temperature gradients. In this work, studying HER at −1.3 V in 1 mol/L KOH (previously optimized condition based on reaction yield and corrosion resistance), an increase in mass-transport-limited current densities was noticed as the temperature increased from 303 K to 343 K, both for Zn and Co-based coatings. This is related to the decrease in the viscosity of the solutions at higher temperatures, which allows faster ion diffusion and a consequent increase in current density. Issues related to mass- and charge-transport variations resulting from temperature changes and their influence on viscosity have also been reported by Fu et al. [36], based on studies on the electrochemical nucleation of copper in ChCl:EG. From the Cottrell Equation [37], it is also possible to verify the impact of the temperature increase on the ionic diffusion coefficient (D), as shown in Table 1. For cobalt coatings, D values varied between $2.6 \times 10^{-7} \pm 0.7 \times 10^{-8}$ cm^2 s^{-1} and $4.4 \times 10^{-7} \pm 0.5 \times 10^{-7}$ cm^2 s^{-1}, while for zinc coatings the variation was from $8.9 \times 10^{-11} \pm 0.8 \times 10^{-11}$ cm^2 s^{-1} to $4.5 \times 10^{-10} \pm 0.3 \times 10^{-10}$ cm^2 s^{-1}. The same trend was observed by Phuong et al. [38] for the nucleation of Co^{2+} ions in 1ChCl:2U, as the temperature increased from 313 K to 343 K.

For comparison purposes, Table 1 also gathers other D values obtained for Co- and Zn-based coatings obtained in different solvents and temperatures [38–44]. For both cases, the values were equivalent to those obtained by other authors who studied coatings produced from the same deep eutectic solvent (7.1×10^{-10} cm^2 s^{-1} at 313 K for Zn^{2+} [43]) or from other compositions, such as ChCl:urea (8.1×10^{-8}–1.1×10^{-7} cm^2 s^{-1} at 313–343 K for Co^{2+} [38]; 7.8×10^{-9} cm^2 s^{-1} at 363 K for Zn^{2+} [41]), EG (2.3×10^{-8} cm^2 s^{-1} at 343 K for Co^{2+} [39]), 1-methyl-imidazolium trifluoromethylsulfonate (7.7×10^{-9} cm^2 s^{-1} at 373 K for Zn^{2+} [40]), urea:1-ethyl-3-methylimidazolium (5.5×10^{-9} cm^2 s^{-1} at 353 K for Zn^{2+} [42]), and hybrid eutectic sulfolane:water (5.0×10^{-12} cm^2 s^{-1} for Zn^{2+} [44]). However, D values for Co^{2+} ions in 1ChCl:2EG were higher than those for Zn^{2+} ions recorded under the same experimental conditions. This is due to the formation of a smaller solvation sphere for Co^{2+} ions, giving them greater mobility than Zn^{2+} ions [31,45]. Regardless of the precursor, all coatings remained electrochemically stable at the different HER potentials evaluated, i.e., −0.4, −0.8 and −1.3 V.

3.3. Composition and morphology studies

Fig. 2 presents the percentage elemental composition of electrodeposits obtained by EDS, as well as surface morphological features observed by SEM micrographs, before and after immobilizing the coatings. According to Fig. 2a, the proportion of Zn and Co atoms present in the electrodeposits is very close to their molar concentration contained

Table 1
Comparison of diffusion coefficients obtained for Co^{2+} and Zn^{2+} ions at different temperatures and electrolytes.

Temperature/ K	Electrolyte	D/ $cm^2 s^{-1}$	Reference
Co^{2+}			
303	1ChCl:2EG	$2.6 \times 10^{-7} \pm 0.7 \times 10^{-8}$	This work
313	1ChCl:2EG	$3.0 \times 10^{-7} \pm 0.8 \times 10^{-8}$	This work
323	1ChCl:2EG	$3.4 \times 10^{-7} \pm 0.5 \times 10^{-7}$	This work
343	1ChCl:2EG	$4.4 \times 10^{-7} \pm 0.5 \times 10^{-7}$	This work
313	1ChCl:2U	8.1×10^{-8}	[32]
323	1ChCl:2U	1.1×10^{-7}	[32]
333	1ChCl:2U	1.1×10^{-7}	[32]
343	1ChCl:2U	1.5×10^{-7}	[32]
343	Ethylene glycol	2.3×10^{-8}	[33]
Zn^{2+}			
303	1ChCl:2EG	$8.9 \times 10^{-11} \pm 0.8 \times 10^{-11}$	This work
313	1ChCl:2EG	$1.4 \times 10^{-10} \pm 0.1 \times 10^{-10}$	This work
323	1ChCl:2EG	$2.9 \times 10^{-10} \pm 0.5 \times 10^{-11}$	This work
343	1ChCl:2EG	$4.5 \times 10^{-10} \pm 0.3 \times 10^{-10}$	This work
373	1-methylimidazolium trifluoromethylsulfonate	7.7×10^{-9}	[34]
363	1ChCl:2U	7.8×10^{-9}	[35]
353	urea/1-ethyl-3-methylimidazolium	5.5×10^{-9}	[36]
313	1ChCl:2EG	7.1×10^{-10}	[37]
–	hybrid eutectic sulfolane/water	5.0×10^{-12}	[38]

in the electrolytes: 94% Zn and 6% Co from 0.4 mol L^{-1} $ZnCl_2$ + 0.025 mol L^{-1} $CoCl_2$; and 97% Co and 3% Zn from 0.025 mol L^{-1} $ZnCl_2$ + 0.4 mol L^{-1} $CoCl_2$. This shows that the use of 1ChCl:2EG allows excellent control of the desired chemical composition for Zn-Co deposits.

As for morphology, Fig. 2b illustrates the copper substrate surface after mechanical grinding and polishing processes, where only the inherent grooves of metal erosion are observed. The results also indicated that all electrodeposits ensured a complete surface coating, proving the efficiency of the electrochemical conditions employed. For Zn coating (Fig. 2c), individual crystallites are seen, while the Co coating (Fig. 2d) exhibits dendritic shapes. The same characteristics are seen when any one of these cations is present as a major part of the electrolyte. Regardless of the proportion tested for each cation, observing at a higher magnification, the Zn-Co coatings (Fig. 2e and f) showed cracked morphological patterns, which have a high surface area and are considered excellent catalysts for electrochemical reactions. Table 2 shows the concentration of precursors tested in each electrolytic bath, in addition to the percentage of Zn, Co and Zn-Co measured by EDS in each coating.

XRD analyses were conducted to evaluate the crystalline structure of Zn, Co, and Zn-Co films. Fig. 3 shows the diffraction patterns before and after modification of copper substrates in deep eutectic solvent. According to ICDD/JCPDS database, the XRD data obtained indicate characteristic peaks associated with Cu with a face-centered cubic structure (card 85-1326), hexagonal metallic forms of Zn (card 03-065-5973), Co (card 15-0806), $Zn_{96}Co_4$ and Zn_3Co_{97} alloys (card 23-1390), besides rhombohedral $Co_2(OH)_3Cl$ (space group R-3m #166). The presence of the coatings also denotes high quality of the modifications carried out on the electrode substrate (see also the surface plasmon resonance results, Fig. S4 in Supplementary Material). On the other hand, the presence of $Co_2(OH)_3Cl$ shows that when Co^{2+} is electroimmobilized individually, parallel equilibria can be formed, leading to the formation of soluble salts and loss of coating stability. Although the same trend has not been registered for Zn^{2+}, Zn-Co coatings tend to be

Table 2
Composition of metallic coatings estimated by energy dispersive X-ray spectroscopy.

Bath	Precursor concentration (mol L^{-1})		Coatings composition (%)		Sample label
	$ZnCl_2$	$CoCl_2$	Zn	Co	
I	0.4	–	100	0	Zn
II	0.4	0.025	96	4	$Zn_{96}Co_4$
III	0.025	0.4	3	97	Zn_3Co_{97}
IV	–	0.4	0	100	Co

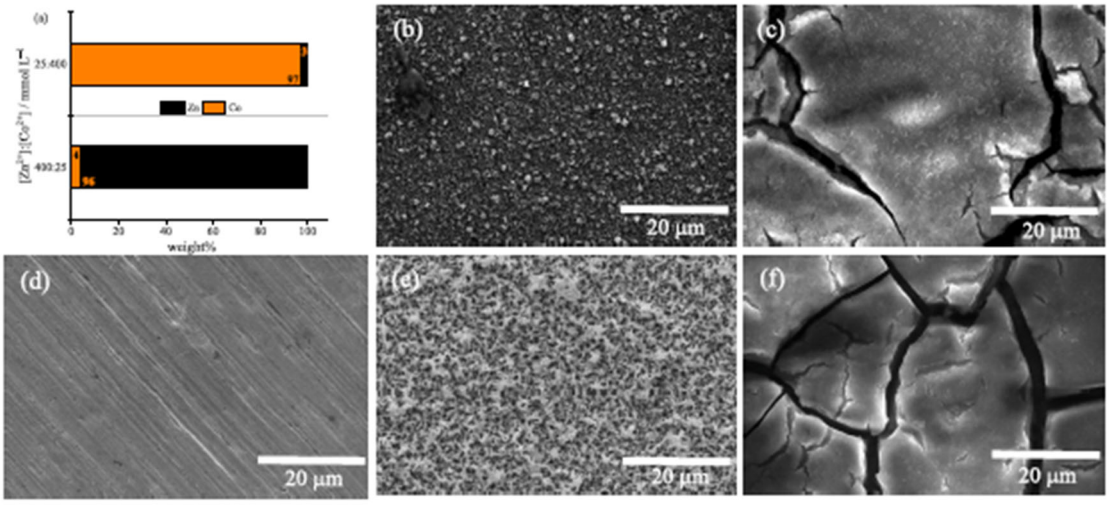

Fig. 2. (a) Metallic composition, along with the SEM images of (b) Cu substrate, (c) Cu/Zn, (d) Cu/Co, (e) Cu/$Zn_{96}Co_4$ and (f) Cu/Zn_3Co_{97}. The micrographs illustrated in b-d and e-f were recorded with 500- and 1000-times magnification, respectively.

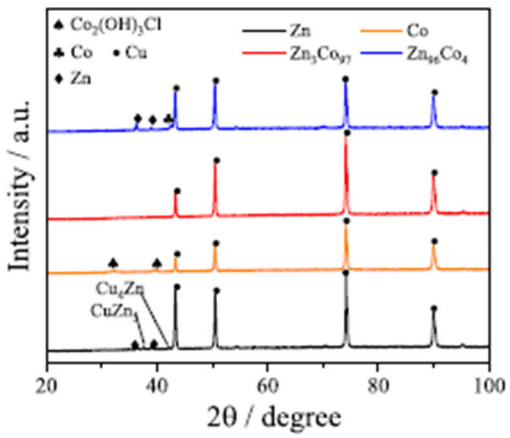

Fig. 3. XRD pattern of Zn, Co, and Zn-Co coatings, electrodeposited on Cu substrate.

more stable and suitable as electrocatalysts, as will be demonstrated later. No peaks resulting from impurities were detected, reaffirming the success in the electrosynthesis of the different metallic materials.

3.4. HER electrocatalysis

The overall performance of metallic substrates and coatings towards HER electrocatalysis is summarized in Fig. 4. The steady state curves obtained by LSV at 5 mV s^{-1} (Fig. 4a), using 1 mol/L KOH at 333 K as electrolyte, indicate the following onset potential order: Zn_3Co_{97} < $Zn_{96}Co_4$ < Co < Zn < Cu. This result proves that Zn-Co alloys are more promising as HER electrocatalysts, in addition to providing higher hydrogen production yields at lower potentials [46]. Even so, it is important to point out that all tested coatings performed better than the unmodified copper substrate, used as one of the standard electrode materials in studies with hydrogen production by water splitting.

Under alkaline conditions, the Tafel diagrams (Fig. 4b) are concentrated in a narrow overpotential range (≈ 150–320 mV dec^{-1}), suggesting that the HER mechanism for all the films is not affected by their thickness [47]. However, observing the Tafel fits, there are changes in slope values and, consequently, greater reaction rate on the Zn_3Co_{97} coating (kinetic constant = 108.2 ± 0.74 mV dec^{-1}). About the surface stability, evaluated by potential variations at a current density of 10 mA cm^{-2} applied for 100 h of electrolysis (Fig. 4c), the greatest stability trend is seen for coatings that work at lower overpotentials (Co- and Zn_3Co_{97}-based coatings), possibly because they are less exposed to corrosion conditions and/or surface fouling by reaction by-products, which lead to variations in ohmic resistance. The electrochemical behavior demonstrated by the Cu substrate, Cu/Zn and Cu/$Zn_{96}Co_4$ is like that registered for AISI 304 stainless steel (overpotential variation from 100 mV to 300 mV during electrolysis), requiring higher potentials to promote HER and showing that the presence of cobalt contributes positively to catalyze this electrochemical reaction, including as an additive in metallic alloys. Zn_3Co_{97} coatings had the lowest overpotential variation among all the analyzed materials.

Values of electrochemical active surface area (ECSA) for catalysts were estimated from them electric double layer capacitance (C_{dl}). Cyclic voltammetric profiles of Zn, $Zn_{96}Co_4$, Zn_3Co_{97} and Co electrodes were recorded in a non-Faradic region (±0.05 V vs. reversible hydrogen electrode (RHE) in relation on E_{OCP} (t = 180 s)) at different scan rates (2.5, 5, 10 and 15 mV s^{-1}) in 1 mol/L KOH (Figs. S1 and S2 in the

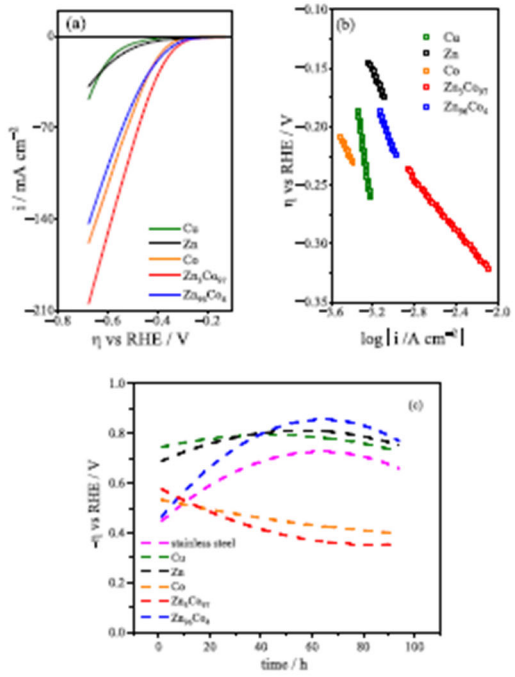

Fig. 4. (a) Polarization curves carried out with different catalysts at 0.5 mV s^{-1}. (b) The corresponding Tafel slopes. (c) Electrochemical stability tests of the catalysts, evaluated at 10 mA cm^{-2} and 333 K for 100 h. Supporting electrolyte: 1 mol L^{-1} KOH.

Supplementary Material). For comparison purposes, Table 3 presents Tafel coefficients (^{-}b), exchange current densities (i_0) and estimated overpotentials (|η|) for HER on each catalyst, obtained from fitting LSV data at 5 mV s^{-1} and using 1 mol L^{-1} KOH at 298.15 K. Now the values were normalized by geometric area and ECSA, as can be seen in Fig. S2 and Table S1 (in the Supplementary Material). These results corroborate the SEM images obtained in Fig. 3: the coating with the highest electroactive area ($Zn_{96}Co_4$) showed higher roughness, accompanied by Zn_3Co_{97}, which showed cracks.

As already stated earlier, the Cu substrate requires a highest |η| value (546 mV) to achieve a current density of 10 mA cm^{-2} during HER, followed by Zn (509 mV), Co (372 mV), $Zn_{96}Co_4$ (355 mV) and Zn_3Co_{97} (333 mV), reiterating the better electrocatalytic effect of the latter [48]. This sequence does not change even working at 10 times higher current densities. In addition, according to Banoth, Kandula and Kollu, it is desirable that an electrocatalytic material presents low values of Tafel slope accompanied by high values of exchange current [49]. When this occurs, high operating current densities can be achieved without a significant increase in overvoltage, which leads to lower operating costs [49]. Thus, the ^{-}b and i_0 values presented by the Zn_3Co_{97} and Co coatings are also indicative of their higher electrocatalytic activity compared to the others.

For Zn_3Co_{97}, comparing the Tafel parameters obtained in this study with previously published ones (Table 3), the values of ^{-}b and |η| were higher than those reported with Zn-Co-S, CoZn, NiCoZn e $Zn_{85}Ni$ coatings, but i_0 values were lower [46,48,50–52]. Since water molecules are precursors of HER by electrolysis, variations in the Tafel parameters may be due to uncompensated ohmic drop, so that small stoichiometric changes are sufficient to cause significant influences on the electrochemical reaction. Therefore, even more satisfactory results than those

Table 3
Electrochemical parameters obtained with different metallic coatings developed to produce hydrogen in 1 mol L^{-1} KOH at 298.15 K.

Catalyst	$-b$ mV dec^{-1}	i_0 A cm^{-2}	$i_{0\ RSA}$ A cm^{-2}	$\lvert\eta\rvert_{(10\ mA\ cm^{-2})}$ mV	$\lvert\eta\rvert_{(100\ mA\ cm^{-2})}$ mV	Reference
Copper	622.2 ± 2.04	2.27 × 10^{-4} ± 1.80 × 10^{-5}	–	546	–	this work
Zn	233.1 ± 64.3	1.20 × 10^{-4} ± 2.86 × 10^{-5}	1.09 × 10^{-6} ± 2.60 × 10^{-7}	509	–	this work
$Zn_{36}Co_4$	247.6 ± 15.5	1.24 × 10^{-4} ± 5.33 × 10^{-5}	9.63 × 10^{-8} ± 5.42 × 10^{-8}	355	600	this work
Zn_3Co_{97}	108.2 ± 0.74	8.57 × 10^{-6} ± 3.28 × 10^{-7}	2.12 × 10^{-8} ± 8.12 × 10^{-10}	333	524	this work
Co	191.4 ± 3.20	2.52 × 10^{-5} ± 2.56 × 10^{-6}	8.42 × 10^{-8} ± 8.53 × 10^{-9}	372	578	this work
Zn-Co-S	86.3	–	–	176	–	[50]
CoZn	96	3.80 × 10^{-2}	–	–	240	[51]
NiCoZn	81	1.62 × 10^{-2}	–	–	140	[51]
$Zn_{83}Ni$	–	0.30 × 10^{-4}	–	95*	–	[46]

*not mentioned.

obtained in this work can be achieved from more detailed studies about the reaction mechanism and surface reactivity of the coatings.

4. Conclusions

Zn, Co, and Zn-Co alloys, produced electrochemically from 1ChCl:2EG DES, are functional materials to produce hydrogen in an alkaline medium, achieving remarkable electrocatalytic effect. The potentiostatic electrodeposition of these coatings allows a good stoichiometric control of the metallic constituents, and these materials achieved a better performance at higher temperatures, due to the reduction in electrolyte viscosity, charge-transfer resistance and increase in the diffusion coefficient of the precursor cations. Increasing Co content in coatings leads to morphological organization changes, resulting in cracked surfaces that have high surface area and directly contribute to HER electrocatalysis. Among the coatings studied, Zn_3Co_{97} was the one that showed the best performance in terms of ^{-}b, i_0 and $|\eta|$, therefore it is the most promising to produce hydrogen by water splitting.

CRediT authorship contribution statement

Deomar N. Rodrigues-Júnior: Investigation, Methodology, Writing – original draft, Formal analysis. **Natalia G. Sousa:** Investigation, Formal analysis. **F. Murilo T. Luna:** Resources. **Thiago M.B.F. Oliveira:** Writing – review & editing. **Dierle S. Abreu:** Investigation, Formal analysis, Writing – review & editing. **Walther Schwarzacher:** Writing – review & editing. **Pedro de Lima-Neto:** Resources. **Adriana N. Correia:** Conceptualization, Resources, Writing – review & editing, Supervision, Project administration, Funding acquisition.

Declaration of Competing Interest

The authors declare that they have no known competing financial interests or personal relationships that could have appeared to influence the work reported in this paper.

Acknowledgments

This study was financed in part by the Coordenação de Aperfeiçoamento de Pessoal de Nível Superior - Brazil (CAPES) – Finance Code 001. The authors thank the financial support given by the following Brazilian funding agencies: Coordenação de Aperfeiçoamento de Pessoal de Nível Superior (CAPES), Conselho Nacional de Desenvolvimento Científico e Tecnológico (CNPq) and Fundação Cearense de Apoio ao Desenvolvimento Científico e Tecnológica (FUNCAP). A.N. Correia gratefully acknowledges funding provided by CNPq (proc. 405596/2018-9 and 305136/2018-6). P. de Lima-Neto thanks the financial support received from CNPq (proc. 408626/2018-6 and 304152/2018-8). N. G. Sousa thanks CNPq for her grant (proc. 141171/2021-9). D. S. Abreu thanks FINEP (CV. 01.22.0174.00 BIONANO SPR) and CNPq (proc. 407954/2022-8) for financial support. The authors would like to thank the Central Analítica-UFC/CT-INFRA/MCTI-SISANO/Pró-Equipamentos CAPES for the support.

Appendix A. Supplementary data

Supplementary data to this article can be found online at https://doi.org/10.1016/j.jelechem.2023.117785.

References

[1] R. Shilpa, K.S. Sibi, S.R. Sarath Kumar, R.K. Pai, R.B. Rakhi, Electrocatalysts for hydrogen evolution reaction, in: Mater. Hydrog. Prod. Conversion, Storage, Wiley, 2023: p. 115–146. doi: 10.1002/9781119829584.ch5.
[2] C. Pi, Z. Zhao, X. Zhang, B. Gao, Y. Zheng, P.K. Chu, L. Yang, K. Huo, In situ construction of γ-MoC/VN heterostructured electrocatalysts with strong electron coupling for highly efficient hydrogen evolution reaction, Chem. Eng. J. 416 (2021), 129130, https://doi.org/10.1016/j.cej.2021.129130.
[3] C. Feng, B. Xin, H. Li, Z. Jia, X. Zhang, B. Geng, Agaric-like cobalt diselenide supported by carbon nanofiber as an efficient catalyst for hydrogen evolution reaction, J. Colloid Interface Sci. 610 (2022) 854–862, https://doi.org/10.1016/j.jcis.2021.11.130.
[4] X. Wang, R. Su, H. Aslan, J. Kibsgaard, S. Wendt, L. Meng, M. Dong, Y. Huang, F. Besenbacher, Tweaking the composition of NiMoZn alloy electrocatalyst for enhanced hydrogen evolution reaction performance, Nano Energy 12 (2015) 9–18, https://doi.org/10.1016/j.nanoen.2014.12.007.
[5] Z. Xu, Q. Zhu, X. Xi, M. Xing, J. Zhang, Z-scheme CdS/WO_3 on a carbon cloth enabling effective hydrogen evolution, Front. Energy 15 (2021) 678–686, https://doi.org/10.1007/s11708-021-0768-6.
[6] L. Chang, Z. Sun, Y.H. Hu, 1T phase transition metal dichalcogenides for hydrogen evolution reaction, Electrochem. Energy Rev. 4 (2021) 194–218, https://doi.org/10.1007/s41918-020-00087-y.
[7] H. Wu, C. Feng, L. Zhang, J. Zhang, D.P. Wilkinson, Non-noble metal electrocatalysts for the hydrogen evolution reaction in water electrolysis, Electrochem. Energy Rev. 4 (2021) 473–507, https://doi.org/10.1007/s41918-020-00086-z.
[8] M. Plevová, J. Hnát, K. Bouzek, Electrocatalysts for the oxygen evolution reaction in alkaline and neutral media. A comparative review, J. Power Sources 507 (2021), 230072, https://doi.org/10.1016/j.jpowsour.2021.230072.
[9] T. Lim, S.-K. Kim, Non-precious hydrogen evolution reaction catalysts: Stepping forward to practical polymer electrolyte membrane-based zero-gap water electrolyzers, Chem. Eng. J. 433 (2022), 133681, https://doi.org/10.1016/j.cej.2021.133681.
[10] M. Nemiwal, T.C. Zhang, D. Kumar, Graphene-based electrocatalysts: Hydrogen evolution reactions and overall water splitting, Int. J. Hydrog. Energy 46 (2021) 21401–21418, https://doi.org/10.1016/j.ijhydene.2021.04.008.
[11] V.D. Nithya, Recent advances in Co6e2 electrocatalysts for hydrogen evolution reaction, Int. J. Hydrog. Energy 46 (2021) 36080–36102, https://doi.org/10.1016/j.ijhydene.2021.08.157.
[12] S. Zhang, X. Zhang, Y. Rui, R. Wang, X. Li, Recent advances in non-precious metal electrocatalysts for pH-universal hydrogen evolution reaction, Green Energy Environ. 6 (2021) 458–478, https://doi.org/10.1016/j.gee.2020.10.013.
[13] A. Ali, F. Long, P.K. Shen, Innovative strategies for overall water splitting using nanostructured transition metal electrocatalysts, Electrochem. Energy Rev. 5 (2022) 1, https://doi.org/10.1007/s41918-022-00136-8.
[14] R. Zahra, E. Pervaiz, M. Yang, O. Rabi, Z. Saleem, M. Ali, S. Farrukh, A review on nickel cobalt sulphide and their hybrids: Earth abundant, pH stable electro-catalyst for hydrogen evolution reaction, Int. J. Hydrogen Energy 45 (2020) 24518–24543, https://doi.org/10.1016/j.ijhydene.2020.06.236.
[15] M. Đurović, J. Hnát, K. Bouzek, Electrocatalysts for the hydrogen evolution reaction in alkaline and neutral media. A comparative review, J. Power Sources 493 (2021), 229708, https://doi.org/10.1016/j.jpowsour.2021.229708.

[16] G. Gao, W. Wang, Y. Wang, Z. Fu, L. Liu, Y. Du, Z. Li, Y. Liu, L. Wang, Synergistic coupling of NiCoS nanorods with NiCo-LDH nanosheets towards highly efficient hydrogen evolution reaction in alkaline media, J. Electroanal. Chem. 943 (2023), 117622, https://doi.org/10.1016/j.jelechem.2023.117622.
[17] Z. Zhai, H. Li, C.-a. Zhou, H. Zheng, Y. Liu, W. Yan, J. Zhang, Anisotropic Strain Boosted Hydrogen Evolution Reaction Activity of F-NiCoMo LDH for Overall Water Splitting, J. Electrochem. Soc. 170 (3) (2023) 036509.
[18] C.L. Fan, D.L. Piron, H.J. Miao, M. Rojas, Hydrogen evolution in alkaline water on cobalt electrodeposits prepared from baths containing different anions, J. Appl. Electrochem. 23 (1993) 985–990, https://doi.org/10.1007/BF00266119.
[19] A. Maurya, S. Suman, A. Bhardwaj, L. Mohapatra, A.K. Kushwaha, Substrate dependent electrodeposition of Ni–Co alloy for efficient hydrogen evolution reaction, Electrocatalysis 14 (2023) 68–77, https://doi.org/10.1007/s12678-022-00773-x.
[20] V.S. Kublanovsky, Y.S. Yaponteva, Electrocatalytic properties of Co-Mo alloys electrodeposited from a citrate-pyrophosphate electrolyte, Electrocatalysis 5 (2014) 372–378, https://doi.org/10.1007/s12678-014-0197-y.
[21] T. Ling, T. Zhang, B. Ge, L. Han, L. Zheng, F. Lin, Z. Xu, W.-B. Hu, X.-W. Du, K. Davey, S.-Z. Qiao, Well-dispersed nickel- and zinc-tailored electronic structure of a transition metal oxide for highly active alkaline hydrogen evolution reaction, Adv. Mater. 31 (2019) 1807771, https://doi.org/10.1002/adma.201807771.
[22] C.K. Sumesh, Zinc oxide functionalized molybdenum disulfide heterostructures as efficient electrocatalysts for hydrogen evolution reaction, Int. J. Hydrog. Energy 45 (2020) 619–628, https://doi.org/10.1016/j.ijhydene.2019.10.235.
[23] Q. Cao, Z. Cheng, J. Dai, T. Sun, G. Li, L. Zhao, J. Yu, W. Zhou, J. Lin, Enhanced hydrogen evolution reaction over co nanoparticles embedded n-doped carbon nanotubes electrocatalyst with Zn as an accelerant, Small 18 (2022) 2204827, https://doi.org/10.1002/smll.202204827.
[24] S.S.V. Tatiparti, F. Ebrhimi, Potentiostatic versus galvanostatic electrodeposition of nanocrystalline Al–Mg alloy powders, J. Solid State Electrochem. 16 (2012) 1255–1261, https://doi.org/10.1007/s10008-011-1522-5.
[25] F. Endres, D. MacFarlane, and A. Abbott, Electrodeposition from ionic liquids, Electrodeposition from Ionic Liquids. p. 1-387, 2008, doi: 10.1002/9783527622917.
[26] K. Li, T. Ren, Z.Y. Yuan, T.J. Bandosz, Electrodeposited P-Co nanoparticles in deep eutectic solvents and their performance in water splitting, Int. J. Hydrog. Energy 43 (2018) 10448–10457, https://doi.org/10.1016/j.ijhydene.2018.04.136.
[27] C. Lei, H.F. Alesary, F. Khan, A.P. Abbott, K.S. Ryder, Gamma-phase Zn-Ni alloy deposition by pulse-electroplating from a modified deep eutectic solution, Surf. Coat. Technol. 403 (2020), 126434, https://doi.org/10.1016/j.surfcoat.2020.126434.
[28] A.P. Abbott, D. Boothby, G. Capper, D.L. Davies, R.K. Rasheed, Deep eutectic solvents formed between choline chloride and carboxylic acids: versatile alternatives to ionic liquids, J. Am. Chem. Soc. 126 (2004) 9142–9147, https://doi.org/10.1021/ja048266j.
[29] A. Srivastava, P. Sahu, M. S. Murali, Sk. M. Ali, M. Sahu, J. S. Pillai, and N. Rawat, New deep eutectic solvents based on imidazolium cation: Probing redox speciation of uranium oxides by electrochemical and theoretical simulations, J. Electroanal. Chem. vol. 901, p. 115752, 2021.
[30] A.S.C. Urcezino, L.P.M. Dos Santos, P.N.S. Casciano, A.N. Correia, P. De Lima-Neto, Electrodeposition study of Ni coatings on copper from choline chloride-based deep eutectic solvents, J. Braz. Chem. Soc. 28 (2017) 1193–1203, https://doi.org/10.21577/0103-5053.20160278.
[31] J.C. Pereira, L.P.M. Santos, A.A.C. Alcanfor, H.B. de Sant'Ana, F.X. Feitosa, O. S. Campos, A.N. Correia, P.N.S. Casciano, P. de Lima-Neto, Effects of electrodeposition parameters on corrosion resistance of ZnSn coatings on carbon steel obtained from eutectic mixture based on choline chloride and ethylene glycol, J. Alloy. Compd. 886 (2021), 161159, https://doi.org/10.1016/j.jallcom.2021.161159.
[32] J.C. Pereira, L.P.M. Santos, A.A.C. Alcanfor, O.S. Campos, P.N.S. Casciano, A. N. Correia, P. de Lima-Neto, Electrochemical corrosion evaluation of new Zn-Sn-In coatings electrodeposited in a eutectic mixture containing choline chloride and ethylene glycol, Electrochim. Acta 407 (2022), 139647, https://doi.org/10.1016/j.electacta.2021.139647.
[33] L.P.M. dos Santos, R.M. Freire, S. Michea, J.C. Denardin, D.B. Araújo, E.B. Barros, A.N. Correia, P. de Lima-Neto, and Pedro de Lima-Neto, Electrodeposition of 1-D tellurium nanostructure on gold surface from choline chloride-urea and choline chloride-ethylene glycol mixtures, J. Mol. Liq. 288 (2019) 111038.
[34] H.F. Alesary, S. Cihangir, A.D. Ballantyne, R.C. Harris, D.P. Weston, A.P. Abbott, K. S. Ryder, Influence of additives on the electrodeposition of zinc from a deep eutectic solvent, Electrochim. Acta 304 (2019) 118–130, https://doi.org/10.1016/j.electacta.2019.02.090.
[35] Q. Chu, J. Liang, J. Hao, Electrodeposition of zinc-cobalt alloys from choline chloride–urea ionic liquid, Electrochim. Acta 115 (2014) 499–503, https://doi.org/10.1016/j.electacta.2013.10.204.
[36] X. Fu, C. Zhan, R. Zhang, B. Wang, H. Sun, J. Sun, Effect of temperature on mechanism and kinetics of electrochemical nucleation of copper in ChCl–based deep eutectic solvents, J. Solid State Electrochem. 26 (2022) 2713–2722, https://doi.org/10.1007/s10008-022-05282-z.
[37] M.V. Tesakova, S.M. Kuzmin, V.I. Parfenyuk, Electrodeposition of films of individual 5,10,15,20-tetrakis(3-aminophenyl)porphyrin metal complexes and their composite for electrocatalytic oxygen reduction, Inorg. Chem. Commun. 135 (2022), 109106, https://doi.org/10.1016/j.inoche.2021.109106.
[38] T.D.V. Phuong, L.M. Quynh, N.N. Viet, L.V. Thong, N.T. Son, V.-H. Pham, P. D. Tam, V.H. Nguyen, T.L. Manh, Effect of temperature on the mechanisms and kinetics of cobalt electronucleation and growth onto glassy carbon electrode using reline deep eutectic solvent, J. Electroanal. Chem. 880 (2021), 114823, https://doi.org/10.1016/j.jelechem.2020.114823.
[39] G. Panzeri, A. Accogli, F. Gibertini, S. Varotto, C. Rinaldi, L. Nobili, L. Magagnin, Electrodeposition of cobalt thin films and nanowires from ethylene glycol-based solution, Electrochem. Commun. 103 (2019) 31–36, https://doi.org/10.1016/j.elecom.2019.04.012.
[40] M. Li, Y. Li, Electrodeposition of zinc from zinc oxide and zinc chloride in 1-methylimidazolium trifluoromethylsulfonate ionic liquid, Prot. Met. Phys. Chem. Surfaces 56 (2020) 180–188, https://doi.org/10.1134/S2070205120010141.
[41] H. Yang, R.G. Reddy, Electrochemical kinetics of reduction of zinc oxide to zinc using 2:1 urea/ChCl ionic liquid, Electrochim. Acta 178 (2015) 617–623, https://doi.org/10.1016/j.electacta.2015.08.050.
[42] W. He, L. Shen, Z. Shi, B. Gao, X. Hu, J. Xu, Z. Wang, Zinc electrodeposition from zinc oxide in the urea/1-ethyl-3-methylimidazolium chloride at 353 K, Electrochemistry 84 (2016) 872–877, https://doi.org/10.5796/electrochemistry.84.872.
[43] K. Wang, J. Phelps, R. Abdolvand, J. Carter, H.A. Hamedani, Zinc nanoparticles electrodeposited on TiO2 nanotube arrays using deep eutectic solvents for implantable electrochemical sensors, ACS Appl. Nano Mater. 6 (2023) 8238–8249, https://doi.org/10.1021/acsanm.3c00511.
[44] C. Li, R. Kingsbury, A.S. Thind, A. Shyamsunder, T.T. Fister, R.F. Klie, K.A. Persson, L.F. Nazar, Enabling selective zinc-ion intercalation by a eutectic electrolyte for practical anodeless zinc batteries, Nat. Commun. 14 (2023) 3067, https://doi.org/10.1038/s41467-023-38460-2.
[45] T.K. Dang, N. Van Toan, C.M. Hung, N. Van Duy, N.N. Viet, L.V. Thong, N.T. Son, N. Van Hieu, T.u. Le Manh, Investigation of zinc electronucleation and growth mechanisms onto platinum electrode from a deep eutectic solvent for gas sensing applications, J. Appl. Electrochem. 52 (2) (2022) 299–309.
[46] G. Sheela, Zinc–nickel alloy electrodeposits for water electrolysis, Int. J. Hydrog. Energy 27 (2002) 627–633, https://doi.org/10.1016/S0360-3199(01)00170-7.
[47] F. Bao, E. Kemppainen, I. Dorbandt, R. Bors, F. Xi, R. Schlatmann, R. van de Krol, S. Calnan, Understanding the hydrogen evolution reaction kinetics of electrodeposited nickel-molybdenum in acidic, near-neutral, and alkaline conditions, ChemElectroChem 8 (2021) 195–208, https://doi.org/10.1002/celc.202001436.
[48] H. Ren, L. Yu, L. Yang, Z.H. Huang, F. Kang, R. Lv, Efficient electrocatalytic overall water splitting and structural evolution of cobalt iron selenide by one-step electrodeposition, J. Energy Chem. 60 (2021) 194–201, https://doi.org/10.1016/j.jechem.2021.01.002.
[49] P. Banoth, C. Kandula, and P. Kollu, Introduction to electrocatalysis, In: Noble metal-free electrocatalysts: new treads in electrocatalysts for energy applications, vol. 2, ch. 1, p. 1-37, 2022, doi: 10.1021/bk-2022-1432.ch001.
[50] B. Zhang, G. Yang, C. Li, K. Huang, J. Wu, S. Hao, J. Feng, D. Peng, Y. Huang, Phase controllable fabrication of zinc cobalt sulfide hollow polyhedra as high-performance electrocatalysts for the hydrogen evolution reaction, Nanoscale 10 (2018) 1774–1778, https://doi.org/10.1039/C7NR08097B.
[51] A. Döner, R. Solmaz, G. Kardaş, Enhancement of hydrogen evolution at cobalt–zinc deposited graphite electrode in alkaline solution, Int. J. Hydrog. Energy 36 (2011) 7391–7397, https://doi.org/10.1016/j.ijhydene.2011.03.083.
[52] R. Solmaz, G. Kardaş, Fabrication and characterization of NiCoZn–M (M: Ag, Pd and Pt) electrocatalysts as cathode materials for electrochemical hydrogen production, Int. J. Hydrog. Energy 36 (2011) 12079–12087, https://doi.org/10.1016/j.ijhydene.2011.06.101.

APÊNDICE B – MATERIAL SUPLEMENTAR DO MANUSCRITO 1 - $Zn_xCo_{(1-x)}$ *COATINGS FROM CHOLINE CHLORIDE-ETHYLENE GLYCOL DEEP EUTECTIC SOLVENT AS ELECTROCATALYSTS FOR HYDROGEN EVOLUTION REACTION* - PUBLICADO NO PERIÓDICO *JOURNAL OF ELECTROANALYTICAL CHEMISTRY*

Supplementary Material

$Zn_xCo_{(1-x)}$ coatings from choline chloride-ethylene glycol deep eutectic solvent as electrocatalysts for hydrogen evolution reaction

Deomar N. Rodrigues-Júnior[a], Natalia G. Sousa[a], F. Murilo T. Luna[b], Thiago M.B.F. Oliveira[c], Dieric S. Abreu[d], Walther Schwarzacher[e], Pedro de Lima-Neto[a], Adriana N. Correia[a,*]

[a] Grupo de Eletroquímica e Corrosão, Departamento de Química Analítica e Físico-Química, Centro de Ciências, Universidade Federal do Ceará, Campus do Pici, Fortaleza - CE, 60440-900, Brazil

[b] Grupo de Pesquisa em Separações por Adsorção, Departamento de Engenharia Química, Centro de Tecnologia, Universidade Federal do Ceará, Campus do Pici, Fortaleza - CE, 60455-760, Brazil

[c] Laboratório de Química Aplicada, Centro de Ciência e Tecnologia, Universidade Federal do Cariri, Juazeiro do Norte - CE, 63048-080, Brazil

[d] Laboratório de Materiais e Dispositivos, Departamento de Química Analítica e Físico-Química, Centro de Ciências, Universidade Federal do Ceará, Campus do Pici, Fortaleza, CE

60440-900, Brazil

[e] H. H. Wills Physics Laboratory,

University of Bristol, Tyndall Avenue, Bristol, BS8 1TL, United Kingdom

Figure S1. Cyclic voltammetry curves for effective electrochemical active surface area tests (ECSA) in 1 mol L^{-1} KOH for (a) Zn, (b) $Zn_{96}Co_4$, (c) Zn_3Co_{97} and (d) Co. The capacitive currents are collected at ±0.05 V (from the open circuit potential) from 2.5 up to 15 mV s^{-1}.

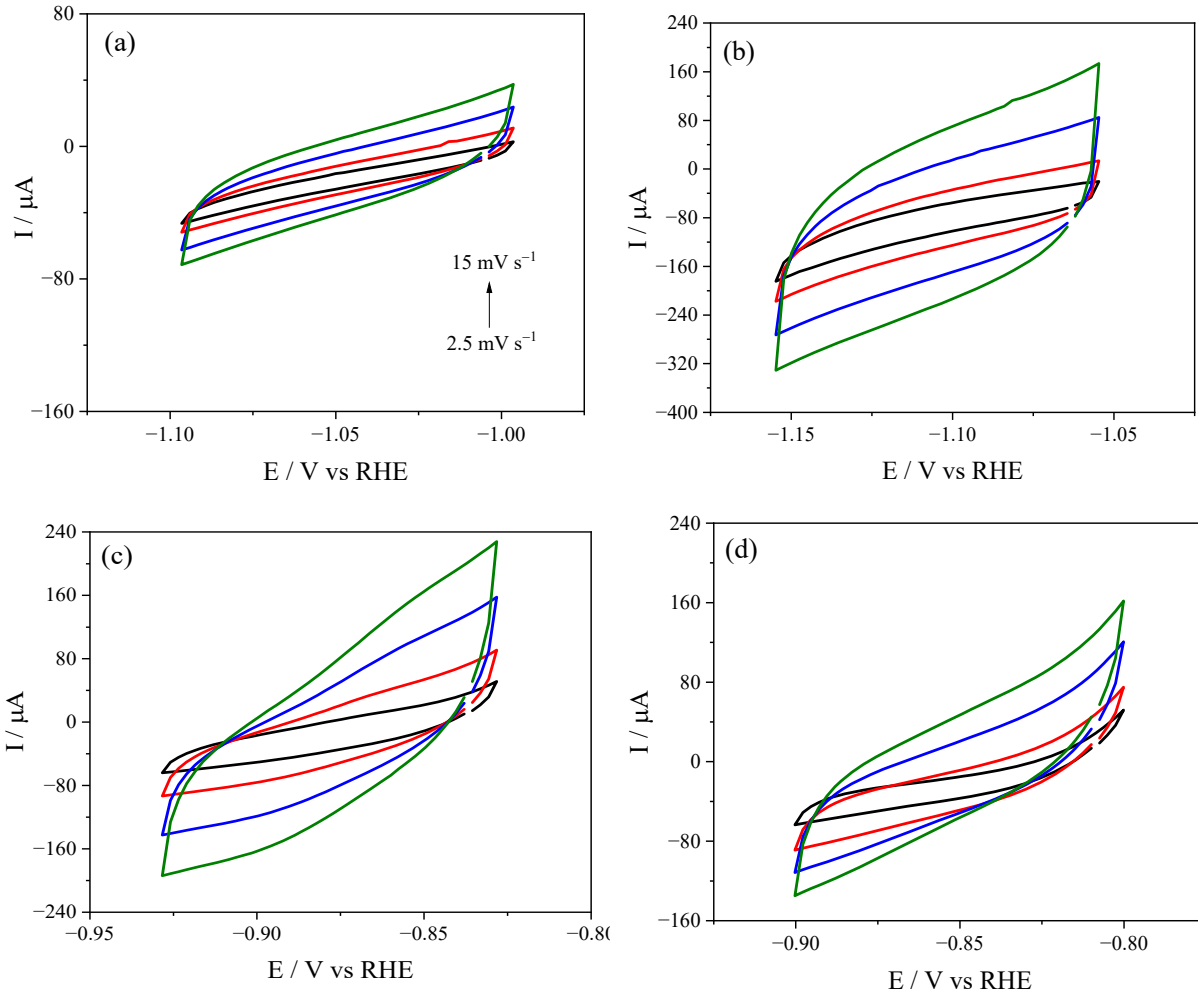

Figure S2. The charging current density differences plotted against scan rates of Zn, Co, Zn_3Co_{97}, and $Zn_{96}Co_4$ electrodes.

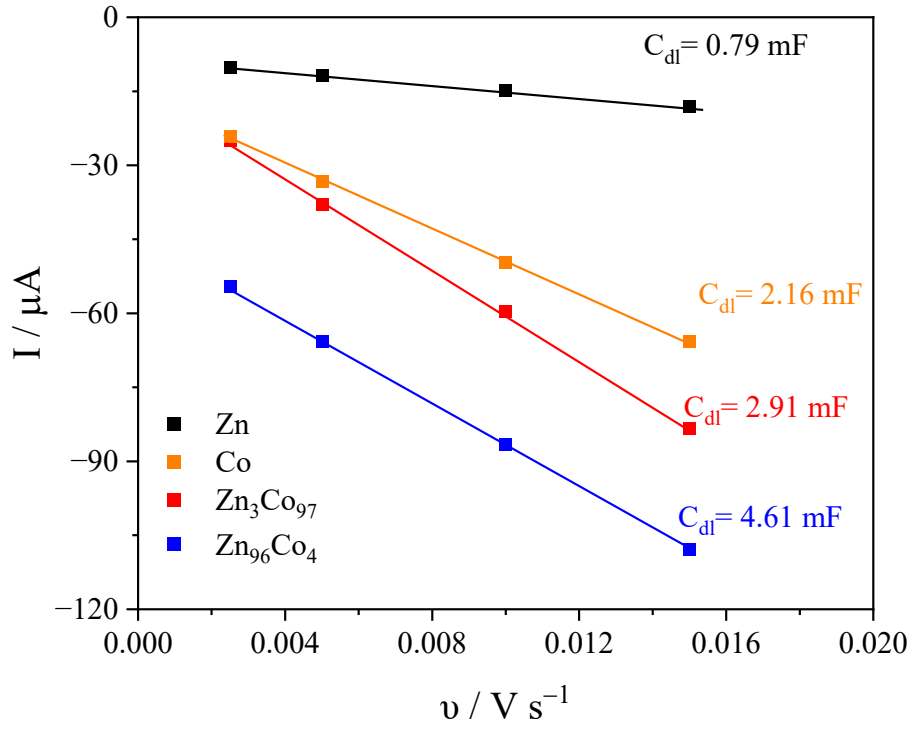

For these calculations, the value of the C_s used was 0.040 mF cm^{-2}. [R1 and R2] Considering these relative surface areas, it was possible to normalize the electrochemical data to determine the values of Tafel slope and exchange current density and the results are summarized in Table 3.

References

[R1] P. Mukherjee, K. Sathiyan, R. S. Vishwanatha and T. Zidki, Anchoring MoS2 on an ethanol-etched Prussian blue analog for enhanced electrocatalytic efficiency for the oxygen evolution reaction, ***Mater. Chem. Front.***, **vol. 6, p.** 1770-1778, 2022, https://doi.org/10.1039/D2QM00183G.

[R2] H. Liang, D. Jiang, S. Wei, X. Cao, T. Chen, B. Huo, Z. Peng, C. Li and J. Liu, 3D cellular CoS1.097/nitrogen doped graphene foam: a durable and self-supported bifunctional electrode for overall water splitting, *J. Mater. Chem. A*, vol. 6, p. 16235-16245, 2018, https://doi.org/10.1039/C8TA05407J.

Table S1. Benchmarking parameters for catalysts studied in 1 mol L^{-1} KOH.

Catalyst	$C_{dl}=\frac{(\text{anodic slope} - \text{cathodic slope})}{2}$	$ECSA=\frac{C_{dl}}{C_s}$
Zn	0.79 mF	19.8 ± 4.2
$Zn_{96}Co_4$	4.61 mF	115.2 ± 51.6
Zn_3Co_{97}	2.91 mF	72.8 ± 23.6
Co	2.16 mF	53.9 ± 2.7

Fig.S3. (a) Polarization curves performed at 0.5 mV s^{-1} at 298 K and (b) Tafel slopes with linear fittings, considering normalized ECSA in 1 mol L^{-1} KOH for Zn (black line or symbol), Co (orange line or symbol), Zn_3Co_{97} (red line or symbol) and $Zn_{96}Co_4$ (blue line or symbol).

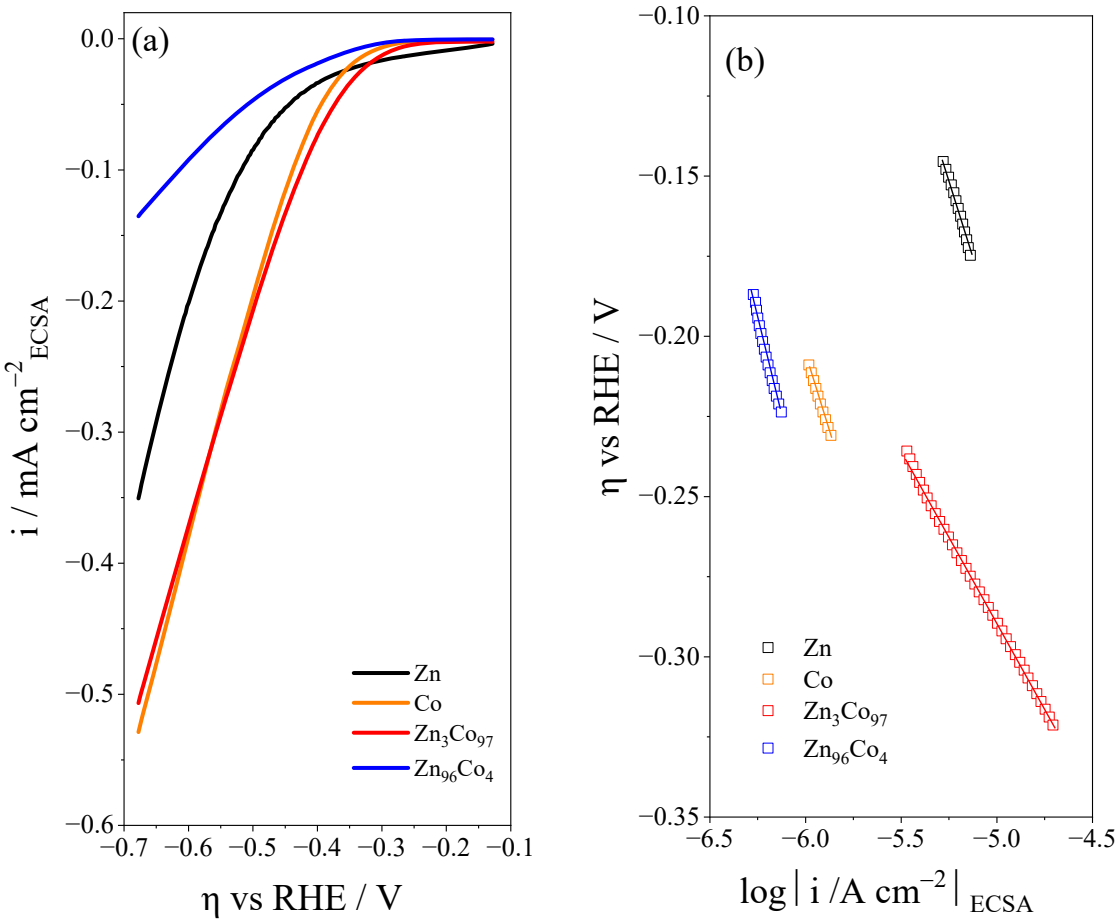

Surface Plasmon Resonance (SPR)

SPR experiments of Zn-Co metal coatings was performed on MP-SPR Navi™ 200 OTSO (Bionavis, Sweden) equipped with two laser channels (670nm and 785 nm) in angular scan mode on two separate spots on the surface. The SPR curves were taken first in air and later in water with a flow rate of 100 µL/min during a measure of 60 minutes. The thin film Zn-Co metal coatings were characterized in terms of layer thickness (d), using dedicated MP-SPR Navi™ LayerSolver™ software. Zn and Co were electrodeposited on a SPR Au-substrate (2

nm Cr adhesion layer and 50 nm Au layer). Prior to electrodeposition, the SPR Au-substrate were cleaned in Piranha solution (H_2SO_4: H_2O_2, 3:1 v/v) for 2 min and rinsed with Milli-Q water. Then, clean SPR Au-slide were placed in electrochemical cell as work electrode to perform electrodeposition of metallic coatings (see *Section 2.3*). The resultant SPR Au-substrate with Zn-Co coatings (Au-substrate + Zn, Au-substrate + Co, Au-substrate + $Zn_{96}Co_4$, and Au-substrate + Zn_3Co_{97}) was promptly washed with water and isopropanol and dried under nitrogen prior to use in SPR. The results are presented in Figure S4.

The SPR curves in Figure S4 show the peak minimum intensity shifted upwards and the peak showed significant broadening with respect to gold due to presence of absorbing layers of Zn-Co metal coatings with optical constants very different from those of gold substrate. Also, due to the nom-plasmonic metallic nature of Zn and Co coatings on gold in the 670 nm and 785 nm wavelengths region and the high values of extinction coefficient for Co (k = 6.5355), [SPR#1] the SPR curves vanishes for those coatings with high composition of Co (i.e., Co and Zn_3Co_{97}). That behavior indicates a high ordered and dense thin film,[SPR#2] corroborating with powder DRX results (see *Section 3.3*). In addition, SPR curves obtained with water flux for 1h (Figure S4. (b) and (d)) indicate no change in optics properties of coatings, also confirming their stabilities.

Figure S4. SPR curves for the Co, Zn, Zn_3Co_{97} and $Zn_{96}Co_4$ metal coatings on Au-substrate. Measurements were performed with 785 nm wavelength in (a) air and (b) water, and with 670 nm wavelength in air (c) and (d) water.

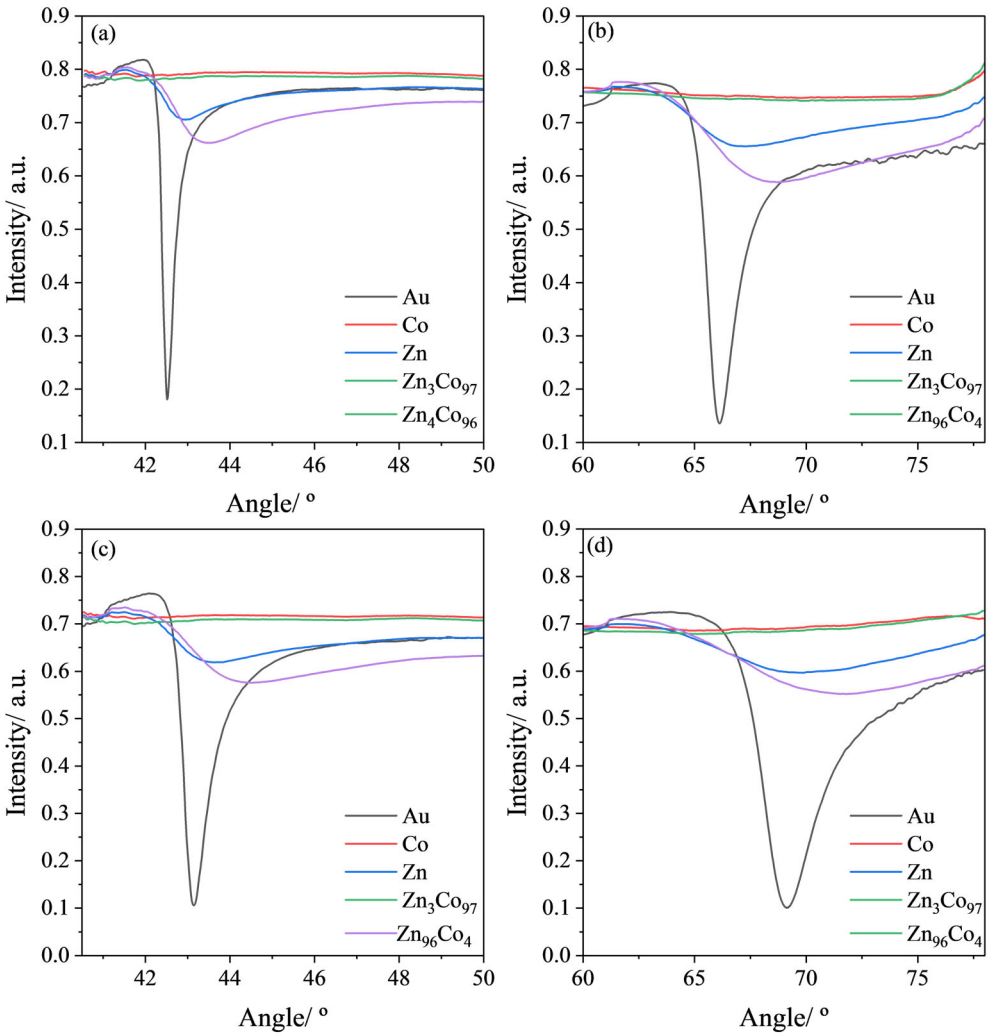

References

[SPR#1] Wolfgang S. M. Werner, Kathrin Glantschnig, Claudia Ambrosch-Draxl; Optical Constants and Inelastic Electron-Scattering Data for 17 Elemental Metals. *Journal of Physical and Chemical Reference*, vol. 4, p. 1013–1092, 2009, https://doi.org/10.1063/1.3243762.

[SPR#2] Popov, K. I., Djokić, S. S., Nikolić, N. D., & Jović, V. D.. Electrodeposition of Metals with Hydrogen Evolution. *Morphology of electrochemically and chemically deposited metals,* p. 171-203. Switzerland: Springer. 2016. https://doi.org/10.1007/978-3-319-26073-0_5.